STABLE ISOTOPIC RESPONSE TO THE LATE EOCENE EXTRATERRESTRIAL IMPACT EVENTS

by

AIMEE E PUSZ

A thesis submitted to the

Graduate School-New Brunswick

Rutgers, The State University of New Jersey

in partial fulfillment of the requirements

for the degree of

Master of Science

Graduate Program in Geological Sciences

written under the direction of

Dr. Kenneth G. Miller

and approved by

_____

_____

_____

New Brunswick, New Jersey

[October, 2007]

ABSTRACT OF THE THESIS

Stable Isotopic Response to the Late Eocene Extraterrestrial Impact Events

by AIMEE ELIZABETH PUSZ

Thesis Director:
Dr. Kenneth G. Miller

Two large and near synchronous late Eocene (~35.4 - 35.5 Ma based on radiometric ages) impact events (Popigai and Chesapeake Bay) produced well-preserved structures, yet the environmental response to these impacts is poorly understood. Impact events generate ejecta deposits that surround source craters creating characteristic strewn fields. The Chesapeake Bay and Popigai impactors produced strewn fields that serve as stratigraphic markers for these impact events and the late Eocene. The late Eocene global temperature history and carbon budget are poorly constrained because of sparsely sampled $\delta^{18}O$ and $\delta^{13}C$ records. In this thesis: 1) the Chesapeake Bay microtektite layer is shown to be stratigraphically younger than the Popigai cpx-bearing (or microkrystite) layer, by ~ 4 kyr; 2) a first order correlation of the late Eocene ejecta layers identified in ODP Site 1090 to the geomagnetic polarity timescale in Chron C16n.1n (279 mbsf) is provided with a corresponding magnetochronologic age of 35.43 Ma, consistent with published radiometric ages; 3) new stable isotopic data is presented from Site 1090 and DSDP Site 612 that show a large and transient $\delta^{13}C$ excursion (~0.5‰) associated with the impacts. At Site 1090, late Eocene benthic foraminifera are well preserved, the identified ejecta horizon is marked by an Ir anomaly (~950 pg/g), and the published magnetostratigraphic age control is excellent. Site 1090 $\delta^{13}C$ and $\delta^{18}O$ records of benthic foraminifera across

the ejecta layer from 34.6 - 35.8 Ma (8 kyr sampling) and 33.7 - 36 Ma (16 kyr sampling) and a high-resolution (2 kyr sampling) bulk-carbonate record (278 - 279.5 mbsf) are presented. Coeval benthic foraminiferal records show a $\delta^{13}C$ excursion from: 1) new benthic data from Southern Ocean Site 1090 show a 0.5‰ anomaly; 2) new benthic data from New Jersey slope Site 612 show a 0.5‰ change, though this record is partially truncated by an unconformity; 3) Southern Ocean Site 689 published data shows a 1.0‰ excursion; and 4) Pacific Ocean Site 1218 published data shows a 0.4‰ anomaly. The $\delta^{13}C$ excursion is suggested to reflect a perturbation in the global carbon cycle and to be directly related to the late Eocene impactor(s).

Acknowledgements

I would like to thank my fantastic advisor, Ken Miller, for providing me with this opportunity. I cannot thank Ken enough for his continuous support, guidance, and advice. He is truly an amazing advisor who taught me everything from how to manage my files, to my money, and even my life.

I sincerely thank Jim Wright, an amazing teacher not only of stable isotopes and paleoceanography, but of scientific completeness and ultimately merit.

An essential and tremendous thank you, to Dennis Kent, for developing and funding such an insightful and eclectic project. I thank Dennis for his great advice I will carry throughout my career. And for showing me things that seem so obvious now!

A very special thank you, to Mimi Katz who taught so much about benthic foraminifera. She opened my eyes to these breathtakingly beautiful little creatures. Her encouragement, support, and advice are forever remembered and truly appreciated.

Thank you dearly, to Jim Browning, for the many times he was there to help and for all the little details.

A profound thank you, to my mother and father, who taught me how to teach a flawless lesson is by leading through example. I would not be able to achieve my ambitions or live my dream without the support and illustration of my father and mother, respectively. Thank you to my brother, Matthew, my buddy through life, who questioned long ago "why don't you become a geologist?"

Last, but never least, thank you to Brennan, for his endless support, understanding, and love.

Table of Contents **Page**

Abstract ii

Acknowledgements iv

Table of Contents v

List of Tables viii

List of Figures ix

List of Appendices xiv

1. Introduction 1

2. Background 3

2.1 Carbon Isotope Excursions and Mass Extinctions 3

2.1 Cretaceous-Tertiary (K-T) Boundary 3

2.1 Permian-Triassic (P-Tr) Boundary 5

2.1 Triassic-Jurassic (Tr-J) Boundary 5

2.1 Paleocene-Eocene Thermal Maximum (PETM) 6

2.2 Cenozoic Strewn Fields 6

2.2 North American Strewn Field (NASF) 8

2.2 Popigai Strewn Field 9

2.2 Nd and Sr Isotopes 10

2.3 Stable Isotopes 11

2.3 Carbon Isotopes and the 'Long-term' Global Carbon Cycle 11

2.3 'Short-term' Global Carbon Cycle 17

2.3 'Abrupt' Term Global Carbon Cycle 19

Table of Contents **Page**

2.3 Abyssal Circulation and the Global Carbon Cycle 20

2.3 Oxygen Isotopes 22

2.4 Late Eocene Impact Stratigraphy 23

2.4 Barbados, Bath Cliff Section 23

2.4 Caribbean Sea 24

2.4 Massignano, Italy 25

2.4 Southern Ocean ODP Site 689 27

2.4 St. Stephen's Quarry (SSQ), Alabama 29

2.4 Southern Ocean ODP Site 1090 30

2.4 Deep Sea Drilling Project (DSDP) Site 612 31

3. Methods 34

3.1 ODP Sites 1090, and 612, and St. Stephens Quarry (SSQ) 34

3.1 Site 1090 Impact Stratigraphy 34

3.1 Site 1090 Isotopic Analysis 34

3.1 Site 612 Isotopic Analysis 36

3.1 SSQ Microspherules 36

4. Results 37

4.1 Site 1090 37

4.1 Calibration of Impactites to the GPTS (1992,1995) 37

4.1 Site 1090 Benthic Foraminifera 38

4.1 Site 1090 Benthic Carbon Isotopes 38

Table of Contents **Page**

4.1 Site 1090 Bulk-Carbonate Carbon Isotopes 40

4.1 Site 1090 Benthic Oxygen Isotopes 40

4.1 Site 1090 Bulk-Carbonate Oxygen Isotopes 41

4.1 Site 1090 Ejecta Deposits 42

4.2 DSDP Site 612 43

4.2 Site 612 Benthic Carbon Isotopes 43

4.2 Site 612 Benthic Oxygen Isotopes 44

4.3 St. Stephens Quarry (SSQ) 45

4.3 SSQ Microspherule Deposits 45

5. Discussion 48

5. Abyssal Circulation 48

5. Impact Events and Climate 49

5. Impactor Diameter 51

5. Impact Events and Carbon Isotope Excursions 54

5. Impact Events and Mass Extinctions 56

6. Conclusions 58

References 60

Tables 89

Figures 102

Appendix A 129

List of Tables **Page**

Table 1.	Size in gigatons (Gt) and the isotopic ratio of the exchangeable carbon reservoirs.	89
Table 2.	Site 1090 Benthic genus *Cibicidoides* abundances.	90
Table 3.	Site 1090 benthic stable isotope data.	94
Table 4.	Site 1090 bulk-carbonate stable isotope data.	97
Table 5.	Calculated amounts of cometary C inputs required to change the C system by a given isotopic value.	98
Table 6.	Calculated amounts of ordinary chondritic C inputs required to change the C system.	99
Table 7.	Magnitude of K-T boundary C isotope anomaly relative to the exchangeable C reservoirs.	100
Table 8.	Calculated amounts of carbonaceous chondritic C inputs required to change the C system.	101

List of Figures **Page**

Figure 1. Global map showing the location of the CBIS and Popigai crater, DSDP Site 612, ODP Sites 689, 1090 and 1218, RC9-58, SSQ, and Massignano. 102

Figure 2. Regional map showing the CBIS (modified from Gohn et *al*., 2006). 103

Figure 3. Location of South Atlantic ODP Site 1090. 104

Figure 4a. Carbon isotope and Ir data across the K-T boundary at DSDP Site 524 (modified from Hsu et *al*., 1982). 105

4b. Carbon isotope and Ir data across the P-Tr boundary in northern Italy (modified from Holser et *al*., 1989). 106

Figure 5a. Map showing the four Cenozoic Strewn Fields (modified from Koeberl, 1994). 107

5b. Distribution of sites with late Eocene cpx-spherules (modified from Glass, 2004). 107

List of Figures **Page**

Figure 6 Shipboard measurements of inclination (Gersonde et *al*., 1999) and magnetic polarity (Channell et *al*., 2003). 108

Figure 7. Top illustration depicts the distribution of $\delta^{13}C$ of DIC in today's oceans using GEOSECS data (Kroopnick, 1985), after Wright and Miller (1992). Bottom illustrates the position of South Atlantic ODP Site 1090 relative to NADW and CDW (modified from Hodell et *al*., 2002). 109

Figure 8. Biostratigraphy, tephrastratigraphy, and $\delta^{18}O$ stratigraphy of the Bath Cliff section, Barbados (modified from Saunders et *al.,* 1984). 110

Figure 9a. Biostratigraphy, magnetostratigraphy, stable isotopes, and Ir anomalies of the GSSP of the Eocene/Oligocene boundary at Massignano, Italy (Bodiselitsch et *al*., 2004). 111

9b. Stable isotope and Ir data of the GSSP of the Eocene/Oligocene boundary at Massignano, Italy for the entire section (Bodiselitsch et *al*., 2004). 112

List of Figures **Page**

Figure 10.	Biostratigraphy, magnetostratigraphy, stable isotopes, Ir data (Montanari et *al*., 1993), and microsperule abundances (Glass and Koeberl, 1999) from South Atlantic ODP Site 689.	113
Figure 11.	SSQ, Alabama age-depth plot with biostratigraphy, magnetostratigraphy, and sequence stratigraphy (Modified from Miller et *al*., 2006).	114
Figure 12.	Age-depth plot for South Atlantic ODP Site 1090.	115
Figure 13.	DSDP Site 612 biostratigraphy, stable isotopes, and microspherule counts (Glass, 1989).	116
Figure 14.	Stratigraphic distribution of SSQ microspherules.	117
Figure 15a.	SEM image magnified 272x of an SSQ microspherule.	118
b.	SEM image magnified 1,100x of an SSQ microspherule.	118

List of Figures **Page**

Figure 16a. South Atlantic ODP Site 1090 benthic $\delta^{13}C$ vs. depth (mbsf). 119

b. Site 1090 benthic $\delta^{13}C$ vs. age (Ma). 120

Figure 17. Site 1090 bulk-carbonate and benthic $\delta^{13}C$ data. 121

Figure 18. Site 1090 benthic $\delta^{18}O$ vs. age (Ma). 122

Figure 19. Site 1090 bulk-carbonate and benthic $\delta^{18}O$ data. 123

Figure 20a. SEM image magnified 306x of a Site 1090 microtektite. 124

b. SEM image magnified 4,460x of a Site 1090 microtektite. 124

Figure 21. Site 612 benthic stable isotope data across the cpx-bearing ejecta layer (Glass, 1989). 125

Figure 22a. Plot of Al_2O_3 (top) and CaO (bottom) vs. SiO_2 weight percent (wt.%) concentrations SSQ microspherules. 126

b. Plots of MgO (top) and FeO (bottom) vs. SiO_2 weight percent (wt.%). 127

List of Figures **Page**

Figure 23. Late Eocene/early Oligocene benthic $\delta^{13}C$ and $\delta^{18}O$ data from Sites 1090, 612 (new data from this thesis and Miller et *al*., 1991), and 1218 (data from Lear et *al*., 2004). 128

List of Appendices **Page**

Appendix A:	Back-scattered electron microscope (BEM) images of SSQ microspherules taken by C. Koeberl at the University of Vienna, Austria.	129

1. Introduction

The late Eocene marks one of the largest transitions in Earth's climate system of the past 50 myr. The Paleocene to early Eocene is characterized by an increase in global deep-water temperatures and in surface waters at high-latitudes (Shackleton and Kennett, 1975; Savin et *al*., 1975; Miller et *al*., 1987, 1992; Stott et *al*., 1990; Barrera and Huber, 1991; Zachos et *al*., 2001). Tropical terrestrial flora (Wolfe, 1980; Greenwood and Wing, 1995) are found at high latitudes that indicate warmer and wetter conditions (Estes and Hutchison, 1980; Axelrod, 1984; Francis, 1988). The continents were largely ice-free during the Paleocene and early Eocene (Shackleton, 1986; Miller et *al*., 1987; Zachos et *al*., 1994; Zachos et *al*., 2001). A significant progressive cooling followed the warm climate conditions throughout the middle to late Eocene (Miller et *al*., 1987; Boersma et *al*., 1987; Zachos et *al*. 2001; Bohaty and Zachos, 2003; Sexton et *al*., 2006). Temperatures declined significantly and global ice-volume increased immediately after the Eocene-Oligocene boundary (~33.8 Ma) suggested by a positive $\delta^{18}O$ shift in benthic and planktonic foraminifera (Miller and Fairbanks, 1985; Zachos et *al*., 2001; Bohaty and Zachos, 2003; Coxall et *al*., 2005). Only a limited number of high-resolution stable isotope curves for the middle to late Eocene from deep-sea sediments exist today (e.g., Miller et *al*., 1987; Zachos et *al*., 2001). However, these records do not have the proper resolution needed to accurately document 10 kyr-scale changes during the late Eocene to early Oligocene.

The late Eocene was a time of several extraterrestrial impact events with two of the largest being: 1) Chesapeake Bay Impact Structure (CBIS); and 2) Popigai impact crater (Figure 1) (Grieve, 2001). The CBIS is an 80 km-wide crater located on the

eastern shore of North America with a radiometric age of ~35.5 Ma (Figure 2) (Obradovich et *al*., 1989; Poag et *al*., 1994). The ~35.7 Ma, 100 km Popigai impact crater is found in northern Siberia (Bottomley et *al*., 1997; Masaitis et *al*., 1972, 2005). The CBIS is the 7th largest crater found on Earth and holds great significance because it is one of the best preserved structures identified to date (Sanford, 2004). Although the crater is well preserved, the global stable isotopic response (if any), biotic effects, and climatic changes to the impact event are poorly known. The late Eocene provides a good opportunity to study the relationships between extraterrestrial impact events and global climate. Determining if a $\delta^{13}C$ anomaly was associated with the CBIS holds a broader importance in improving our knowledge of past perturbations in Earth's climate, their triggers, threshold limits, response times, and feedback mechanisms.

The Cretaceous-Tertiary (K-T) (~ 65 Ma), Permian-Triassic (P-Tr) (~ 251 Ma), Paleocene-Eocene Thermal Maximum (PETM) (~ 55.5 Ma), and Triassic-Jurassic (~ 200 Ma) mass extinctions are associated with notable changes in the global carbon system (e.g., Zachos et *al*., 1986; Holser et *al*., 1989; Olsen et *al*., 2002; Hesselbo et *al*., 2002; Kennett and Stott 1990, 1991). These boundary events associated with $\delta^{13}C$ excursions have been hypothesized to be linked to extraterrestrial impact events, although only the K-T boundary episode is well substantiated as an impact event (e.g., Alvarez et *al*., 1980). A global change in Earth's carbon system would be predicted for the late Eocene impact events based on evidence from previously studied mass extinctions, carbon isotopic anomalies, and/or extraterrestrial impacts.

In this thesis the relationship between extraterrestrial impact events and the response of global climate is evaluated by: 1) reviewing the literature on a known (K-T)

and three hypothesized (P-Tr, Tr-J, and PETM) extraterrestrial impact events and their relationships with $\delta^{13}C$ and $\delta^{18}O$ data and biotic effects. An overview of the relationships for the K-T, P-Tr, Tr-J, and PETM events is provided and detailed reconstructions for upper Eocene sections and their associated impact layers in Barbados, Caribbean, Gulf of Mexico, Massignano in Italy, and South Atlantic ODP Site 689 (Figure 1) are given; 2) Sixteen microspherules were found in an upper Eocene section of core from St. Stephens Quarry, Alabama (Figure 1); 3) New stable isotopic data from South Atlantic ODP Site 1090 (Figure 3) is presented. This data provides a first-order correlation of carbon and oxygen isotopic curves with magnetostratigraphy of the GPTS (1992,1995) and upper Eocene ejecta layers that quantify a 0.4 - 0.5‰ decrease of $\delta^{13}C$ in benthic foraminifera in Chron C16n1n; and 4) DSDP Site 612 on the NJ continental slope (Figure 1) was revisited to obtain new high-resolution stable isotope data that is associated with upper Eocene impact layers over a 3 kyr equivalent sampling interval.

2. Background

2.1 Carbon Isotope Excursions and Mass Extinctions

2.1 Cretaceous-Tertiary (K-T) Boundary

The K-T boundary is marked by the 5th greatest mass extinction in Earth's history (Raup and Sepkoski, 1982). This 65 Ma impact event (Swisher et *al*., 1992) is characterized by numerous mass extinctions including terrestrial plants, marine plankton, and dinosaurs (Ryder, Fastovsky, and Gartner eds., 1996). Alvarez et *al*. (1980) originally suggested an extraterrestrial impact event was responsible for the massive

extinctions seen at the K/T boundary. This hypothesis argues an extraterrestrial impact event caused increased concentrations of atmospheric dust particles that lowered light levels and subsequently suppressed global photosynthesis. The discovery of the Chicxulub impact structure on the Yucatan peninsula, Mexico, dated to ~ 65 Ma (Swisher et *al*., 1992), became a good candidate for the source crater (e.g. Hildebrand et *al*., 1991; Pope et *al.*, 1993; Sharpton et *al*., 1993). An extraterrestrial impact event is predominantly accepted as the primary mechanism for the mass extinctions seen at K-T boundary.

K-T boundary sediments are associated with a large (1.5 - 2.0‰), negative $\delta^{13}C$ anomaly in planktonic foraminifera and bulk-carbonate (Figure 4a) (Brennecke and Anderson, 1977; Hsu et *al*., 1982; Perch-Nielsen et *al*. 1982; Zachos and Arthur, 1986; 1989). A limited number of benthic foraminiferal stable isotope records show a negative $\delta^{13}C$ excursion across K-T boundary sediments (Stott and Kennett, 1990). $\delta^{13}C$ values decreased for ~ 40 - 50 kyr following the K/T boundary and took ~ 300 - 400 kyr to recover to pre-boundary levels. Hsu and McKenzie (1985) developed the 'strangelove' ocean hypothesis to explain $\delta^{13}C$ anomalies lasting on the order of 10 - 100 kyr. This hypothesis describes how impact-induced mass mortality can cause a decrease in surface water productivity and ultimately photosynthetic fractionation of ocean basins. A 'strangelove' ocean model is described in further detail in the carbon isotope section of this thesis. Additional research (Hsu et *al*., 1982; Zachos and Arthur, 1986) reported the surface-to-deep water $\delta^{13}C$ gradient collapsed to zero in K/T boundary sediments because of a rapid (<10,000 years) cessation of marine export productivity (Figure 4a). Stott and Kennett (1990) reported one of the first continuous $\delta^{13}C$ records of K/T boundary

sediments using single benthic and planktonic foraminiferal species showing a 1.5 - 2‰ $\delta^{13}C$ decrease in the South Atlantic that persisted for approximately 300 kyr.

2.1 Permian-Triassic (P-Tr) Boundary

The P-Tr boundary is characterized by the extinction 90% of all marine species (Raup, 1979; Erwin, 1993; Jin et *al*., 2000) occurring at ~ 251 Ma (Bowring et *al.,* 1998; Mundil et *al*., 2001). A negative carbon-isotope anomaly of ~2 - 4‰ is documented in marine sediments across P-Tr boundary (Figure 4b) (Magaritz et *al*. 1988; Baud et *al*. 1989; Holser et *al*. 1989; Oberhansli et *al*. 1989). Recent zircon dating studies constrained the negative $\delta^{13}C$ pulse to a duration of ~ 165 kyr (Bowring et *al*., 1998). The origin of the P-Tr boundary episode is uncertain and has not yet been definitively linked to an extraterrestrial impact event, though Becker (2001) have suggested a major impact at this time.

2.1 Triassic-Jurassic (Tr-J) Boundary

The Tr-J boundary extinction is considered one of the five largest extinction events of the entire Phanerozoic Eon effecting the marine and terrestrial realms (Raup and Sepkoski, 1982, 1986; Hesselbo et *al*., 2002). The Tr-J boundary is radiometrically dated to ~ 200 Ma on U-Pb zircons (Palfy et *al*., 2000). A negative $\delta^{13}C$ excursion of ~ 2‰ is associated with the boundary in C_{org} and bulk-CO_3 (Ward et *al*., 2001; Hesselbo et *al*., 2002, 2007). The Tr-J boundary event has not been unequivocally associated with any extraterrestrial impact event and its origin remains unknown.

2.1 Paleocene-Eocene Thermal Maximum (PETM)

The PETM is characterized by a significant global temperature increase recorded as a negative $\delta^{18}O$ excursion in planktonic and benthic foraminifera (Kennett and Stott, 1991; Zachos et *al*., 1993). The end Paleocene (~ 55.5 Ma) marks the largest extinction of Cenozoic benthic foraminifera (Tjalsma and Lohmann, 1983; Thomas, 1990; Kennett and Stott, 1991; Pak and Miller, 1992; Kaiho, 1994) and is also associated with terrestrial mammalian extinctions (Koch et *al*., 1992; Maas et *al*., 1995; Hooker, 1996; Bowen et *al*., 2002; Gingerich, 2003; Hooker and Dashzeveg, 2003). The PETM is associated with a large, rapid, and negative $\delta^{13}C$ anomaly of approximately ~2.5 - 3‰ (Kennett and Stott 1990, 1991; Koch et *al*. 1992; Pak and Miller, 1992; Schmitz et *al*. 1996; Stott et *al*. 1996; Bralower et *al*. 1997; Schmitz et *al*., 2001). The source for the PETM extinctions and $\delta^{13}C$ anomaly is still debated and has not yet been definitively linked to any impact event, though Kent et *al*. (2003) did suggest a major impact event at this time.

2.2 Cenozoic Strewn Fields

Tektites and microtektites are composed of natural chemically homogeneous glass generated from melting and quenching of terrestrial or marine rocks during impact with an extraterrestrial object. By definition, tektites are 1 mm or greater and microtektites are < 1 mm. The quenching process usually produces glassy spheres, but tektites and microtektites come in many different structural forms such as droplets, dumbbells, and flattened pancakes. Tektites and microtektites with similar physical, chemical, and petrological properties and of the same age are distributed geographically over specified areas termed strewn fields (O'Keefe, 1976). There are currently four tektite/microtektite

strewn fields of Cenozoic age found on the Earth today (Figure 5a): 1) the North American; 2) Central European (moldavite); 3) Ivory Coast; 4) and Austrailasian (O'Keefe, 1976; Koeberl, 2001; Glass et *al*., 2004a). The Austrailasian is the youngest strewn field dated around the time of the Brunhes Matuyama magnetic reversal boundary at ~ 800 kyr (Burns, 1989; Schneider et *al*., 1992; Lee and Wei, 2000). No source crater has been identified for the Austrailasian strewn field, however, it is predicted to be located somewhere in the Indochina region (Figure 5a) (Glass, 2003). The Ivory Coast strewn field is restricted to a small region off the coast of western Africa (Figure 5a). The Ivory Coast strewn field was deposited within 8 - 30 kyr after the onset of the Jaramillo normal polarity subchron (0.97 Ma) and 40 kyr before its terminiation (0.90 Ma) (Mankinen et *al*., 1980; Schneider and Kent, 1990; Glass et *al*., 1991). Ivory Coast tektites are thought to have originated from the Bosumtwi impact crater in Ghana (Zahringer, 1963; Gentner et *al*., 1967, 1970; Durrani and Kahn, 1971; Koeberl et *al*., 1989, 1997, 1998). The Central European strewn field is composed of tektites called moldavites, and interestingly, no microtektites are known for this strewn field. Moldavites have an age of 15 Ma (Staudacher et *al*., 1982) and are associated with the upper layers of the Ries impact structure in Southern Germany (Figure 5a) (Delano and Lindsley, 1982; Shaw and Wasserburg, 1982; Engelhardt et *al*., 1987).

The fourth and oldest strewn field is the late Eocene North American and is the focus of this thesis (Figure 5a). The North American strewn field is dated to ~35.5 Ma (Obradovich et *al*., 1989) and the source crater is the Chesapeake Bay impact structure (CBIS) off the North American continental slope (Poag et *al*., 1994). Some upper Eocene deep-sea sections contain two or more ejecta layers in close proximity to one

another: 1) the previously mentioned NASF (Figure 5a); and 2) a second layer derived from the Popigai impact structure, northern Siberia (Figure 5b). Previous studies have indicated that North American microtektites are slightly younger than Popigai's clinopyroxene-bearing spherules, or "microkrystites" (Glass et *al*. 1985; Keller et *al*. 1987; Glass and Koeberl 1999). The Chesapeake Bay tektite and Popigai krystite ejecta layers are separated by approximately 10-20 kyr (Miller et. *al*. 1991; Glass et. *al*. 1998; Glass and Koeberl 1999).

2.2 North American Strewn Field (NASF)

Original evidence that an impactor struck the eastern North American seaboard came from distal ejecta that comprise a portion of the North American tektite strewn field (NASF). The first North American (NA) tektites found in the Jackson Formation in eastern Texas are called bediasites (Barnes, 1939, 1951; O'Keefe, 1976). Tektites were also found in Dodge County, Georgia (Bruce, 1959; Howard, 1968) and one in Cuba (Garlick et *al*., 1971). None of these are stratigraphically in-situ. Tektites, microtektites, shocked minerals, and rock fragments were discovered at Deep Sea Drilling Project (DSDP) Leg 95 Site 612 off the NJ coast (Figure 1) (Keller,1986a; Thein, 1987; Keller et *al*., 1987; Glass, 1988; Bohor et *al*., 1988). Original efforts to locate the source crater depended on physical and chemical properties of the ejecta layer at Site 612. Several studies concluded the source crater must be in close proximity (a few hundred km) to Site 612 based on the large size, high abundance, and chemical composition of ejecta deposits (Thein, 1987; Glass, 1989; Koeberl, 1989; Stecher et *al*., 1989; Glass et *al*., 1998). Poag et *al*. (1994) discovered the Chesapeake Bay Impact Structure (CBIS) that proved to be a

good candidate for the source crater. Koeberl et *al*. (1996) performed geochemical analysis of the Exmore breccia that confirmed the CBIS as the source crater (Figure 2). Deutsch and Koeberl (2006) used trace element data and isotopic compositions of target lithologies, crater fill breccias, and post-impact CBIS sediments to verify it as the source for the NASF.

The NASF is made up of tektites, microtektites, coesite, stishovite, and other shocked mineral grains such as quartz and zircons (Glass, 1989; Glass and Wu, 1993; Glass et *al*., 1998; Glass and Liu, 2001; Glass 2002). Glass et *al*. (1986) determined an age of 35.4 ± 0.6 on tektite fragments from Barbados using $^{40}Ar/^{39}Ar$ laser-probe dating. The ejecta layer at site 612 was originally dated to 35.5 ± 0.3 Ma by Obradovich et *al*. (1989) using $^{40}Ar/^{39}Ar$ isotopes. Additional studies by Poag and Aubry (1995) determined an age between 35.3 ± 0.3 and 35.5 ± 0.3 Ma using radiometric $^{40}Ar/^{39}Ar$ step-heating of DSDP Site 612 microtektite glass. Radiometric dates by Horton and Izett (2005) determined a weighted-mean total-fusion $^{40}Ar/^{39}Ar$ age of 35.3 ± 0.1 Ma on tektites fragments in the Langley, Virgina core.

2.2 Popigai Strewn Field

The second and stratigraphically older layer of late Eocene impact-generated crystal-bearing microspherules is found in sediments from numerous sites across the globe (Figure 5b) (Glass et *al*., 1985; Keller et *al*., 1987; Glass et *al*., 1998; Glass and Koeberl, 1999; Vonhof and Smit, 1999; Glass, 2000; Liu and Glass, 2001). Glass and Burns (1988) first proposed the term ‘microkrystites’ to distinguish the stratigraphically older layer of primary crystalline-bearing microspherules from non-crystalline containing

microtektites. The microkrystite layer is composed of clinopyroxene-bearing (cpx) tektites and microtektites (Montanari and Koeberl, 2000). Whitehead et *al*. (2000) identified the source crater for the cpx spherule layer in northern Siberia as the Popigai impact structure. Additional studies by Kettrup et *al*. (2003) confirmed Popigai as the source crater for the cpx-spherule layer (Figure 5b). Kettrup et *al*. (2003) used geochemical and isotopic data of target and impact melt lithologies to confirm Popigai's upper sediment layers are the origin for the cpx-microspherules and their associated microtektites. The Popigai impact structure is radiometrically dated to 35.7 ± 0.8 Ma (Bottomley et *al*., 1997). The microkrystite layer has been shown to be associated with an Ir anomaly in many locations (Glass et *al*., 1985; Keller et *al*., 1987; Vonhof and Smit, 1999; Kyte and Liu, 2002).

2.2 Nd and Sr Isotopes

The geochemical composition of NA microtektites and cpx- microspherules can be similar if comparing certain elements such as silica, iron, or magnesiumin (Glass et *al*., 2004a). However, their Sm-Nd and Rb-Sr isotopic signatures differ significantly because these isotope ratios remain unchanged during and after the impact event. Recent work (Liu et *al*., 2006) analyzed Nd and Sr isotopes in cpx-spherules from Site 1090 and microtektites from Site 689 to determine their source crater. This new study disputes their previous hypothesis that claims Site 1090 microtektites belong to the NASF, even though the microtektites could not be linked with a specific rock type, including ones above Popigai. Other studies disagree (Vonhof and Smit, 1999) by pointing out Site 689 microtektites are somewhat chemically different from other NA microtektites, such as in

Na and have dissimilar Sr isotopic compositions. Additionally, Popigai strewn field microtektites are chemically similar to the glass of their associated cpx-microspherules, but Site 689 microtektites are distinctly dissimilar to the glass of the Popigai microkrystites. In regards to this thesis, it is irrelevant if Site 1090 microtektites belong to the NASF because the cpx-microspherule layer is located in the same stratigraphic interval. If the microtektite layer at Site 1090 belongs to the NASF, it is still not possible to separate the isotopic response to the Popigai and Chesapeake Bay impactors using this site alone because the layers are virtually indistinguishable (Figure 6).

2.3 Stable Isotopes

2.3 Carbon Isotopes and the 'Long-term' Global Carbon Cycle

$\delta^{13}C$ values of benthic foraminifera tests and bulk-CO_3 sediments are used as a proxy to reconstruct paleoceanographic conditions. They are also utilized to detect perturbations in the global carbon system. $\delta^{13}C$ values of foraminifera tests respond to chemical changes in ambient seawater. These chemical changes reflect fundamentally distinct modes of carbon-cycling on different geologic timescales. There are several factors contributing to perturbations of the global carbon cycle over 'long-term' timescales ($\geq 10^6$-year). Weathering and tectonic processes, such as sea-floor spreading and volcanism, constitute the major reservoirs controlling variations of $\delta^{13}C$ ocean values on $\geq 10^6$-year timescales (Berner, 1990, 2004; Kump and Arthur, 1999).

Volcanic, metamorphic, and diagenetic outgassing serve to input carbon with a low $\delta^{13}C$ value (-5‰) into the oceans and atmosphere in the form of CO_2 (Table 1)

(Deines, 1992). This $\delta^{13}C$ value of mantle carbon is very similar to the $\delta^{13}C$ ratio of today's rivers. Volcanic out-gassing, metamorphic, and diagenetic decarbonization controls the influx of CO_3 minerals and C_{org} from sediments into the oceans and atmosphere (Kump and Arthur, 1999; Berner, 2004). Increasing the rate of carbon input from volcanism alone only causes a small decrease in the $\delta^{13}C_{carb}$ composition of mean oceanic DIC, also requiring an extensive amount of volcanic activity to achieve this.

Tectonic processes including, uplift and mountain building, can alter weathering rates to change the global carbon system sufficiently on long-term timescales (Raymo, 1991). Weathering comprises a variety of physical and chemical processes transferring C_{carb} and C_{org} from Earth's lithosphere, sediments, soils, and atmosphere, into its rivers and oceans. Silicates, C_{org}, and C_{carb} constitute the weathering products entering the worlds' rivers and oceans. The $\delta^{13}C$ value of rivers averages -5‰ (Lasaga et *al*., 1985), but it can vary widely based on its source rocks. Rocks with different ratios of C_{org} (-25‰) and C_{carb} (~0‰) influence the $\delta^{13}C$ values of the rivers and oceans (Table 1) (Craig, 1953; Keith and Weber, 1964; Faure, 1986; Schidlowski, 2001; Berner, 2004; Sundquist and Visser, 2005). Bicarbonate ions (HCO_3^-) are sourced from CO_3-rich rocks, soils, groundwater, and the atmosphere and carried eventually into rivers (Berner, 2004). Almost one third of most rivers' HCO_3^- flux comes from CO_3-rich rocks (Holland, 1978). Rates of CO_3 weathering are regulated by temperature with respect to atmospheric CO_2 levels, orbital variations, and continental movement. CO_3 weathering is also controlled by uplift, erosion, runoff, and terrestrial vegetation (Berner, 2004). Increased erosion of CO_3-rich rocks can force the $\delta^{13}C$ value of rivers in a positive direction (Kump and Arthur, 1999).

Carbon burial in sediments and Earth's crust also influences paleoceanographic changes on long-term timescales of ≥ 10^6 years. C_{carb} and C_{org} burial in marine sediments provides an important sink for C removal from the world's oceans. Output of carbon via sediment burial can influence the ocean's $\delta^{13}C$ composition depending on the type of carbon that is deposited. CO_3 sedimentation rates are dependent upon the influx of carbon to the oceans and atmosphere, which is controlled by volcanic out-gassing and global weathering (Berner, 2004). Within the ocean reservoir, CO_3 sedimentation is a function of the fractionation of CO_3 burial between the deep ocean basins and shallower continental shelf (Sundquist, 1985). Exposing continental shelves by means of lowering sea-level serves to decrease available space for deposition of CO_3 carbon. Shallow water CO_3 accumulation decreases during glacial maxima and deep-water deposition of C_{org} increases (Curry and Lohmann, 1985). Excess DIC is deposited in deeper waters so that the ocean can balance its internal reservoir (Berner, 2004).

Silicate and CO_3 weathering remove bicarbonate ions and transport them into rivers, and eventually the world's oceans (Berner, 2004). However, weathering of silicates takes longer and directly affects atmospheric CO_2 levels through uptake and subsequent burial of CO_2 by Ca and Mg carbonate minerals. Uplift and topographic relief holds a strong influence on CO_3 and silicate weathering. Low relief mountainous regions will first accumulate less resistant weathered clay deposits that trap the underlying silicate rocks and protect them from further erosion (Berner, 2004). Silicate weathering rates are also controlled by temperature in relation to atmospheric greenhouse gases, solar radiation, and continental movement. Increased amounts of terrestrial vegetation and runoff both accelerate rates of silicate weathering (Berner, 2004). A

decrease in silicate weathering rates can decrease atmospheric pCO_2 by transforming C_{carb} in atmospheric CO_2 to C_{org} in the form of oceanic bicarbonate (Kump and Arthur, 1999). Reducing silicate weathering by exposing less silicate-bearing rocks produces a decrease in the composition of mean oceanic DIC $\delta^{13}C$ (Raymo and Ruddiman, 1992; Kump and Arthur, 1997, 1999). The input of carbon into a steady-state ocean from continental weathering is balanced by the sum of the C_{org} and C_{carb} removed through burial in marine sediments.

Weathering rates of organic-rich deposits are a function of erosion, runoff, terrestrial temperatures, temperatures with respect to CO_2, solar change, and possibly atmospheric O_2 levels (Berner, 2004). High weathering rates of sedimentary organic matter will increase the amount of C_{org} being delivered to rivers and temporarily decrease the $\delta^{13}C$ composition of mean oceanic DIC (Kump and Arthur, 1999) because the $\delta^{13}C$ ratio of all terrestrial vegetation (-25‰) is lower than the DIC of mean ocean water (0‰) (Table 1) (Schidlowski, 2001). Input of various types of terrestrial vegetation can influence mean ocean water in distinct ways because today's terrestrial plants use two types of chemical pathways (C3 and C4) for photosynthesis causing them to have different $\delta^{13}C$ compositions (Schidlowski, 2001). Terrestrial vegetation utilizing the C4 pathway, such as tropical and marsh grasses, has $\delta^{13}C$ compositions between -25 and -5‰. Other types of vegetation, including most of the higher plants, which use the C3 pathway have lower $\delta^{13}C$ ratios between -23 and -35‰ (Schidlowski, 2001). A global switch to C4 plants would increase the $\delta^{13}C$ composition of mean oceanic DIC.

Oceanic DIC $\delta^{13}C$ values will eventually increase when C_{org} is removed from the system through burial. Decaying C_{org} in soils and detritus has similar $\delta^{13}C$ compositions

to living terrestrial vegetation (-25‰) (Table 1) (Sundquist and Visser, 2005) and provides an output for C_{org} in the carbon system. Increasing the fraction of C_{org} to C_{carb} buried in ocean sediments leads to positive excursions in ocean DIC $\delta^{13}C$. The present day steady state partitioning between C_{org} to C_{carb} in the sedimentary reservoir is roughly 1:4 (Schidlowski, 2001). This is determined by calculating the present-day isotopic mass balance of the system maintained with a $\delta^{13}C$ output value for mantle carbon equaling -5‰ and $\delta^{13}C$ input values for C_{org} and C_{carb} equaling -25 and 0‰, respectively (Table 1). An increase in the rate of C_{org} to C_{carb} burial is achieved by several means, such as increasing the riverine contribution of phosphate into the oceans (Kump and Arthur, 1999). An additional mechanism involves increasing the ratio of phosphate controlled new production that fails to undergo decomposition, ultimately getting buried. Lastly, higher deposition rates of organic matter are achieved by increasing the rate of deepwater sinking, which causes more phosphate to returned to the euphotic zone (Kump and Arthur, 1999). Removing a higher fraction of C_{org} relative to C_{carb} through sediment burial serves to increase the whole-ocean $\delta^{13}C$ value.

Previous work (Vincent and Berger, 1985) reported a notable positive $\delta^{13}C$ anomaly persisting for 4 myr in Miocene benthic and planktonic foraminifera from the Indian Ocean. The 1‰ $\delta^{13}C$ increase is attributed to a switch to greater burial of C_{org} relative to C_{carb}. C_{org} was deposited along ocean-margins. Strong zonal winds and a permanent thermocline led to intensive coastal upwelling and ultimately the deposition of organic-rich diatomaceous sediments. Vincent and Berger (1985) termed this phenomenon the Monterey hypothesis and claimed it definitively led to a decrease in atmospheric CO_2 concentrations that ultimately resulted in further cooling. Cyclical $\delta^{13}C$

variations on the order of ≤10 myr with amplitudes of ~1‰ occurred during the Oligocene to middle Miocene in benthic and planktonic foraminifera (Shackleton et *al*., 1984; Vincent et *al*., 1984; Miller and Fairbanks, 1985; Vincent and Berger, 1985). The $\delta^{13}C$ cycles are considered to be global, recording changes in the Atlantic and Pacific basins in both benthic and planktonic foraminifera (Miller and Fairbanks, 1983,1985). Previous work (Miller and Fairbanks, 1985) show cyclical $\delta^{13}C$ variations result from output changes in the ratio of C_{org} to C_{carb} burial. Increased $\delta^{13}C$ values are attributed to a decrease in the fraction of C_{carb} deposited in marine sediments, while assuming the ratio of C_{org} output remained unchanged (Miller and Fairbanks, 1985).

Long-term storage of carbon in the form of natural gases, petroleum, coal, and kerogen has typical $\delta^{13}C$ values similar to the C_{org} in the tissues of living organisms. Present day average $\delta^{13}C$ values for coal equal -25‰ and petroleum is -28‰ (Stahl, 1979; Faure, 1986). Liberating ^{12}C-rich C_{org} from long-term storage in the form of fossil fuels can serve to decrease the $\delta^{13}C$ composition of the whole-ocean reservoir. The present-day burning of fossil fuels has already increased Earth's atmospheric CO_2 content significantly and decreased its $\delta^{13}C$ composition (Faure, 1986). Studies reported (Farmer and Baxter, 1974) the combustion of fossil fuels has increased atmospheric CO_2 concentrations by 10% from 280 - 290 ppm in 1900 AD to 323 ppm in 1972 AD. More recent work shows an increase in atmospheric CO_2 concentrations from 355 ppm in 1992 (Siegenthaler and Sarmiento, 1993) to 370 ppm in 2000 AD (Blasing and Jones, 2002). Trapped gases from ice-cores record pre-industrial atmospheric CO_2 $\delta^{13}C$ compositions of ~ -6.4‰ (Friedli et *al*., 1986; Francey et *al*., 1999), while values decreased to ~ -7.9‰ in the 21st century (Francey et *al*., 1999).

2.3 'Short-term' Global Carbon Cycle

The world's oceans retain 50 times more carbon in the form of DIC than our present day atmosphere (Table 1) (Falkowski, 2005). For this reason, oceans play a major role in buffering global carbon cycle changes on shorter timescales because variations occur over periods similar to the residence time of carbon in the oceans (on the order of 10^5 years) (Froelich et *al*., 1982; Kump and Arthur, 1999). Mean present day ocean water has a $\delta^{13}C$ composition equal to 0‰, North Atlantic Deep-Water is 1‰, and the deep Pacific is -0.2‰ (Kroopnick et *al*., 1972; Broecker and Peng, 1982).

During photosynthesis, ^{12}C is preferentially extracted (or fixed) from the dissolved inorganic carbon (DIC) pool of ambient seawater by surface-dwelling foraminifera. This process increases the ratio of $^{13}C/^{12}C$ in surface waters, which is then reflected in the shells precipitated by planktonic foraminifera. During high surface water productivity the dead and decaying CO_3 shells (0‰) and organic matter (-25‰) (Table 1) eventually fall through the water column or are essentially 'pumped' into bottom waters causing deep-water $\delta^{13}C$ values to decrease (Keith and Weber, 1964; Schidlowski, 2001). Low values are effectively recorded in the shells precipitated by benthic foraminifera. Low dissolved oxygen and low $\delta^{13}C$ values of deep-water result from high productivity and increased nutrient levels in surface waters (Kroopnick, 1985). Higher surface-water productivity leads to an increased $\delta^{13}C$ gradient between surface and deep waters, although an increased surface-to-deep water $\delta^{13}C$ gradient can also reflect changes in deep water circulation. A coeval change in $\delta^{13}C$ compositions of surface and deep waters indicate a transfer among carbon reservoirs. If change occurs within the whole-ocean reservoir it indicates an external mechanism is controlling the perturbation.

Natural variability in Pleistocene $\delta^{13}C$ records display high-amplitude (~0.5 - 1‰) and periodic fluctuations (10^4 - 10^5 yr) in benthic and planktonic foraminifera from several ocean basins (Shackleton et *al*., 1983; Mix and Fairbanks, 1984; Fairbanks and Mix, 1984; Cramer et *al*., 2003; Wade and Palike, 2004). Periodic climate change is shown to respond to cyclical variations in Earth's orbital parameters that influence the distribution of latitudinal and seasonal solar radiation (Broecker and van Donk, 1970; Shackleton and Opdyke, 1976; Imbrie et *al*., 1992, 1993). The Milankovitch hypothesis explains the link between cyclical variations in orbital parameters that drive global temperature changes and the repeated growth and decay of global ice-volume (Milankovitch, 1941; Hays et *al*., 1976). Eccentricity operates on 100, 400, and 2,400 kyr timescales, obliquity on 40 kyr, and precession on 19 - 23 kyr (Hays et *al*., 1976). On glacial-to-interglacial timescales, natural oceanic DIC $\delta^{13}C$ variations have an amplitude of ~0.3 - 0.5‰ (Curry et *al*., 1988; Duplessy et *al*., 1988; Sarnthein et *al*., 1988; Ku and Luo, 1992; Crowley, 1995). During glacial periods, large-scale continental ice-sheets replaced previously vegetated regions leading to the global transfer of terrestrial C_{org} into the oceans (Broecker, 1970, 1982; Shackleton, 1977; Adams et *al*., 1990). Low oceanic DIC $\delta^{13}C$ values during glacial episodes reflects the input of C_{org} from the terrestrial biosphere, expansion of grasslands, and exposure of organic-rich deposits on continental shelves during times of lower sea-level (Shackleton, 1977; Curry et *al*., 1988; Duplessy et *al*., 1988).

2.3 'Abrupt' Term Global Carbon Cycle

Abrupt perturbations of the global carbon cycle occurring timescales of only a few thousand years (i.e. K-T and PETM) are of particular interest to many scientists having difficultly constraining the precise mechanism that led to significant changes in global C system. Previous work (Hsu and McKenzie 1985) established the hypothesis of a "Strangelove" ocean to explain variations in the marine carbon-isotope record across the K-T boundary on the order of 10 - 100 kyrs. In a "Strangelove" ocean, photosynthesis is suppressed through increased amounts of atmospheric dust particles that derived from extraterrestrial impact events (Hsu and McKenzie 1985; Alvarez et *al*., 1980; Toon et *al*., 1994). This leads to a global reduction in ocean productivity. Hsu and McKenzie (1990) later developed a 'respiring' ocean model to explain reversed carbon isotope surface to deep water gradients on the order of 10^6 years. $\delta^{13}C$ values of surface waters are lower than deep waters under such conditions. Respiration and bacterial activity are the principal controls of $\delta^{13}C$ of dissolved bicarbonate in surface waters of a 'respiring' ocean. This idea is modeled after an ocean where photosynthetic fractionation in surface waters is competing unsuccessfully with respiration and bacterial activity. Both respiration and bacterial sulfate reduction of organic matter release ^{12}C-enriched CO_2 into surface waters at a faster pace then uptake by photosynthetic fractionation. They proposed mass mortality created empty niches that bacteria occupied subsequently. The bacteria in surface waters would immediately reduce the newly photosynthesized organic matter. This process would have continually released ^{12}C-enriched CO_2 into surface waters and reversed the surface-to-deep water $\delta^{13}C$ gradient for 500 kyr in certain regions. Hsu and McKenzie (1990) state a 'respiring' ocean model relies on the

condition that particles falling through the water column remain long enough for bacterial activity to fully decay the material. They suggest such a phenomenon occurred in areas where zooplankton were rare or picoplankton abundant.

Extraterrestrial impact events can also affect the global carbon cycle on 10^5 to 10^6 yr by injecting significant amounts of ^{12}C into the ocean-atmospheric system. Cometary carbon has a $\delta^{13}C$ composition anywhere between -1 to -120‰ (Table 1) (Messenger, 2000; Wyckoff et *al*., 2000; Arpigny et *al*., 2003). The mean $\delta^{13}C$ value for comets and interplanetary dust particles is -45‰ (Table 1) (Messenger, 2000; Wyckoff et *al*., 2000; Arpigny et *al*., 2003). Kent et *al*. (2003) hypothesized the amount of extraterrestrial carbon from a comet with a $\delta^{13}C$ ratio of -45‰ to explain a portion of the PETM $\delta^{13}C$ negative anomaly in the exchangeable oceanic-atmospheric carbon reservoir. A calculated ~ 8 km diameter cometary impactor could be responsible for a portion (~ 2‰) of the $\delta^{13}C$ decrease. These predictions (Kent et *al*., 2003) are considered to be virtually instantaneous with respect to the atmosphere, with later effects in ocean surface waters. Deep waters have the longest response time compared to the atmosphere and surface waters.

2.3 Abyssal Circulation and the Global Carbon Cycle

The ocean's internal biological pump is influenced not only upon microorganisms themselves, but also to changes in deep-water circulation patterns and rates. Today, increased $\delta^{13}C$ values can be found in high-latitude deep-water masses that have recently been in contact with the atmosphere (Figure 7) (Kroopnick, 1985). Equilibrium of CO_2 between the atmosphere and surface-waters occurs as cold surface waters sink. This

process generates deep water (Broecker and Peng, 1982) that forms at high latitudes from northern and southern end member components.

Southern Component Water (SCW) is composed of Weddell Sea Bottom Water that flows through the Vema Passage into the deep western Atlantic (Carmack and Foster, 1975; Broecker and Peng, 1982; Broecker et *al*. 1985). Northern Component Water (NCW) consists of Iceland-Faroe Overflow Water, Labrador Sea Water, and Denmark Straits Overflow Water, Mediterranean Overflow Water, and entrained Antarctic and North Atlantic Bottom Water (Worthington, 1976; Broecker and Peng, 1982). NCW mixes with ambient waters creating nutrient-depleted North Atlantic Deep Water (NADW) with high $\delta^{13}C$ values (1.0‰) (Kroopnick, 1985). SCW combines with surrounding waters to produce Antarctic Bottom Water (AABW). AABW is relatively low in $\delta^{13}C$ (0.4‰) because it contains less surface waters than NADW (Kroopnick, 1985). NADW flows south, mixing with AABW as it enters the Southern ocean to combine with re-circulated Pacific Deep Water (PDW) and forms Circumpolar Deep Water (CPW) (0.4‰) (Figure 7) (Kroopnick, 1985). PDW is high in nutrients and consequently has the lowest $\delta^{13}C$ values (0.0‰) (Kroopnick, 1985). PDW has more time for oxidation of ^{12}C-enriched organic matter to rain through the water column because deep-water does not form in the Pacific today. Present day $\delta^{13}C$ values of Atlantic deep water are 1‰ higher than Pacific deep-water measurements (Kroopnick et al., 1972; Kroopnick 1974, 1980, 1984; Curry and Lohmann, 1983). The distribution of $\delta^{13}C$ in the world's oceans is used reconstruct the relative 'ages' and mixing between deep-water masses based on these processes.

In this thesis, deep-water circulation patterns are reconstructed for the late Eocene (33.7 - 36 Ma) when the ejecta layers were deposited. The North Atlantic is represented by Site 612 (1,404 m present day water depth, paleowater depth ~ 1,000 m (Miller and Katz, 1987)), the South Atlantic by Site 1090 (present day water depth 3,702 m, paleowater depth 3,200 m (Miller, pers. comm., 2006)), and the equatorial Pacific by Site 1218 (present day water depth 4,826 m, paleowater depth 3,700 m (Lyle et *al*., 2002)) (Figure 1).

2.3 Oxygen Isotopes

Oxygen isotope measurements of marine microfossils in sediments have long been used in Quaternary chronologic interpretations (e.g. Shackleton and Opdyke, 1973; Imbrie et *al*., 1984; Prell et *al*., 1986; Martinson et *al*., 1987). The $\delta^{18}O$ composition of benthic and planktonic foraminifera are used as a proxy for reconstructing past changes in global ice-volume, marine temperatures, and local salinity (Urey, 1947; Epstein et *al*., 1953; Emilani, 1955; Shackleton, 1967; Shackleton and Opdyke, 1973). This proxy is based upon preferential chemical and physical isotopic fractionation of water molecules of different molecular weights during evaporation and precipitation. Evaporation and condensation of surface waters preferentially extracts the lighter isotope (^{16}O) during fractionation causing the ambient seawater to be enriched in ^{18}O. Higher rates of evaporation increase the $\delta^{18}O$ value of surrounding surface-water that is recorded in the shells of marine microfossils precipitating their tests in equilibrium with ambient sea-water (Epstein et *al*., 1951, 1953; Emilani, 1955). $\delta^{18}O$ measurements are therefore a function of both temperature and sea-water isotopic composition. $\delta^{18}O$ measurements on

benthic foraminifera can help to reconstruct past deep-water circulation patterns when used in conjunction with $\delta^{13}C$.

Natural variability on glacial to interglacial timescales in oceanic DIC $\delta^{18}O$ (1 - 2‰) are caused by changes in global ice-volume and temperatures caused by differing amounts of latitudinal and seasonal insolation driven by periodic fluctuations in Earth's orbital parameters (Milankovitch, 1941; Hays et *al*., 1976; Imbrie et *al.*, 1984; Broecker, 1986). A 1‰ increase in the $\delta^{18}O$ composition of sea-water corresponds to a ~4°C global temperature decrease (Epstein et *al*., 1951, 1953). Early Eocene deep-water temperatures were determined to be 13ºC warmer than today's based on benthic foraminiferal $\delta^{18}O$ measurements (Miller et *al*., 1987).

2.4 Late Eocene Impact Stratigraphy

2.4 Barbados, Bath Cliff Section

A single microtektite layer is identified in Bath Cliff section, Barbados at approximately 100 m (Figure 8) (Saunders et *al*., 1984). The ejecta horizon is located in the middle of the *T. cerroazulensis* planktonic foraminifera (P16) zone, the radiolarian biozone *C. ornata*, and the nannofossil zones NP20 and CP15b (Figure 8). Previous work estimated a maximum age of ~ 35 Ma for the microtektite layer at Bath Cliff based on biostratigraphy and sedimentation rates (Saunders et *al*., 1984; Berggren et *al*., 1985). The tektite fragments and microtektites are determined to be part of the NASF based on the appearance, major oxide compositions, and previously reported K/Ar and $^{40}Ar/^{39}Ar$ ages (Glass et *al*., 1984). No clinopyroxene-bearing glass spherules are found near the

NA microtektites at Barbados. Glass et *al*. (1986) radiometrically dated the microtektite layer to 35.4 ± 0.6 Ma using the $^{40}Ar/^{39}Ar$ laser-probe method.

Additional work (Sanfilippo et *al*., 1985; Keller et *al*., 1987) identified an iridium anomaly located ~26 cm below the microtektite layer at Bath Cliff (Figure 8). The Ir anomaly is located at the *C. bandyca/C. ornate* radiolarian subzone boundary, and in the planktonic foraminifera zone *T. cerroazuiensis* (P16) and calcareous nannofossil zone NP20 (Figure 8). The distance between the microtektite layer and Ir anomaly is equivalent to 13 - 14 kyr, using the 2 cm/kyr sedimentation rates reported at Bath Cliff (Saunders et *al*., 1985; Berggren et *al*., 1985). Previous work (Montanari et *al*., 1993) used biostratigraphy to correlate the Ir anomaly within the latest 0.25 myr of C16n (~35.3 to 35.5 Ma).

2.4 Caribbean Sea

Microtektites are identified in Lamont Doherty Earth Observatory (LDEO) core RC9-58 from the Caribbean Sea (Figure 1) (Glass et *al*., 1973) and DSDP Site 149 Core 31 located in the Venezuelan Basin (Donnelly and Chao, 1973). Upper Eocene microtektites were found in core RC9-58 with the highest abundance occurring at ~250 cm (Glass et *al*., 1973). Geochemical analysis determined the Caribbean microtektites are part of the NASF (John and Glass, 1974). A clinopyroxene-bearing microspherule layer is located 20 cm (John and Glass, 1974) to 30 cm (Ganapathy, 1982) below the peak abundance of microtektites in core RC9-58. Additional work (Ganapathy, 1982) identified an Ir anomaly of 4.1 ppb located at 279.5 cm in the core, which is in close proximity to the stratigraphically lower microkrystite layer. Previous

work (Alvarez et *al*., 1982) of DSDP Caribbean core 149 identified the presence of an Ir anomaly coinciding with the highest abundance of microtektites in upper Eocene sediments.

The North American microtektite horizon in core RC9-58 coincides with the extinction of four radiolarian species: *Thyrsocyrtis bromia, T. tetracantha, T. triacantha,* and *Calocyclas turris* (Maurrasse and Glass, 1976; Glass and Zwart, 1977; Glass and Burns, 1987) and with five species including, *Thyrsocyrtis finalism* in DSDP Cores 94 and 149 (Glass and Zwart, 1977). These radiolarian extinctions are also identified in western equatorial Pacific DSDP site 292 associated with the lower cpx-spherule layer (Keller et *al*. 1987). More recent work in the equatorial Pacific at ODP Site 1218 (Funakawa et *al*. 2006) reported a significant reorganization of radiolarian assemblages in magnetochron C16n.1r with an interpolated magnetochronologic age between 35.5 - 35.7 Ma. This assemblage turnover occurs in calcareous nannofossil biozone CP15 and upper planktonic zone P15.

2.4 Massignano, Italy

Massignano, Italy is internationally recognized as the Global Stratotype Section and Point (GSSP) for the Eocene-Oligocene boundary (Figure 1) (Premoli Silva and Jenkins, 1993). Two Ir anomalies separated by 0.5 m are identified in planktonic foraminifera zone P15 and calcareous nannofossil zones NP19-20 and CP15b (Figures 9a & b) (Montanari et *al*., 1993). The lower and stratigraphically older Ir anomaly equal to ~250 ppt is located at ~5.6 m in the section (Montanari et *al*., 1993; Pierrard et *al*., 1998)

and the stratigraphically younger peak of ~250 ppt is found at 6.2 m (Figures 9a & b) (Bodiselitsch et *al*., 2004). A high concentration of Ir (350 ppt) was also found at 10.25 m in the section (Montanari et *al*., 1993). The stratigraphically older Ir anomaly at 5.6 m is associated with shocked quartz grains (Clymer et *al*., 1996; Langenhorst, 1996) and flattened smectite spherules coated with Ni-rich spinel crystals (Pierrard et *al*., 1998). Previous work suggests the flattened smectite spherules are diagenetically altered microkrystites that are derived from the Popigai impact event (Glass et *al*., 2004b). However, Bodiselitsch et *al*. (2004) claim to have found a small number of spherules between 6.15 and 6.18 m, suggesting the 6.2 m Ir anomaly (and spherules) could be associated with the Chesapeake Bay impact event.

Two different magnetostratigraphic interpretations exist for Massignano (Figures 9a & b) (Bice and Montanari, 1988; Lowrie and Lanci, 1994). The 5.6 m Ir anomaly is located in magnetochron C16n.2n and the 6.2 m Ir anomaly in Chron C16n.1r according to the original published magnetostratigraphy (Bice and Montanari, 1988). This interpretation provides an interpolated magnetochronologic age of ~35.59 Ma for the 6.2 m Ir anomaly and 35.89 Ma for the 5.6 m anomaly. Later work (Lowrie and Lanci, 1994) developed a different interpretation placing both Ir anomalies (5.6 and 6.2 m) in Chron C16n (Figures 9a & b). Assuming the bottom of the section is also the bottom of C16n.2n and sedimentation rates in C16n equal 6.76 m/myr, the 6.2 m Ir anomaly has an interpolated age of 35.43 Ma and the 5.6 m anomaly an age of 35.51 Ma. The average sedimentation rate for the entire section using Lowrie and Lanci (1994) equals 8.3 m/myr. Extrapolating from the top of C16n, the interpolated age of for the upper Ir anomaly is 35.41 Ma and 35.48 Ma for the lower.

The 5.6 m Ir anomaly has an interpolated radiometric age of 35.7 ± 0.4 Ma based on K/Ar, $^{40}Ar/^{39}Ar$, U/Th/Pb, and Rb/Sr analysis of biotite-rich ashes at Massignano (35.4 ± 0.3 Ma) and Contessa (36.4 ± 0.4 Ma) (Montanari et *al*. 1985, 1988; Odin et *al*., 1991). Recent studies combined new radiometric dates to the previous ones at Massignano (Oberli and Meier, 1991; Odin et *al*., 1991) to produce a new interpolated radiometric age for the 5.6 m Ir anomaly is 35.63 Ma. The 6.2 m anomaly has an interpolated radiometric age of 35.56 Ma.

Previous work (Bodiselitsch et *al*., 2004) performed high-resolution $\delta^{13}C$ and $\delta^{18}O$ analyses on bulk-carbonate samples (6.4 to 6.0 m) across the upper Ir anomaly located at 6.2 m (Figures 9a & b). This work (Bodiselitsch et *al*., 2004) reported a decrease in both $\delta^{13}C$ and $\delta^{18}O$ from the bulk-carbonate samples (Figures 9a & b). However, other researchers (e.g., Vonhof et *al*. 2000) opted not to perform analyses on samples from Massignano because severe diagenesis affected the foraminifera.

Samples from Massignano were analyzed for changes in marine biota across the ejecta horizon (Coccioni et *al*., 2000; Spezzaferri et *al*. 2002). These studies revealed a bloom in the dinoflagellate species *T. pelagica* above the impact horizon (5.6 m) that may be indicative of cooling in surface waters or possibly an increase in productivity (Coccioni et *al*., 2000; Spezzaferri et *al*. 2002).

2.4 Southern Ocean ODP Site 689

ODP Site 689 is located on Maud Rise (64°S, 3°E) in the Weddell Sea (Figure 1) at 2080 m present day water depth. Late Eocene (~35 Ma) paleo-waterdepth was 1650 m (Kennett and Stott, 1990). Site 689 is located near the present day source of AABW that

flows northward from the Weddell Sea (Carmack and Foster, 1975; Broecker and Peng, 1982; Broecker et *al*., 1985). Discrepancies in the magnetostratigraphic interpretations of Site 689 exist that offer several options for the placement of the identified upper Eocene ejecta layers (Figure 10) (Speiß, 1990; Kennett and Stott, 1990; Cande and Kent, 1992,1995; Glass and Koeberl, 1999; Vonhof and Smit, 1999). A peak concentration of microtektites is located ~ 1 - 2 cm above a second peak abundance of microkrystites (Figure 10) (Glass and Koeberl, 1999). The age difference between the two layers is equivlent to ~ 4 kyr (sedimentation rate ~5 m/myr) (Barker et *al*. 1988). Site 689 microtektites are traced to the NASF and the cpx-spherules belong to Popigai (Glass and Koeberl, 1999; Vonhof and Smit, 1999).

An Ir peak of 150 ppt, is also identified in upper Eocene normally magnetized sediments from Site 689 (128.7 mbsf) (Core 14H, Section 6; 100 - 110 cm) (Figure 10) (Montanari et *al*., 1993). The originally published ODP magnetostratigraphy places the Ir peak in Chron C15n.1 with an interpolated age of 35.05 Ma based on the Berggren et *al*. (1985) timescale (Spieß, 1990; Montanari et *al*., 1993). A second magnetostratigraphic option places the Ir peak in Chron C16n.1-2 (Kennett and Stott, 1990) with an interpolated age of 35.41 Ma (sed. rate 5.71 m/myr) (Figure 10) (Kennett and Stott, 1990). More recent (Florindo and Roberts, 2005) magnetostratigraphic interpretations show a similar sedimentation rate of 5.70 m/myr in Chron C15r. This work reported a hiatus located below the ejecta layers and Ir anomaly (128.7 mbsf) in a core-break at 129.9 mbsf (Figure 10). Florindo and Roberts (2005) interpreted this missing section to include Chron C16n.1r. If this interpretation is correct, it places the ejecta layers and Ir anomaly at Site 689 in Chron C16n.1n.

High-resolution stable isotopic work is published on benthic foraminifera and bulk-sediments from Site 689 (Figure 10) (Vonhof et *al*., 2000). Benthic foraminiferal $\delta^{13}C$ values decrease by ~1‰ across the ejecta horizon (Figure 10), but fine fraction CO_3 (calcareous nannofossils) increase by 0.5‰ (Vonhof et *al*., 2000). Benthic foraminifera (Figure 10) and fine-fraction CO_3 $\delta^{18}O$ values increase by 0.5‰.

2.4 St. Stephen's Quarry (SSQ), Alabama

St. Stephens Quarry, Alabama (Figure 1) provides a good continental shelf record through its precise age chronology from the integrated bio-, litho-, magneto-stratigraphic interpretations with isotopic and sequence stratigraphic data of Miller and Kent (1987) and Miller et *al*. (1993, *in press*) (Figure 11). SSQ sequences are shallow-water deposits (late Eocene paleodepth is < 200 m) comprised of clays, silts, and carbonate, siliciclastic, and glauconitic sands. The late Eocene is represented by the Jackson Stage, which includes the Moodys Branch, North Twistwood Creek Clay, and Yazoo Clay Formations (Figure 11). The youngest Yazoo Clay Formation includes the upper Eocene Cocoa Sand and Pachuta Marl and the lower Oligocene Shubuta members (Miller et *al*., 1993, in press). The SSQ stratigraphic section is complicated by several short erosional or non-depositional hiatuses (Figure 11) (Miller et *al*., *in press*); however, all unconformities were identified and the timing and duration of these events was estimated from the well-preserved nature of this section (Miller et *al*., *in press*). Stratigraphically in-place late Eocene microtektites or microkrystites are absent from the terrestrial record in North America (Koeberl, 2001). SSQ provides a good North

Amreican section with integrated age chronology to search for the occurrence of NA microtektites.

2.4 Southern Ocean ODP Site 1090

South Atlantic ODP Site 1090 is located on the southern flank of the Agulhas Ridge (Figure 3) and currently is located above the calcite compensation depth (CCD) at 3,702 m water depth. Paleowater depths (34 Ma) are in the range of 3,200 m (Miller, pers. comm., 2006). ODP Site 1090 is located in a region that is well-suited to monitor the changes in Cenozoic paleoceanographic conditions with a higher degree of accuracy. This site is situated near the meeting of NADW with underlying Circumpolar Deep Water (CDW) in the present day ocean basins (Figure 7).

The age-model is generated with integrated biostratigrapic and magnetostratigraphic data from the published literature (Figure 12). Channell et *al*. (2003) used calcareous nannoplankton (Marino and Flore5s, 2002) and planktonic foraminifera (Galeotti et *al*., 2002) biostratigraphy to correlate the middle Eocene to middle Miocene magnetostratigraphic inclination at Site 1090 to the GPTS of Cande and Kent (1992; 1995) (Figure 6). Magnetostratigraphic interpretations of Site 1090 reveal two alternative geochronologies. Option 1 uses data from the calcareous nannofossil biostratigraphy of Marino and Flores (2002). Option 2 utilizes the planktonic foraminiferal biostratigraphy of Galeotti et *al*. (2002). These two magnetostratigraphic interpretations differ only near the Eocene-Oligocene boundary. Channell et *al*. (2003) utilized $^{87}Sr/^{86}Sr$, $\delta^{18}O$, and $\delta^{13}C$ values to illustrate that option 1 is the best fit to the GPTS. This is because the $\delta^{18}O$ and $\delta^{13}C$ Oi-1a shift from Miller et *al*. (1991) proves to

be too young when option 2 is used. Option 1 from the published Channell et *al*. (2003) magnetostratigraphy is utilized in this thesis based on its best fit to the GPTS (1992,1995).

Kyte (2001) identified impact spherules and peak Ir concentrations at Site 1090 in the 177-*Scientific Results* volume. Microspherules are found in core 30X-5 between 95 - 126 cm (278.95 - 279.26 mbsf) (Figures 6 & 12). Kyte (2001) found the Ir peak (954 ppt) in core 30X-5, 105-106 cm (279.05 mbsf). Further analyses (Liu et *al*., 2000) identified two distinct Ir anomalies. The larger Ir peak of 970 ppt is found at the same depth that Kyte (2001) located it in core 30X-5 at 105-106 cm. The older Ir anomaly (780 ppt) is located 10 cm below the larger peak at 115-116 cm. Liu et *al*. (2000) also identified two separate microtektite and cpx-microspherule layers in Core 30X-5 at Site 1090. No distinct stratigraphic separation is found between the microtektite and microkrystite layers at Site 1090, although each is recognized as its own layer (Liu et *al*., 2000; Kyte and Liu, 2002). The peak abundance of both microtektites (106/gm) and microkrystites (562/gm) is located in Core 30X-5; 114 - 115 cm (279.14 mbsf) (Figure 6).

2.4 Deep Sea Drilling Project (DSDP) Site 612

DSDP Site 612 is a well-studied, yet unresolved record of late Eocene extraterrestrial impact stratigraphy off the NJ continental slope (Figure 1). Site 612 present day water depth is 1,404 m and Eocene paleowater depth was ~1,000 m (Miller and Katz, 1987). The discovery of upper Eocene impact-generated deposits at Site 612 is reported in the *Initial Reports* volume from Leg 95 (Poag et *al*., 1987). Additional

studies confirmed the presence of upper Eocene microtektites, microkrystites, shocked minerals, glass fragments, and high-pressure polymorphs in Core 21 Section 5 (Figure 13) (Cousin and Thein, 1987; Glass and Burns, 1987; Poag and Low, 1987; Thein, 1987; Bohor et *al*., 1988; Glass, 1989; Koeberl, 1989; Miller et *al*., 1991; Poag and Aubry, 1995). Analyses (Glass, 1989) show an abundance of tektite glass within 8 cm of sediment in Core 21. The highest concentration of microtektites occurs at 112 - 113 cm (Figure 13) (Glass, 1989). An increased number of clinopyroxene-bearing microspherules is concentrated in the lower part of the tektite layer. The highest abundance of microkrystites occurs from 115 to 117 cm (Figure 13). The microkrystite layer is 4 - 5 cm below the microtektite horizon. A radiometric $^{40}Ar/^{39}Ar$ plateau age of 35.5 ± 0.3 Ma at Site 612 is obtained from microtektities and tektite fragments (Obradovich et *al*., 1989).

A high degree of discrepancy exists between various studies on the nature of the impact-generated deposits and the location of the stratigraphically older unconformity at Site 612 (Figure 13). One study (Poag and Low, 1987) places the unconformity in Core 21 Section 5 at 115 cm (181.35 m) between foraminiferal zones P15 and P11 (Figure 13). However, additional work (Cousin and Thein, 1987) locates the unconformity at 119 cm (181.39 mbsf). Further studies (Keller et *al*., 1987) place the unconformity at the microkrystite layer (115 - 117 cm) or below because of the presence of reworked middle Eocene planktonic foraminifera at the microkrystite layer. This depth is only 4 cm above the alternative unconformity location at 119 cm, which is well-within range of typical bioturbation. Keller et *al*. (1987) noted a major decrease in foraminiferal biodiversity at the microkrystite layer and 28 cm above attributed to fertility and nutrient changes in

ocean chemistry. Later studies (Glass, 1989; Macleod et *al*., 1990; Miller et *al*., 1991) determined the depth of the unconformity is 119 cm. They determined the microtektite layer in planktonic foraminiferal zone *P. semiinvoluta*. Miller et *al*. (1991) concluded that 4 cm of separation between the layers represents ~1.2 kyr by interpolating sedimentation rates between radiometric dates and biostratigraphic datum levels. According to the work of Miller et *al*. (1991), the sedimentation rate equals ~ 3.5 cm/kyr based on the FO of *T. cerroazulensis cunialensis* and the FO of *Isthmolithus recurvus*. More recent work (Poag and Aubry, 1995) interprets the entire ~23 cm section from 181.39 - 181.16 m, immediately above the middle/late Eocene unconformity, to be a debritite that accumulated instantly (Figure 13). This would mean the biostratigraphic and isotopic data across the 23 cm interval is erroneous because of chaotic and disturbed sedimentation.

In this thesis, the biostratigraphic and isotopic chronology from Miller et *al*. (1991) and the impact stratigraphy of Glass (1989) is utilized. Major elemental oxide composition of Site 612 microtektites linked them to the NASF (Glass, 1989; Glass et *al*., 1998). New work (Glass et *al*., 1998) disputed the previous studies that associate Site 612 upper Eocene microtektites with the Toms Canyon structure (Poag et *al*., 1992; Poag and Aubry, 1995; Poag and Poppe, 1998) based on ejecta mineralogy, glass composition, and the geographic variation in ejecta layer thickness. Glass et *al*. (1998) reaffirmed that Site 612 upper Eocene microtektites were derived from the CBIS. The biostratigraphic and isotopic data from Miller et *al*. (1991) was adopted for reasons that both the planktonic foraminiferal zones and calcareous nannofossil biozones closely match those of later studies by Poag and Aubry (1995). Uncertainty remains in the nature of the

sediments directly above the unconformity at 181.39 mbsf. Whether or not this part of the section is undisturbed will be addressed later in my study with additional data from this thesis.

3. Methods

3.1 ODP Sites 1090 and 612, and St. Stephens Quarry (SSQ)

3.1 Site 1090 Impact Stratigraphy

The magnetic chronozone interpretations of Channell et *al*. (2003) from option 1 are correlated to the microtektite and microkrystite abundance data of Liu et *al*. (2000) and Kyte and Liu (2002) (Figure 6). This is a first-order correlation of microtektites and microkrystites to the normal magnetic polarity Chron C16n.1n. Liu et *al*. (2000) provided geochemical evidence showing the microtektites at Site 1090 are equivalent to the NASF. They also demonstrated the microkrystites at Site 1090 are related to the cpx-bearing spherule Popigai strewn field.

3.1 Site 1090 Isotopic Analysis

Benthic foraminifera display very good preservation throughout the 40 m section, although they also show low diversity. A total of 160 samples were taken between ~239.3 and 291.4 mbsf for stable isotopic analysis of benthic foraminifera. Approximately 20 cm^3 of sediment was sampled every 20 cm across the ejecta layer. The sampling interval decreased to 40 cm at 10 m above (269.5 mbsf) and 10 m below

(286 mbsf) the ejecta layer. Planktonic foraminifera are too sporadic to generate a reliable stable isotope record.

All samples to be picked for benthic foraminifera were weighed, dried at 90°C for ~ 48 hours, and reweighed. Samples were soaked in ~ 150 ml of Calgon for ~ 4 to 5 hours before being washed through a 63 μm sieve. The washed samples were dried overnight at 90°C and reweighed. Dried samples were separated into fine (<150 μm) and coarse size (≥ 150 μm) fractions with a dry sieve. All samples weighing ≥ 0.20 gm were placed into a splitter and separated into working and archival halves. Samples weighing ≤ 0.19 gm were not split as to avoid any unnecessary loss of sediment. Working halves were handpicked under a binocular microscope for all planktonic and benthic foraminifera. Benthic foraminifera were identified using the taxonomy of Tjalsma and Lohmann (1983), van Morkhoven et *al*. (1986), and Katz et *al*. (2003). An average of 4 to 5 benthic specimens of the genus *Cibiciboides* were selected for stable isotopic analysis. To minimize any possible contamination or diagenetic effects the non-fragile *Cibiciboides* tests were sonicated for approximately 30 to 90 seconds. Samples were analyzed on a Micromass Optima mass spectrometer in the Stable Isotope Laboratory at Rutgers University. Samples were reacted with phosphoric acid at 90°C in a multi-prep peripheral device and reported against the V-PDB (Vienna PeeDee Belemnite) standard. Samples are analyzed in sets of 32 that include 8 internal laboratory standards. Duplicate samples were often included to ensure the data analyses are consistent. The laboratory standard is checked regularly against NBS-19, which has a $\delta^{18}O$ offset equal to 0.04‰ and a $\delta^{13}C$ offset of 0.01‰. The laboratory standard for a 1-σ error is equal to 0.08‰ for $\delta^{18}O$ and 0.05‰ for $\delta^{13}C$.

3.1 Site 612 Isotopic Analysis

Benthic foraminifera were identified from previously processed samples and picked from 20 new samples for oxygen and carbon stable isotopic analysis. Benthic foraminifera were identified from 20 samples in Core 21X section 5, 100 - 118 cm (181.2 - 181.38 mbsf). About 4 to 5 specimens per sample of the genus *Cibiciboides* were selected for stable isotopic analysis. Samples were analyzed on the mass spectrometer in the Stable Isotope Laboratory at Rutgers University, NJ.

3.1 SSQ Microspherules

To search for the occurrence of microtektites and microkrystites the published magnetostratigraphy (Miller et *al*., 1993) was used to calculate a target depth in Chron C16n.1n to be between 62.8 - 64.9 m (Figure 11). I sampled approximately 20 cm^3 of sediment every 0.09 m between 62.6 - 63.8 m. Four additional samples were also taken: 1) two at 65.2 m and 67.0 m; and 2) two at 60.9 m and 59.4 m. A total of 17 samples were weighed, dried at 90°C for ~ 48 hours, and reweighed. They were then soaked in ~150 ml of Calgon for ~ 4 to 5 hours before being washed through a 63 μm sieve. Washed samples were dried overnight at 90°C and reweighed. Dried samples were separated into four size fractions of fine (<150 μm), medium (150 - 212 μm), medium-coarse (212 - 250 μm), and coarse (≥ 250 μm) with dry sieves. I searched for microtektites in all size fractions under a binocular microscope and found a total of 16 (Figure 14) discussed in the results.

Scanning electron microscope (SEM) images of a microspherule was taken from 62 m (204.75 ft) (Figures 15a & b). Bridget Wade produced the SEM images at Rutgers

University in Piscataway, NJ. SEM images at different magnifications show a 250 μm microspherule with a highly fibrous-like, or shingled, surface. SEM images alone are inadequate to accurately determine the microspherules true composition, and presumably origin. C. Koeberl performed geochemical analyses and took backscattered electron (BSE) images of the microspherules at the University of Vienna, Austria (Appendix A). Major elemental oxide compositions were determined using EDS (Energy Dispersive System) analysis from a JEOL SEM instrument or by wavelength-dispersive spectrometry using an ARL-SEMQ electron microprobe for quantification of 8 to 9 of the sixteen microspherules (C. Koeberl, pers. comm. 2007).

4. Results

4.1 Site 1090

4.1 Calibration of Impactites to the GPTS (1992,1995)

A first order correlation of the upper Eocene ejecta layers to the GPTS (1992,1995) is established using the published magnetostratigraphy from Channell et *al*. (2003) (Figure 6). Correlating magnetic tie-points to the spherule layers from Liu et *al*. (2000) gives both the microtektite and cpx ejecta layers an interpolated age of 35.429 Ma (Figures 6 and 12). The stratigraphically younger Ir anomaly has an interpolated age of 35.426 Ma. The Ir anomaly and the two impact ejecta layers are located in Chron C16n.1n and separated by approximately 4 kyr at Site 1090 (Figure 6).

4.1 Site 1090 Benthic Foraminifera

Site 1090 show a switch in abundance and diversity of the benthic foraminiferal genus *Cibicidoides* directly above the ejecta layer. Species diversity and test size are significantly larger in samples below the ejecta layer (Table 2). Species diversity becomes mono-specific above the impact horizon only being represented by *C. bradyi*. This genus is exceptionally delicate and rather small compared to other late Eocene species of *Cibicidoides* at Site 1090. Site 1090 changes in epi-faunal benthic foraminiferal *Cibicidoides* spp. is interpreted to reflect a deepwater: 1) increase in carbonate dissolution; 2) change in temperature or ventilation; or 3) change in nutrient or food supply.

4.1 Site 1090 Benthic Carbon Isotopes

Site 1090 $\delta^{13}C$ data from this thesis are reported for *Cibicidoides praemundulus, C. eoceanus, C. dickersoni, C. bradyi,* and *C. grimsdalei* (Figures 16a & b) (Table 3). A very small number of samples (> 5) include values expressed as *C. havaensis* and *C. laurisae*. Duplicate samples are averaged because laboratory offsets are consistent within an error range of ~ 0.10‰. $\delta^{13}C$ values of *C. grimsdalei* show a consistent offset from all other species, including *C. praemundulus, C. eoceanus, C. dickersoni,* and *C. bradyi.* The observed offset has a constant value of ~ 0.10‰, resulting from vital effects between species (Vinot-Bertouille and Duplessy, 1973; Erez, 1978).

The lower limit of my record (291.41 mbsf) (Figure 16a) has a magnetostratigraphic interpolated age of ~ 36 Ma (Figure 16b). Upper limits

(239.32 mbsf) (Figure 16a) reach an extrapolated age of ~ 33.79 Ma (Figure 16b). The entire signal spans ~ 2.2 myr of the late Eocene through early Oligocene (Figure 16b). $\delta^{13}C$ values generally center around ~ 0.9‰ from 36 to ~35.4 Ma (Figure 16b). A minor transient excursion equaling ~ -0.3‰ occurs in the early part of Chron C16n.2n equivalent to ~ 35.72 Ma. At most, the initiation of this event occurs within ~ 8.6 kyr. The brief departure persists for ~ 8.1 kyr before beginning a 9 kyr return to previous values at ~ 0.9‰.

A significant $\delta^{13}C$ decrease occurs within ~ 75 - 100 kyr of the ejecta layer, relative to values directly below the horizon (Figure 16b). $\delta^{13}C$ values range between 0.8 - 0.9‰ below the ejecta layer and between 0.2 - 0.3‰ above the layer (Figure 16b). The negative $\delta^{13}C$ excursion has an amplitude of ~ 0.5‰. Pre-impact (35.3 - 36 Ma) natural variability in the benthic $\delta^{13}C$ record from Site 1090 from has a standard deviation of 0.15‰ (Figures 16a & b). The standard deviation for the entire record (33.7 - 36 Ma) equals 0.18‰.

Approximately 40 kyr after the initial drop, a small increase of ~ 0.2‰ occurs in the middle of Chron C15r (Figure 16b). Values reach 0.4 - 0.5‰, but do not fully recover to those below the impact horizon. The signal begins to decrease in the middle of C15r (34.940 - 35.343 Ma) reaching ~ 0.10‰ by 34.9 Ma (Figure 16b). Low values persist throughout all of C15n (34.655 - 34.940 Ma) before increasing to ~ 0.5 - 0.6‰ by ~ 34.6 Ma. A steady decline beginning around 34.6 Ma continues for ~ 260 kyr, reaching the lowest $\delta^{13}C$ values of the entire record at ~ 34.3 Ma (Figure 16b). Located in the middle of this trend at ~ 34.4 Ma is a transient positive perturbation. It is difficult to decipher the authenticity of this data point without performing a duplicate sample

analysis. The trend begins to steadily increase at 34.3 Ma, but with a much larger range of amplitude.

4.1 Site 1090 Bulk-Carbonate Carbon Isotopes

The $\delta^{13}C$ composition of Site 1090 bulk-CO_3 sediments were analyzed with a smaller sampling interval at every 5 cm (equivalent to ~2 kyr) over a 1.5 m section (Figure 17) (Table 4). Site 1090 $\delta^{13}C$ values of bulk-CO_3 are higher then benthic values because of preferred extraction of the lighter ^{12}C isotope during photosynthetic fractionation in surface waters (Kroopnick, 1972; Broecker and Peng, 1982). The upper part of the record (278.05 mbsf) has an interpolated age of ~35.38 Ma and the lowest data point in the record (279.49 mbsf) has an interpolated age of ~35.44 Ma (Figure 17). Bulk-CO_3 $\delta^{13}C$ values center around 2.1 - 2.2‰ below the ejecta layer (Figure 17). Values decrease to 1.8‰ 5 cm below the ejecta layer and to 1.6‰ exactly at the ejecta layer (Figure 17). Values immediately increase 5 cm above the ejecta layer, returning to 2.1‰. Bulk-CO_3 $\delta^{13}C$ compositions center in the range of 2.0 - 2.2‰ for 50 cm (~ 20 kyr) above the decrease found at the ejecta layer. At 278.5 mbsf, $\delta^{13}C$ values increase slightly to 2.2 - 2.3‰ for an additional 20 cm (~8 kyr) when they decrease again to the pre-impact range between 2.1 and 2.2‰.

4.1 Site 1090 Benthic Oxygen Isotopes

Site 1090 data show $\delta^{18}O$ values range between 0.6 - 0.7‰ throughout the oldest part of the record (Figure 18) (Table 3). The progression is relatively steady with two prominent positive excursions both having an amplitude of ~ 0.3‰. The initial

perturbation occurs near the top of Chron C16n.2n at ~ 35.7 Ma and the second excursion occurs close to the top of Chron C16n.1r at ~ 35.6 Ma (Figure 18). This increase occur ~ 125 kyr after the first. A third rapid positive excursion occurs immediately below (9 - 10 kyr) the impact ejecta horizon (Figure 18). Directly above the impact horizon $\delta^{18}O$ values decrease rapidly. $\delta^{18}O$ ratios reach their lowest point in the entire record ~ 10 - 15 kyr after the impact layer at 35.41 Ma (Figure 18). Subsequently, the signal centers around pre-impact values at ~ 0.6‰. At 276.5 mbsf (~ 35.25 Ma) values begin to increase, reaching ~ 1‰ by 276 mbsf (~ 35.1 Ma). From here, values decline to 0.5‰ at 273 mbsf (~ 34.75 Ma). The curve displays a notable positive increase to values of ~ 1‰ from 273 - 259 mbsf (~ 34.75 to 34.3 Ma). Values increase in variability above 266.5 mbsf (from ~ 34.5 Ma on). At the uppermost data point the record begins to trending towards higher values, possibly Oi-1 (Figure 18).

4.1 Site 1090 Bulk-Carbonate Oxygen Isotopes

$\delta^{18}O$ data from this thesis of bulk-carbonate were analyzed over a 1.5 m section (at every 5 cm; equivalent to ~2 kyr) (Figure 19) (Table 4). The $\delta^{18}O$ composition of bulk-CO_3 is lower than benthic foraminifera (Figure 19) because bulk-CO_3 reflects mainly calcareous nannoplankton that live in warmer surface waters (Epstein et *al*., 1951, 1953; Emilani, 1955). The oldest part of the bulk-CO_3 record has $\delta^{18}O$ values that range between 0.4 and 0.1‰. $\delta^{18}O$ values decrease to -0.25‰ at 5 cm below the ejecta layer. A maximum $\delta^{18}O$ decrease reaches -0.55‰ just at the ejecta layer (Figure 19). The amplitude of the negative $\delta^{18}O$ excursion is ~0.5 - 0.6 ‰ (Figure 19). Values

immediately increase above the ejecta layer and return to 0‰. Bulk-CO_3 $\delta^{18}O$ compositions range between 0 - 0.4‰ for 80 cm (~32 kyr) the ejecta layer (Figure 19). At 278.25 mbsf, $\delta^{18}O$ values decrease to -0.2‰ for 20 cm (~8 kyr). Values begin to increase near the upper part of the record reaching 0.1‰ (Figure 19).

4.1 Site 1090 Ejecta Deposits

All except one of the microspherules found in samples picked for benthic foraminifera from Site 1090 are by definition microtektites (<1 mm) (Figures 20a & b). One spherule is greater than 1 mm so it is classified as a tektite. All microspherules were found in the > 150 μm size fraction. Four microtektites were found at 118.5 - 120 cm in a sample that is 4 cm below the identified microtektite and microkrystite layer (Kyte and Liu, 2002) at 114 cm (Figure 6). Two are sphere-like in shape and two have a 'flattened pancake' or splash-type form. Four microtektites and one tektite were found at 94 - 95.5 cm, ~ 10 cm above the Ir anomaly (105 - 106 cm). The four microtektites and one tektite are sphere-like in shape. The larger tektite exhibits clear signs of etching, gouging, and pit marks when viewed through a magnified lens. One sphere-shaped microtektite was found in a sample 30 cm above the Ir anomaly at 75.5 - 77 cm and also a sphere-shaped microtektite farther up in Core 30 Section 4, 123 - 124.5 cm. This microtektite is located 1.32 m above the impact ejecta layer in Section 5. Reworking from bioturbation (Guinasso and Schink, 1975) most likely dispursed microtektites over this section of core.

An additional microtektite located ~ 9 meters above the impact ejecta layer was found at 270.04 mbsf in Core 29 Section 6, 24 - 25.5 cm (Figure 12). It was found just

above the base of C13r with an interpolated age of ~ 34.63 Ma. I am not convinced the occurrence of one microtektite indicates the presence of an additional ejecta layer. Previous work (Guinasso and Schink, 1975) shows mixing rates for abyssal sediments range from 1 - 10^3 cm^2 kyr^{-1}.

4.2 DSDP Site 612

4.2 Site 612 Benthic Carbon Isotopes

Nine samples were picked for benthic foraminifera across the impact horizon at Site 612 Core 21X Section 5, between 106 - 119 cm for $\delta^{13}C$ analyses (Figure 21). The peak abundance of microtektites is between 112 - 113 cm (181.32 mbsf) and highest concentration of microkrystites is between 115 - 117 cm (181.35 mbsf) (Figure 21). A sampling interval of 1 cm was used to obtain a high-resolution record for this site. Miller et *al*. (1991) estimated a sedimentation rate ~ 3.5 cm/kyr based on nannofossil and planktonic foraminifera biostratigraphy. According to this sedimentation rate, a 1 cm sampling interval is approximately equal to every 285 years. The entire 20 cm sampled section is equivalent to a total of 5.7 kyr.

All isotope values from this work in Figure 21 are reported for *Cibicidoides praemundulus, C. subspiratus C. eoceanus, C. dickersoni,* and *C. bradyi*. A technical error caused only a portion (5) of the total samples (9) to be fully analyzed. Considering that my youngest data point is at 114 cm, a complete high-resolution stable isotope record across the microtektite layer identified by Glass (1989) was not achieved (Figure 21). The data show a small decrease between ~ 117 and 114 cm. This decrease occurs at the peak abundance of microkrystites, suggesting a possible correlation (Figure 21). Values

just below the layer center near ~ 0.7‰ and drop to 0.2‰ directly above it. This makes the entire $\delta^{13}C$ decrease I found in this thesis at Site 612 equal to ~ 0.5‰ (Figure 21). A $\delta^{13}C$ decrease occurring over 2 - 4 cm at Site 612 is equivalent to ~ 550 - 1,150 years.

Previous data plotted with mine (137.6 - 179.3 mbsf) in Figure 13 come from Miller et *al*. (1991). Values from Miller et *al.* (1991) (Figure 13) are reported for *Cibicidoides* spp.. The oldest age in Figure 13 is ~ 35.6 Ma using the corrected timescale from Berggren et *al*. (1995). The youngest point has an extrapolated age of ~ 33.7 Ma, comprising a total record of 1.87 myr. The oldest data point from Miller et *al*. (1991) is located 2 m (~60 kyr) above the impact ejecta layer at 181.32 mbsf (Figure 13). The signal returns to pre-impact values by 60 kyr at this initial data point. The record begins a trend toward higher values in the range of 1‰, which is followed by a gradual decrease from 172 to 160 mbsf. Declining values begin to increase again at the zone P15/16 boundary. A short increase occurs from 160 to 155 mbsf, before the signal begins a step-wise decline throughout the remaining part of the record. Values from the youngest part of the record focus around 0‰ (Figure 13).

4.2 Site 612 Benthic Oxygen Isotopes

Benthic foraminifera oxygen isotope values from this thesis show a decrease across the microkrystite layer at 115 - 117 cm (Figure 21). Beginning at 118 cm, values focus around 0.3‰ and decrease to 0‰ by 114 cm (Figure 21). Using a 3.5 cm/kyr sedimentation rate, the decrease occurs over ~ 570 - 900 years. The oldest data point (Core 21-4, 60 - 64 cm) in Figure 13 shows good correlation to the youngest data point from this study (Core 21-5, 114 - 115 cm) (Figures 13 and 21). Values center in the

vicinity of 0‰ and are separated by 2 m, equivalent to ~ 60 kyr (Figure 13). Values continue to range between 0.2 and 0‰ from 180 to 163 mbsf. The curve shifts toward higher values around 160 mbsf and reaches 0.5‰ by 150 mbsf. Values from the upper portion of the record (135 - 160 mbsf) range between 0.2 and 0.4‰ (Figure 13).

4.3 St. Stephens Quarry (SSQ)

4.3 SSQ Microspherule Deposits

Sixteen microspherules were found at SSQ (62.9 - 63.7 m) within the North Twistwood Creek Formation and highstand systems tract of the Moodys Branch-NTC sequence. The microspherules were found in the calcareous nannofossil zone NP19/20, planktonic foraminiferal zone P15, and magnetic Chron C16n.1n. All microspherules range in size between 212 to 250 μm and have a red-stained color. Some microspherules are cracked or broken and seem to have layered edges. Their stratigraphic distribution is plotted in Figure 14. This plot shows the highest abundance of microspherules occurs at 63.7 m (209 ft).

The major oxide compositions of the SSQ microspherules are; SiO_2 70%, Al_2O_3 15%, K_2O 3%, Na_2O 3%, CaO 0.5%, MgO 0.3%, TiO_2 0.7%, and FeO 0.0075% (C. Koeberl, per. comm., 2006). Compositions and appearance are very similar to glass, however, they a lack high Fe content typical of impact-generated microtektites and microkrystites. The Al_2O_3, CaO, and SiO_2 weight percent compositions of the SSQ microspherules are compared to data from several North America microtektites and Popigai cpx-spherules (Figure 22a) (Glass et *al*., 2004a). The average SiO_2 weight percent for North American microtektites is 73.4% and 70% for the SSQ microspherules.

Cpx-microspherules have 5% less SiO_2 than the NA microtektites and SSQ microspherules (Figure 22a). Average Al_2O_3 compositions match very well for NA microtektites and SSQ microspherules. NA microtektites average 14% Al_2O_3 and SSQ microspherules are only 1% more at 15% (Figure 22a). Cpx-microspherules have half as much Al_2O_3 (7.4%) then NA microtektites and SSQ microspherules. Cpx-microspherules have a higher percentage of CaO relative to SiO_2 then both NA microtektites and SSQ microspherules (Figure 22a). SSQ microspherules have 1% less CaO (0.5%) compared to NA microtektites (1.64%). Cpx-microspherules have an average of almost 10% CaO, which is 20 times more then SSQ microspherules and 6 times more then NA microtektites. Average MgO percentages for the NA microtektites is 1.73% and is 0.32% for the SSQ microspherules (Figure 22b). Cpx-microspherules are approximately 7.5% MgO. Cpx-microspherules have almost four times as much MgO as the NA microtektites and more then 20 times the amount in the SSQ microspherules. Plots show SSQ microspherules have similar SiO_2 (70%), Al_2O_3 (15%), and CaO (0.5%) compositions to NA microtektites (Glass et *al*., 2004a). FeO and MgO plots show the SSQ microspherules lack of typical Fe and Mg concentrations found in both cpx-microspherules and NA microtektites. Low Fe and Mg concentrations are usually indicative of terrestrial origins, as opposed to extraterrestrial. The SSQ microspherules have an organic outer-layer composed of unspecified amounts of C, O, and S. The microspherules are not insect egg shell casings or CO_3 shells because their inner-core composition is similar to glass. Microprobe data show a 91 wt.% total that indicates the microspherules are hydrated. Back-scattered electron (BEI) images were taken at the University of Vienna by C. Koeberl (Appendix A). The BEI images display the layered

structure of SSQ microspherules that is composed of organic material on the outside and glass on the inside. BEI image 3/2 shows pyrite crystals on the inner exposed core and outer layer of the microspherule (Appendix A). A barite crystal is also present in the inner core where it is cracked and exposed (Appendix A).

Microspherules found between 62.8 and 63.7 m (206 - 209 ft) at SSQ have a layered structure consisting of a thin outer skin of organic material surrounding an inner core of glass, which includes minerals such as barite (barium sulfate, $BaSO_4$) and pyrite (iron sulfide, FeS_2) (Appendix A: BEI 3/2). Barite is commonly used as a weighting agent for various types of drilling fluids. Barite is sometimes called a "heavy mud" because of its' high specific gravity (4.5) for a non-metallic mineral and for its use in drilling fluids (Klein, 2002). The majority of barite produced commercially is used to help support drill rods and to prevent blow-outs for drilling petroleum and gas wells. Barite crystals are ground into small sizes before they are used in drilling fluids. The Arkansas State Geological Commission website (*http://www.state.ar.us/agc/barite.htm*) reports 90% of the world's production of barite in 1990 was consumed in drilling fluids. The ARCO Oil and Gas Company in conjunction with the U.S. Geological Survey, Amoco, the Alabama Geological Survey, and the University of Alabama drilled the SSQ borehole in 1987 (Miller et *al*., 1993). The SSQ microspherules are interpreted to be anthropogenic based on the high use of barite in drilling oil/gas wells during the late 1980's. ARCO Oil and Gas Co. executed the drilling operations in 1989. The source of the SSQ microspherules is most likely drilling contamination.

Subsequent to finding the microspherules, M.P. Aubry performed further biostratigraphic analyses of SSQ calcareous nannofossils at Rutgers University. A new

age-model for SSQ incorporated this data (Miller et *al*., 2006 *in press*), which now places the microspherules in an older stratigraphic position than predicted. Based on the new age-model, the microspherules are now located in calcareous nannofossil biozone NP18 and Chron C16r (Figure 11). This violates the published magnetostratigraphic interpretations of Miller et *al*. (1993). The microspherules are still located in the same planktonic foraminiferal biozone P15 according to the new age-model. According to this new age-model our target depth (C16n.1n) is now located in a hiatus.

5. Discussion

5. Abyssal Circulation

$\delta^{13}C$ data of benthic foraminifera from three end-member ocean basins are plotted together to monitor the pattern of deep-water flow between these sites (Figure 23). Deep-water circulation patterns across the ejecta layer are reconstructed using North Atlantic Site 612 (paleowater depth ~1,000 m (Miller and Katz, 1987)), South Atlantic Site 1090 (paleowater depth 3,200 m (Miller, pers. comm., 2006)), and equatorial Pacific Site 1218 (paleowater depth 3,700 m (Lyle et al., 2002)). Higher $\delta^{18}O$ and $\delta^{13}C$ values in benthic foraminifera from the record at Site 612 relative to the South Atlantic and equatorial Pacific records argues that Site 612 may reflect a warmer and more oxygenated intermediate water mass (Figure 23). This can only be inferred because Site 612 lacks the good magnetostratigraphic age control found at Sites 1090 and 1218.

Site 1090 benthic $\delta^{13}C$ values from the older part of the record (36 to

35.4 Ma) exhibit lower variability compared to the younger section (34.5 to 33.7 Ma) (Figure 16b). Increased $\delta^{13}C$ variability in the younger part of the Site 1090 benthic record indicates an enhancement of deepwater ventilation. This is similar to Site 689 that exhibits low productivity variability at the early late Eocene and increases variability during the latest Eocene as a result of the Drake Passage opening (Diester and Zahn, 1996). The late Eocene gateway increased wind stresses in the Southern Ocean during colder periods. This resulted in enhanced up-welling of nutrient rich waters causing productivity to become more variable (Diester and Zahn, 1996).

5. Impact Events and Climate

The lack of significant variation in benthic $\delta^{18}O$ values at Site 1090 and 612 (Figures 18 and 21) relative to the ejecta layers is interpreted to reflect a minimal temperature change in deep-waters caused by the late Eocene impact events. The negative bulk-CO_3 $\delta^{18}O$ excursion of ~ 0.5 - 0.6‰ at Site 1090 is possibly the result of a local surface-water temperature increase.

The 0.5‰ negative $\delta^{13}C$ excursion associated with the ejecta layers identified in benthic foraminifera and bulk-CO_3 from Site 1090 (Figure 16b and 17) and in benthic foraminifera from Site 612 (Figure 21) is interpreted to reflect a major change in the global carbon budget. Evidence of a coeval negative $\delta^{13}C$ excursion in benthic foraminifera from the North Atlantic, Pacific, and Southern Ocean basins (Figure 23) supports the interpretation that the late Eocene impact events caused a perturbation in the global carbon system. Site 1090 bulk-CO_3 $\delta^{13}C$ values at the ejecta layer show a rapid response with an equally quick recovery (Figure 17). The rapid $\delta^{13}C$ response and

recovery at Site 1090 in bulk-CO_3 indicates a short-lived global carbon cycle perturbation. Pre-impact benthic $\delta^{13}C$ values from Site 1090 (35.43 - 36 Ma) (Figure 16b) show a maximum of ~ 0.15 - 0.2‰ (out of 0.5‰) can be attributed to natural variability in the climate system.

The prolonged benthic $\delta^{13}C$ response occurring between 35.1 and 34.6 Ma at Site 1090 is not interpreted to be associated with the late Eocene impact events (Figure 16b). The prolonged negative $\delta^{13}C$ response is attributed to a local decrease in the fraction of C_{org} to C_{carb} being buried. Middle Eocene sediments from Site 689 show productivity maxima that occur during periods of low $\delta^{13}C$ values and high $\delta^{18}O$ values that are interpreted as times of higher input of organic matter (Diester and Zahn, 1996). Local surface water primary productivity may have shifted from secreting C_{carb} tests to Si-rich ones, causing more C_{org} relative to C_{carb} to be buried (Vincent and Berger, 1985; Cervato and Burckle, 2003).

The decreasing nature of the $\delta^{13}C$ signal at Site 612 (118 to 114 cm) (Figure 21) does not support interpretations of Poag and Aubry (1995) that claim this portion of the record is disturbed (Figure 13). It is unlikely that random and chaotic mixing of sediments would produce a smooth trending $\delta^{13}C$ signal or the two distinct, normally distributed impact horizons. $\delta^{13}C$ and $\delta^{18}O$ data provide evidence indicating Site 612 sediments are undisturbed above the unconformity at 119 cm.

At Site 612, onset of the $\delta^{13}C$ excursion began when the Popigai impactor struck Earth (Figure 21). The conclusion is reached that the $\delta^{13}C$ excursion at Site 612 is associated with the late Eocene extraterrestrial impact events. Pending analyses will determine the isotopic response to the Chesapeake Bay impactor using samples at every

1 cm (~ 350 kyr) across the upper microtektite layer. The benthic $\delta^{13}C$ decrease found at Site 1090 and 612 (Figures 16b and 21) associated with the ejecta layers is interpreted to reflect the injection of extraterrestrial carbon from an incoming ^{12}C-rich comet, with a maximum of ~ 0.15 - 0.2‰ attributed to natural climate variability.

5. Impactor Diameter

The elemental and isotopic composition of the Chesapeake Bay and Popigai impactors remains unknown. The Chesapeake Bay impactor's associated ejecta deposits lack typical extraterrestrial concentrations in the form of certain siderophile elements (PGEs), such as Ir (Tagle and Claeys, 2005; Grieve et *al*., 2007). It is also possible the Chesapeake Bay impactor was an achondrite because differentiated achondrites lack of a detectable extraterrestrial component in their target rocks since they are relatively depleted in PGEs (Grieve et *al*., 2007). However, previous work (Lee et *al*., 2006) concluded that the PGE abundance patterns in CBIS melt rocks are unlikely to be explained by a differentiated meteorite (achondrite). More recent work (Fritz et *al*., 2007) even suggested the CB impactor was a piece of material ejected from Earth's moon upon impact. It is suggested that Ni-rich spinel crystals found at Massignano are derived from a cometary impactor, not a chondrite (Pierrard et *al*., 1998). Additional work by Farley et *al*. (1998) at Massignano identified a peak concentration of extraterrestrial ^{3}He at 5.6 m, which they attributed to a comet shower during the late Eocene. A large portion of the scientific community agrees that the Chesapeake Bay impactor was a comet, but no definitive proof is yet available.

The magnitude of the $\delta^{13}C$ excursion associated with the impact event(s) is used to approximate the size of the Chesapeake Bay impactor by assuming it was a comet using the equation (Kent et *al*. 2003) for Tables 1, and 5 - 8. The mean $\delta^{13}C$ composition of comets is -45‰ (Table 1) (Messenger, 2000). A comet with a $\delta^{13}C$ value equaling -45‰ requires approximately 370 Gt of cometary C to produce a negative $\delta^{13}C$ anomaly of 0.45‰ in the deep-ocean reservoir holding ~37,000 Gt of exchangeable carbon (Falkowski and Raven, 1997) (Table 1). In contrast, 150 Gt of cometary carbon is needed for a cometary body with a $\delta^{13}C$ composition of -110‰ to cause a negative $\delta^{13}C$ anomaly of 0.45‰ in the deep-ocean (Table 1). To calculate the size of the predicted Chesapeake Bay impactor it is assumed comets are between 20 - 25 weight % C (Jessberger and Kissel, 1991) with a bulk density of 1500 kg/m^3 (Greenberg, 1998) (Table 1). A 12 km diameter comet ($\delta^{13}C$ equals -45‰) is required to produced the measured benthic $\delta^{13}C$ decrease of 0.4 - 0.5‰ (Table 5) or a 9 km diameter comet (-110‰ $\delta^{13}C$ composition) is required (Table 5). Numerical modeling studies of the CBIS (Collins and Wunnemann, 2005) determined the best estimate for the Chesapeake Bay impactor diameter size is 3.2 km. Additional studies (Poag et *al*., 2003) report a 3 - 5 km diameter impactor. An impactor of this size would only contribute 13 Gt of cometary C into the deep ocean reservoir (Table 5), which would not explain a 0.45‰ global carbon shift. Two 4 km comets would add only ~26 Gt of C to the deep ocean reservoir (Table 5).

The Popigai impactor is determined to be a type of ordinary chondrite OC (L-type) based on chromium isotope ratios and siderophile elements (Masaitis and Raikhlin, 1985; Masaitis, 1992; Kyte et *al*., 2004; Tagle and Claeys, 2004, 2005). L-type

chondrites contain between 0.10 - 0.20 wt. % C (Moore and Lewis 1967; Makjanic et *al*., 1993; Tingle, 1998). OCs (H, L, and LL) average 0.15 to 0.10 wt % C (Otting and Zahringer, 1967; Makjanic et *al*., 1993; Tingle, 1998; Hutchinson, 2004). The density for OCs is 2500 kg/m^3 (Mason, 1963). $\delta^{13}C$ compositions of L-Type chondrites are between -15 to -20‰, with an average isotopic value of -18‰ (Table 1) (Alexander et *al*., 1990, 1998). An L-type chondrite with a $\delta^{13}C$ composition of -18‰ requires ~990 Gt of OC carbon to generate a negative $\delta^{13}C$ anomaly of 0.45‰ in the deep-ocean reservoir (Table 1), which would have a diameter of 80 km. An L-type chondrite with a diameter similar to the predicted 5 km (Tagle and Claeys, 2004) Popigai impactor would introduce 0.26 Gt of chondritic C into the deep ocean reservoir (Table 6). If the two late Eocene impactors were both L-type chondrites with 5 km diameters, a mere 0.52 Gt of chondritic C would enter the deep ocean reservoir (Table 6).

The well-documented Chicxulub impact structure (250 km) was formed 65 Ma from a 10 ± 4 km diameter impactor, with some estimates reaching a maximum of 16 km (Alvarez et *al*., 1980; Chapman and Morrison, 1994; Morrison et *al*., 1994; Chapman, 2004). For comparative purposes, Table 7 lists the size and isotopic ratios of the exchangeable carbon reservoirs with each amount required to change the $\delta^{13}C$ value of the deep ocean reservoir by two differing end members (-1.5 and -2‰) representing the $\delta^{13}C$ anomaly found in K-T boundary sediments (Figure 4a) (e.g., Zachos and Arthur, 1986, 1989; Holser et *al*, 1989). The Chicxulub impactor is reported to have been a carbonaceous chondrite (CC) based on siderophile elemental concentrations and Os and Cr isotope ratios in sediments and projectiles (Ganapathy, 1980; Koeberl et *al*., 1994; Schuraytz et *al*., 1996; Kyte, 1998; Shukolyukov and Lugmair, 1998). CCs can hold

from 1.4 up to 6 wt. % C (Scott and Krot, 2005), average 2 wt. % C for all classes (Hutchison, 2004; Wood, 2005) and have the same average density as OCs (2500 kg/m^3) (Mason, 1963). A 10 km Chicxulub impactor would inject 80 Gt of chondritic C into the ocean atmospheric system (Table 8). Assuming the introduction of CC carbon into the ocean atmospheric system caused the entire $\delta^{13}C$ excursion associated with the K-T boundary (although, this seems unlikely considering the significance of changes in photosynthesis), then ~4,000 Gt of CC carbon is required to alter the global carbon system by the observed anomalies (Table 7). These three exercises demonstrate that $\delta^{13}C$ anomalies associated with extraterrestrial impact events reflect some perturbation in the global carbon system that must be linked to something other than the impact event itself.

5. Impact Events and Carbon Isotope Excursions

The large and rapid $\delta^{13}C$ excursion (-0.5‰) associated with the impact layers at Sites 1090 and 612 (Figures 16b and 21), and from previous work at Site 689 (Figure 10) (Vonhof et *al*., 2000) is interpreted to be global. The negative $\delta^{13}C$ excursion is coeval with the stratigraphically lower microkrystite layer at Site 612 (Figure 21) indicating the anomaly began at the time when the Popigai impactor struck Earth. The sudden onset of a large $\delta^{13}C$ excursion associated with Popigai cannot be explained by C input from an L-type chondrite, which Popigai is attributed to (Masaitis and Raikhlin, 1985; Masaitis, 1992; Kyte et *al*., 2004; Tagle and Claeys, 2004, 2005). Therefore, potential sources of the ^{12}C-rich carbon that produced the observed $\delta^{13}C$ anomaly are interpreted to reflect: 1) the injection of cometary carbon from the late Eocene Chesapeake Bay and Popigai impactors into the global carbon system (e.g. Kent et *al*., 2003; Cramer and Kent, 2005).

It is also possible the Popigai impactor was not an L-type chondrite but a comet, as shown in previous work. Assuming the Chesapeake Bay and Popigai impactors were both comets, they would inject a maximum of 30 to 35 Gt of C into the ocean-atmosphere system (Table 5). Yet, this assumption of two extraterrestrial cometary sources still does not yield enough carbon: six times this amount of cometary C with a mean $\delta^{13}C$ value equal to -45‰ is required to produce the observed $\delta^{13}C$ anomaly (Table 1); 2) the dissociation of massive amounts of methane hydrates stored on continental margins caused by an abrupt change in their temperature or pressure stability fields (e.g., Dickens et *al*., 1995, 1997; Katz et *al*., 1999, 2001; Svenson et *al*., 2004). Methane hydrates are a reservoir capable of abruptly releasing massive amounts of readily oxidized ^{12}C-rich carbon ($\delta^{13}C$ equals -60‰) into the ocean-atmosphere system (Table 1). The total size of carbon stored in methane hydrates globally has a large uncertainty, ranging from 500 to 2,500 Gt (Table 1). Less than 300 Gt of methane hydrate C is required to produce the observed -0.5‰ $\delta^{13}C$ decrease. An important, yet unappreciated, mechanism that can explain such a rapid and large $\delta^{13}C$ excursion is linked to the release of methane hydrates by means of an extraterrestrial impact event (e.g., Cramer and Kent, 2005); 3) a small portion of the observed anomaly is attributed to a decrease in the burial fraction of C_{org} relative to C_{carb}. However, this mechanism typically operates on 10^6 yr timescales (Shackleton, 1987) and requires a significant portion (~ 650 Gt) of the entire C_{org} reservoir to produce the observed $\delta^{13}C$ anomaly (Table 1). The magnitude, abrupt onset, and global nature of the $\delta^{13}C$ anomaly cannot be explained by a decrease in burial of C_{org} relative to C_{carb} alone; 4) a small portion due to the rapid burning of terrestrial organic matter in the form of peat deposits (Kurtz et *al*., 2003). Intense heat from the incoming

comet(s) caused significant wildfires that oxidized terrestrial C_{org} stored in the form of peat deposits. The present day peat reservoir holds 250 to 500 Gt of terrestrial C_{org} (Table 1); however upper Paleocene peat deposits were most likely 30% larger than today's (Beerling, 2000). The entire present-day peat reservoir is required to produce the observed $\delta^{13}C$ decrease.

However, none of these four factors by themselves can explain a very abrupt (<< 10 k.y.r.) and large (0.5 ‰) $\delta^{13}C$ decrease in the ocean-atmosphere reservoir. At this point, a combination of four factors are invoked: 1) injection of cometary C; 2) dissociation of massive amounts of methane; 3) decrease in burial fraction of C_{org} relative to C_{carb}; and 4) rapid burning of terrestrial C_{org} stored in peat deposits, to explain the observed benthic foraminifera and bulk-CO_3 $\delta^{13}C$ anomaly (-0.5‰) associated with the late Eocene extraterrestrial impact events.

5. Impact Events and Mass Extinctions

The K-T boundary mass extinctions and associated $\delta^{13}C$ anomaly are widely accepted to be the result of an extraterrestrial impact event since the discovery of Chicxulub (e.g., Alvarez et *al*., 1980). Disagreement exists as to what caused the P-Tr, Tr-J, and PETM mass extinctions and associated $\delta^{13}C$ anomalies (Figures 4a & b). $\delta^{13}C$ data from benthic foraminifera across the late Eocene impact horizon from this thesis supports the hypothesis that extraterrestrial impact events are capable of causing a global perturbation in the carbon system without producing massive biotic extinctions. It is still unresolved as to whether these boundary events are a response to extraterrestrial impact events.

The impact origin hypothesis for the P-Tr boundary is controversial because previous work found enhanced Ir concentrations (Holser et *al*., 1989; Koeberl et *al*., 2001) and shocked quartz grains (Retallack et *al*., 1998; Kaiho et *al*., 2001) at the P-Tr boundary with no conclusive results as to their origin (terrestrial/extraterrestrial) (Figure 4b). ^{3}He and Ar isotope studies of the P-Tr boundary in Japan (Becker et *al*., 2001) supports the extraterrestrial impact hypothesis, but is disputed by Farley and Mukhopadhyay (2001) who detected no extraterrestrial ^{3}He signature on the same samples. Isozaki (2001) refutes the work of Becker et *al*. (2001) by arguing that faulting displaced and destroyed an unknown amount of section. The hypothesis that an extraterrestrial impact triggered mass extinctions observed at the P-Tr boundary remains controversial and unresolved.

The Tr-J boundary extinctions and δ^{13}C anomaly may have been caused by an extraterrestrial impact event. Olsen et *al*. (1987) initially suggested the 100 km Manicouagan impact structure located in Quebec, Canada (Grieve, 2001) with a radiometric age date of 214 ± 1 Ma (Hodych and Dunning, 1992) for the cause of the Tr-J mass extinctions. Microtektites and shocked minerals are found within 10 Ma of the Tr-J boundary in Britain (Walkden et *al*., 2002). Olsen et *al*. (2002) reported an Ir anomaly of up to ~285 ppt associated with the palynologically recognized Tr-J boundary in the Newark rift basin, however the cause of the associated δ^{13}C anomaly and mass extinctions is still controversial.

The PETM δ^{13}C excursion and mass extinctions may be the consequence of an extraterrestrial impact. Schmitz et *al*. (1997) identified an Ir-rich layer (150 ppt) with high abundances of Ni associated with the PETM δ^{13}C anomaly at Zumaya they

attributed to either volcanic activity or an extraterrestrial impact event. Kent et *al*. (2003) postulated a cometary impact hypothesis to explain a small Ir anomaly occurring at the onset of a $\delta^{13}C$ decrease and the presence of abundant magnetic nannoparticles associated with the PETM in the North Atlantic. No impact crater has been identified around the time of the PETM, so much of the scientific community is reluctant to agree with the bolide hypothesis. However, many dynamic tectonic and sedimentary processes still active on Earth today mask the numerous impact structures that would otherwise be visibly prominent, like that on other planets and their moons.

6. Conclusions

In this thesis: 1) the sixteen glass microspherules found at SSQ are interpreted to be the result of drilling contamination; 2) the Chesapeake Bay microtektite and Popigai cpx-bearing (or microkrystite) layers are shown to be separated by ~ 4 kyr at Site 1090 based on magnetostratigraphic interpolation; 3) a first order correlation is provided of upper Eocene ejecta layers identified in ODP Site 1090 to the geomagnetic polarity timescale in Chron C16n.1n (279 mbsf), with a corresponding magnetochronologic age of 35.430 Ma. The Ir anomaly located 10 cm above has an interpolated magnetochronologic age of 35.426 Ma; 4) benthic foraminiferal $\delta^{13}C$ and $\delta^{18}O$ data from Southern Ocean Site 1090 are presented across the impact ejecta layer from 34.6 - 35.8 Ma (8 kyr sampling) and 33.7 - 36 Ma (16 kyr sampling). Results show a transient $\delta^{13}C$ decrease (277 - 278 mbsf) of 0.5‰ is associated with the impact horizon. The $\delta^{13}C$ anomaly persists for ~ 250 kyr; then the signal returns to 'pre-impact' values. Following recovery from the transient and global $\delta^{13}C$ excursion, no long-term changes

in $\delta^{13}C$ values are associated with the late Eocene impact events. The record shows no significant changes in benthic foraminiferal $\delta^{18}O$ values across the ejecta layers, implying that no major changes in deep-water temperatures occurred; 5) bulk-carbonate $\delta^{13}C$ and $\delta^{18}O$ data from Site 1090 (35.44 to 35.38 Ma) (every ~ 2 kyr) show a negative $\delta^{13}C$ and $\delta^{18}O$ anomaly of ~ 0.5‰ at the ejecta layer (279 mbsf); 6) benthic foraminiferal data from North Atlantic DSDP Site 612 display a negative $\delta^{13}C$ excursion of ~ 0.5‰ across the ejecta horizon. Coeval benthic foraminiferal records show the negative $\delta^{13}C$ excursion in new benthic data from New Jersey slope Site 612 showing a 0.5‰ change, though this record is partially truncated due to a hiatus and new benthic data from Southern Ocean Site 1090 shows a 0.5‰ anomaly. Published data from Southern Ocean Site 689 shows a larger excursion (1.0‰) and Pacific Ocean Site 1218 published data shows a smaller anomaly (0.4‰). The $\delta^{13}C$ excursion is suggested to reflect a perturbation in the global carbon cycle and to be directly related to the late Eocene impactor(s).

References

Adams, J., Faure, H., Faure-Denard, L.,McGlade, J.M., Woodward, F.I., 1990. Increases in terrestrial carbon storage from the Last Glacial Maximum to the present. *Nature*, v. 348, pp. 711-14.

Alexander, C.M., Arden, J.W., Ash, R.D., Pillinger, C.T., 1990. Presolar components in the ordinary chondrites. *Earth and Planetary Science Letters*, v. 99, 220-29.

Alexander, C.M., Russell, S.S., Arden, J.W., Ash, R.D., Grady, M.M., Pillinger, C.T., 1998. The origin of chondritic macromolecular organic matter: A carbon and nitrogen isotope study. *Meteoritics and Planetary Science*, v. 33, pp. 603-22.

Alvarez, L.W., Alvarez, W., Asaro, F., michel, H.V., 1980. Extraterrestrial cause for the Cretaceous-Tertiary extinction. *Science*, v. 208, pp. 1095-1108.

Alvarez, W., Asaro, F., Michel, H.V., Alvarez, L.W., 1982. Iridium anomaly approximately synchronous with terminal Eocene extinctions. *Science*, 216:886-888.

Arpigny, C., Jehin, E., Manfroid, J., Hutsemekers, D., Schulz, R., Stuwe, J., Zucconi, J. M., Ilyin, I., 2003. Anomalous nitrogen isotope ratios in comets. *Science*, v. 301, pp. 1522-24.

Arthur, M.A., and Schlanger, S.O., Cretaceous 'oceanic anoxic events' as casual factors in development of reef-reservoired giant oil fields. *Bulletin Amer. Assoc. Petro. Geologists*, v. 63, pp. 870-85.

Arthur, M.A., Schlanger, S.O., Jenkyns, H.C., 1987. The Cenomanian-Turoian Oceanic Anoxic Event, II. Palaeoceanographic controls on organic-matter production and preservation, *in* Brooks, J., and Fleet, A., (eds) Marine Petroleum Source Rocks: *Geological Society of London Special Publication*, v. 24, pp. 401-20.

Arthur, M.A., Brumsack, H.-J., Jenkyns, H.C., Schlanger, S.O., 1990. Stratigraphy, geochemistry, and paleoceanography of organic-carbon rich Cretaceous sequences. *In: Cretaceous Resources, Events, and Rhythms.* (eds) R.N. Ginsburg and B. Beaudoin, Kluwer Academic, Norwell, MA, pp. 75-119.

Aubry, M.P., and Sanfilippo, A., Late Paleocene-Early Eocene sedimentary history in western Cuba: Implications for the LPTM and for regional tectonic history. *Micropaleontology*, v. 45, pp. 5-18.

Axelrod, D.I., 1984. An interpretation of Cretaceous and Tertiary biota in polar regions. *Palaeogeo., Palaeoclim., Palaeoecology,* v. 45, pp. 105-147.

Bains, S., Corfield, R.M., Norris, R.D., 1999. Mechanisms of climate warming at the end of the Paleocene. *Science*, v. 285, pp. 724-27.

Barker, P.F., Kennett, J.P., et *al*., 1990. *Proceedings of the Ocean Drilling Program, Scientific Results, 113:* 1-785.

Barnes, V.E., 1939. North American Tektites. *University of Texas Publications*, v. 3945, pp. 477-656.

Barnes, V.E., 1951. New Tektite areas in Texas. *Geological Society of America Bulletin*, v. 62, pp. 1422.

Barron, E.J., and Peterson, W.H., 1991. The Cenozoic ocean circulation based on ocean general circulation model results. *Palaeogeography, Palaeoclimatology, Palaeoecology*, v. 83, pp. 1-28.

Barrera, E., and Huber, B.T., 1991. Paleogene and early Neogene oceanography of the Southern Ocean: Leg 119 foraminifer stable isotope results. *Proc. ODP Sci. Res.* 119, 693-717.

Baud, A., Magaritz, M., Holser, W., 1989. Permian-Triassic of the Tethys: Carbon isotope studies. *International Journal of Earth Sciences*, v. 78, no. 2, pp. 649-77.

Becker, L., 2001. Impact event at the Permian-Triassic boundary: evidence from extraterrestrial noble gases in… *Science*, v. 291, no. 5508, pp. 4.

Beerling, D., 2000. Increased terrestrial carbon storage across the Paleocene-Eocene boundary. *Palaeogeography, Palaeoclimatology, Palaeoecology*, v. 161, no. 3-4, pp. 395-405.

Berggren, W.A., Kent, D.V., Flynn, J.J., VanCouvering, J.A., 1985. Cenozoic geochronology. *Geological Society of America Bulletin*, v. 96, no. 11, pp. 1407-1418.

Berggren, W.A., Kent, D.V., Swisher III, C.C., Aubry, M.P., 1995. A revised Cenozoic geochronology and chronostratigraphy. In: Berggren, W.A., Kent, D.V., Swisher III, C.C., Aubry, M.P., Hardenbol, J., (eds) Geochronology, Time Scales and Global Stratigraphic Correlation: SEPM Special Publication no. 54, pp 129-212.

Berner, R.A., 1990. Atmospheric carbon dioxide levels over Phanerozoic time. *Science*, v. 249, 1382-1386.

Berner, R.A., 2002. Examination of hypotheses for the Permo-Triassic boundary extinction by carbon cycle modeling. *Proc. of the National Academy of Sci.,* v. 99, no. 7, pp. 4172-77.

Berner, R.A., 2004. The Phanerozoic Carbon Cycle: CO_2 and O_2, Oxford, Univ. Press, pp. 160.

Berner, R.A., and Raiswell, R., 1983. Burial of organic carbon and pyrite sulfur in sediments over Phanerozoic time: A new theory. *Geochimica et Cosmochimica Acta*, v. 47, pp. 855-62.

Bice, D.M., and Montanari, A., 1988. Magnetic stratigraphy of the Massignano section across the Eocene-Oligocene boundary. In: Premoli Silva, I., Coccioni, R., Montanari, A., (eds) The Eocene-Oligocene boundary in the Marche-Umbria Basin (Italy). International Subcommission on Paleontology and Stratigraphy Special Publication II, pp. 111-117.

Blasing, T.J., and Jones, S., 2002. *Current Greenhouse Gas Concentrations. Trends: A Compendium of Data on Global Change*. Carbon Dioxide Information Analysis Center, US Dept. of Energy, Oak Ridge, TN.

Bodiselitsch, B., Montanari, A., Koeberl, C., Coccioni, R., 2004. Delayed climate cooling in the late Eocene caused by multiple impacts: high-resolution geochemical studies at Massignano, Italy. *Earth and Planetary Science Letters*, v. 223, pp. 283-302.

Boersma, A., Premoli-Silva, I., Shackleton, N.J. 1987**,** Atlantic Eocene planktonic foraminiferal paleohydrographic indicators and stable isotope paleoceanography. *Paleoceanography,* v. 2, no. 3, pp. 287-331.

Bohaty, S. M. and J. C. Zachos, 2003, A significant Southern Ocean warming event in the late middle Eocene. *Geology*. v. 31, pp. 1017-1020.

Bohor, B.F., Betterton, W.J., Foord, E.E., 1988. Coesite, glass, and shocked quartz at DSDP Site 612: Evidence for nearby impact in the late Eocene. *Lunar and Planetary Institute Conference* XIX, pp. 114-15.

Bottomley, R., Grieve, R., York, D., Masaitis, V., 1997. The age of the Popigai impact event and its relation to events at the Eocene/Oligocene boundary. *Nature*, v. 388, pp. 365-68.

Bowen, G.J., Clyde, W.C., Koch, P.L., Ting, S., Alroy, J., Tsubamoto, T., Wang, Y., Wang, Y., 2002. Mammalian dispersal at the Paleocene/Eocene Boundary. *Science*, v. 295, pp. 2062-65.

Bowring, S.A., Erwin, D.H., Jin, T.G., Martin, M.W., Davidek, K., Wang, W., 1998. U/Pb zircon geochronology and tempo of the End-Permian mass extinction. *Science*, v. 280, pp. 1039-45.

Bralower, T., 2002. Evidence of surface water oligotrophy during the Paleocene-Eocene thermal maximum: nannofossil assemblage data from Ocean Drilling Program Site 690, Maud Rise, Weddell Sea. *Paleoceanography*, v. 17, no. 2, pp. 1023.

Bralower, T.J., Sliter, W.V., Arthur, M.A., Leckie, R.M., Allard, D., Schlanger, S.O., 1993. Dysoxic/anoxic episodes in the Aptian-Albian (Early Cretaceous), *In: The Mesozoic Pacific: Geology, Tectonics, and Volcanism, Geophys. Monogr. Ser.,* v. 77, M.S. Pringle et *al.*, (eds), AGU, Washington, DC, pp. 5-37.

Bralower, T., Thomas, D., Zachos, J., Hirschmann, M., Rohl, U., Sigurdsson, H., Thomas, E., Whitney, D., 1997. High-resolution records of the late Paleocene thermal maximum and circum-Caribbean volcanism: is there a casual link? *Geology*, v. 25, pp. 963-66.

Bralower, T.J., CoBabe, E., Clement, B., Sliter, W.V., Osburn, C.L., Longoria, J., 1999. The record of global change in mid-Cretaceous (Barremian-Albian) sections from the Sierra Madre, northeastern Mexico. *Journal of Foraminiferal Research*, v. 29, pp. 418-37.

Brenneke, J.C., and Anderson, T.F., 1977. Carbon isotope variations in pelagic sediments. *EOS, Trans. Am. Geophys. Union,* v. 58 p. 415.

Broecker, W.S., 1970. A boundary condition on the evolution of atmospheric oxygen. *Journal of Geophysical Research*, v. 75, pp. 3553-57.

Broecker, W.S., 1975. Climate change: are we on the brink of a pronounced global warming? *Science*, v. 189, pp. 460-63.

Broecker, W.S., 1982. Ocean chemistry during glacial time. *Geochim. Cosmochim. Acta.* v. 46, pp. 1689-1705.

Broecker, W.S., 1986. Oxygen isotope constraints on surface ocean temperatures. *Quaternary Research*, v. 26, pp. 121-34.

Broecker, W.S., and Peng, T.H., 1982. Tracers in the Sea. Eldigio, Palisades, pp. 691.

Broecker, W.S., and Peacock, S., 1999. An ecologic explanation for the Permo-Triassic carbon and sulfur isotope shifts. *Global Biogeochemical Cycles*, v. 13, no. 4, pp. 1167-72.

Broecker, W.S., Peng, T.-H., Ostlund, G., Stuiver, M., 1985. The distribution of bomb-radiocarbon in the ocean. *Journal of Geophysical Research*, v. 90, pp. 6953-70.

Bruce, G.A., 1959. Tektites in Georgia. *Gems Mineralogy*, v. 264, no. 22-23, pp. 65-9.

Burns, C.A., 1989. Timing between a large impact and a geomagnetic reversal and the depth of NRM acquisition in deep-sea sediments. In Geomagnetism and Paleomagnetism (eds.) Lowes, F.J., et *al*. pp. 253-261, Kluwer Academic Publishers.

Cande, S.C., and Kent, D.V., 1992. A new geomagnetic polarity timescale for the late Cretaceous and Cenozoic. *Journal of Geophysical Research*, v. 97, pp. 13917-51.

Cande, S.C., and Kent, D.V., 1995. Revised calibration of the geomagnetic polarity timescale for the Late Cretaceous and Cenozoic, *Journal of Geophysical Research*, v. 100, pp. 6093-95.

Carmack, E.C., and Foster, T.D., 1975. On the flow of water out of the Weddell Sea. *Deep Sea Research*, v. 22, pp. 711-24.

Cervato, C., and Burckle, L.H., 2003. Pattern of first and last appearance in diatoms: Oceanic circulation and the position of the Polar Fronts during the Cenozoic. *Paleoceanography*, v. 18, no. 2, pp. 33-1-33-9.

Channell, J.T., Galeotti, S., Martin, E., Billups, K., Scher, H.D., and Stoner, J.S., 2003. Eocene to Miocene magnetostratigraphy, biostratigraphy, and chemostratigraphy at ODP Site 1090 (sub-Antarctic South Atlantic). *Geological Society of America Bulletin,* v. 115 no. 5

Chapmann, C.R., 2004. The hazard of near-Earth asteroid impacts on Earth. *Earth and Planetary Science Letters*, v. 222, pp. 1-15.

Chapman, C.R., and Morrison, D., 1994. Impacts on the Earth by asteroids and comets: assessing the hazard. *Nature*, v. 367, pp. 33-40.

Clymer, A.K., Bice, D.M., Montanari, A., 1996. Shocked quartz from the late Eocene: Impact evidence from Massignano, Italy. *Geology*, v. 24, pp. 483-86.

Coccioni, R., Basso, D., Brinkhuis, H., Galeotti, S., Gardin, S., Monechi, S., Spezzaferri, 2000. Marine biotic signals across a late Eocene impact layer at Massignano, Italy: evidence for long-term environmental perturbations? *Terra Nova*, v. 12, pp. 258-63.

Collins, G.S. and Wünnemann, K., 2005. How big was the Chesapeake Bay impact? insight from numerical modeling. *Geology*, v. 33, no. 12, pp. 925-28.

Courtillot, V., Jaupart, C., Manighetti, I., Tapponnier, P., Besse, J., 1999. On causal links between flood basalts and continental breakup. *Earth and Planetary Science Letters*, v. 166, pp. 177-95.

Courtillot, V., and Renne, P.R., 2003. On the ages of flood basalt events. *Comptes Rendus Geoscience*, v. 335, no. 1, pp. 113-40.

Coxall, H.K., Wilson, P.A., Palike, H., Lear, C.H., Backman, J., 2005. Rapid step-wise onset of Antarctic glaciation and deeper calcite compensation in the Pacific Ocean. *Nature*, v. 433, pp. 53-7.

Cousin, M., and Thein, J., 1987. Lithologic and geochemical changes across unconformities at Site 612, New Jersey Transect: *In: Initial Reports of the Deep Sea Drilling Project,* C.W. Poag, A.B. Watts *et al.* (eds), 95, pp. 549-64.

Craig, H., 1953. The geochemistry of the stable carbon isotopes. *Geochimica et Cosmochimica Acta*, v. 3, no. 2-3, pp. 53-92.

Cramer, B.S., and Kent, D.V., 2005. Bolide summer: The Paleocene/Eocene thermal maximum as a response to an extraterrestrial trigger. *Palaeogeography, Palaeoclimatology, Palaeoecology*, v. 224, pp. 144-66.

Cramer, B.S., Wright, J.D., Kent, D.V., Aubry, M.-P., 2003. Orbital climate forcing of $\delta^{13}C$ excursions in the late Paleocene-early Eocene (chrons C24n-C25n). *Paleoceanography*, v. 18, no. 4, 1097, doi:10.1029/2003PA000909.

Crouch, E.M., Heilmann-Clausen, C., Brinkhuis, H., et *al*., 2001. Global dinoflagellate event associated with the late Paleocene thermal maximum. *Geology*, v. 29, pp. 315-18.

Crowley, T.J., 1995. Ice age terrestrial carbon changes revisted. *Global Biogeochemical Cycles*, v. 9, pp. 377-89.

Curry, W.B., and Lohmann, G.P., 1983. Reduced advection into the Atlantic Ocean eastern basins during late glacial maximum. *Nature,* v. 306, pp. 577-580.

Curry, W.B., and Lohmann, G.P., 1985. Carbon deposition rates and deep water residence time in the equatorial Atlantic ocean throughout the last 160,000 years, *In*: Sundquist, E.T., and Broecker, W.S., eds., *The Carbon Cycle and Atmospheric CO2: Natural Variations Archean to Present, Am. Geophys. Un., Geophys. Monograph*: vol. 32*,* pp. 285-301.

Curry, W.B., Duplessy, J.C., Labeyrie, L.D., Shackleton, N.J., 1988. Changes in the distribution of $\delta^{13}C$ of deep water $\sum CO_2$ between the last glaciation and the Holocene. *Paleoceanography*, v. 3, no. 3, pp. 317-341.

Deines, P., 1992. Mantle carbon: concentration, mode of occurrence, and isotopic composition. *In: Early Organic Evolution: Implications for Mineral and Energy Resources*, (eds) M. Schidlowski, et *al*., Springer, Berlin, pp. 133-46.

Delano and Lindsley, 1982. Chemical systematics among the moldavite tektites. *Geochim. Cosmochim. Acta.* v. 46, pp. 2447-2452.

Deutsch, A., and Koeberl, C., 2006. Establishing the link between the Chesapeake Bay impact structure and the North American tektite strewn field: The Sr-Nd isotopic evidence. *Meteoritics and Planetary Science*, v. 41, no. 5, pp. 689-703.

Dickens, G.R., O'Neil, J.R., Rea, D.K., Owen, R.M., 1995. Dissociation of oceanic methane hydrate as a cause of the carbon isotope excursion at the end of the Paleocene. *Paleoceanography*, v. 10, p. 965-71.

Dickens, G.R., Castillo, M.M., Walker, J.C., 1997. A blast of gas in the latest Paleocene: Simulating first-order effects of massive dissociation of oceanic methane hydrate. *Geology*, v. 25, pp. 259-62.

Diester-Haass, L. and Zahn, R., 1996. Eocene-Oligocene transition in the Southern Ocean: History of water mass circulation and biological productivity. *Geology*, v. 24, no. 2, pp. 163-66.

Donnelly, T.W., and Chao, E.C.T., 1973. Microtektites of late Eocene age from the eastern Caribbean Sea. *Initial Reports Deep Sea Drilling Project* 15, p. 1031-37.

Duplessy, J.C., Shackleton, N.J., Fairbanks, R.G., Labeyrie, L., Oppo, D., Kallel, N., 1988. Deepwater source variations during the last climatic cycle and their impact on the global deepwater circulation. *Paleoceanography*, v. 3, pp. 343-60.

Durrani, S.A., and Khan, H.A., 1971. Ivory Coast microtektites: fission track age and geomagnetic reversals. *Nature*, v. 232, pp. 320-23.

Emiliani, C., 1955. Pleistocene temperatures. *Journal of Geology*, v. 63, pp. 538-78.

Engelhardt, W.V., Luft, E., Arndt, J., Schock, H., Weiskirchner, W., 1987. Origin of moldavites. *Geochim. Cosmochim. Acta,* v. 51, pp. 1425- 1443.

Epstein, S., Buchsbaum, R., Lowenstam, H., Urey, H., 1951. Carbonate-water temperature scale. *Geological Society of America Bulletin*, v. 62, pp. 417-26.

Epstein, S., Buchsbaum, R., Lowenstam, H., Urey, H., 1953. Revised carbonate-water isotopic temperature scale. *Geological Society of America Bulletin*, v. 64, pp. 1315-25.

Erbacher, J., Thurow, J., Littke, R., 1996. Evolution patterns of radiolaria and organic matter variations: a new approach to identify sea level changes in mid-Cretaceous pelagic. *Geology*, v. 24, pp. 499-502.

Erez, J., 1978. Vital effect on stable-isotope composition seen in foraminifera and coral skeletons. *Nature*, v. 273, pp. 199-202.

Erwin, D.H., 1993. The great Paleozoic crisis. New York, NY, Columbia Uni. Press, 327 pp.

Estes, R., and Hutchison, J.H., 1980. Eocene lower vertebrates from Ellesmere Island, Canadian Artic Archipelago. *Palaeogeogr., Palaeoclimatol., Palaeoecol.*, v. 30, pp. 325-47.

Falkowski, P.G., 2005. Biogeochemistry of Primary Production in the Sea. *In:* W. H. Schlesinger (ed), Biogeochemistry: *Treatise on Geochemistry*, v. 8, Elsevier Press, Oxford, UK, pp. 185-214.

Falkowski, P.G., and Raven, J.A., 1997. "Carbon acquisition and assimilation." Aquatic Photosynthesis. Malden: Blackwell Science Pubs., 128-162.

Farley, K.A., and Mukhopadhyay, S., 2001. An extraterrestrial impact at the Permian-Triassic Boundary? *Science*, v. 293, no. 5539, p. 2343a.

Farley, K.A., Montanari, A., Shoemaker, E.M., and Shoemaker, C.S., 1998. Geochemical evidence for a comet shower in the late Eocene. Science, v. 280, pp. 1250-53.

Farmer, J.G., and Baxter, M.S., 1974. Atmospheric carbon dioxide levels as indicated by the stable isotope record in wood. *Nature*, v. 247, pp. 273-75.

Faure, G. 1986. Principles of Isotope Geochemistry 2nd ed. New York: John Wiley.

Florindo, F., and Roberts, A.P., 2005. Eocene-Oligocene magnetobiochronology of ODP Sites 689 and 690, Maud Rise, Weddell Sea, Antarctica. *GSA Bulletin*, v. 117, no. 1-2, pp. 46-66.

Francois, L.M., Godderis, Y., Warnant, P., Ramstein, G., de Noblet, N., Lorenz, S., 1999. Carbon stocks and isotopic budgets of the terrestrial biosphere at mid-Holocene and last glacial maximum times. *Chemical Geology*, v. 159, pp. 163-89.

Francey, R.J., Allison, C.E., Etheridge, D.M., Trudinger, C.M., Enting, I.G., Leuenberger, M., Langenfelds, R.L., Michel, E., Steele, L.P., 1999. A 1000-year high precision record of delta ^{13}C in atmospheric CO_2. *Tellus Series B-Chemical and Physical Meteorology*, v. 51, 170-93.

Friedli, H., Lotscher, H., Oeschger, H., Siegenthaler, U., Stauffer, B., 1986. Ice core record of the $^{13}C/^{12}C$ ratio of atmospheric CO_2 in the past two centuries. *Nature*, v. 324, pp. 237-38.

Fritz, J., Tagle, R., Artemieva, N., 2007. Raining moon and the late Eocene asteroid shower. *Proc. of Lunar and Plant. Sci. Conf.* XXXVIII, (abs) 1069.

Froelich, P.N., Bender, M.L., Luedthe, N.A., Heath, G.R., DeVries, T., 1982. The marine phosphorous cycle. *American Journal of Science*, v. 282, pp. 474-511.

Funakawa, S., Nishi, H., Moore, T.C., Nigrini, C.A., 2006. Data report: Late Eocene-early Oligocene radiolarians, ODP Leg 199 Holes 1218A, 1219A, and 1220A, central Pacific. *In:* Wilson, P.A., Lyle, M., Firth, J.V., (eds), *Proc. ODP, Sci. Results,* 199: College Station, TX (Ocean Drilling Program), 1-74.

Galeotti, S., Coccioni, R., and Gersonde, R., 2002. Middle Eocene-Early Pliocene Subantarctic planktic foraminiferal biostratigraphy of Site 1090, Agulhas Ridge. *Marine Micropaleontology,* v. 45, pp. 357-381.

Galli, M.T., Jadoul, F., Bernasconi, S.M., Weissert, H., 2005. Anomalies in global carbon cycling and extinction at the Triassic-Jurassic boundary: evidence from a marine C-isotope record. *Palaeogeography, Palaeoclimatology, Palaeoecology*, v. 216, pp. 203-14.

Ganapathy, R., 1980. A major meteorite impact on the earth 65 million years ago: Evidence from the Cretaceous-Tertiary boundary clay. *Science*, v. 209, pp. 921-23.

Ganapathy, R., 1982. Evidence for a major meteorite impact on the Earth 34 million years ago: Implication for Eocene extinctions. *Science*, v. 216, pp. 885-86.

Garlick, G.D., Naeser, C.W., O'Neil, J.R., 1971. A Cuban tektite. *Geochimica, Cosmochimica Acta*, v. 35, pp. 731-34.

Gentner, W., Kleinman, B., Wagner, G.A., 1967. New K-Ar and fission track ages of impact glasses and tektites. *Earth and Planetary Science Letters*, v. 2, pp. 83-6.

Gentner, W., Glass, B.P., Storzer, D., Wagner, G.A., 1970. Fission track ages and ages of deposition of deep-sea microtektites. *Science*, v. 168, pp. 359-61.

Gersonde, R., Hodell, D.A., Blum, P., et al., 1999. *Proc. ODP, Init. Repts*., 177[CD-ROM]. Available from: Ocean Drilling Program, Texas A&M University, CollegeStation, TX 77845-9547, U.S.A.

Gingerich, P., 2003. Mammalian responses to climate change at the Paleocene-Eocene boundary: Polecat Bench record in northern Bighorn Basin, Wyoming. *In: Causes and Consequences of Globally Warm Climates in the Early Paleogene, Geological Society of America Special Publication*, 369, Geological Society of America, Boulder, CO, pp. 463-78.

Glass, B.P., 1989. North American tektite debris and impact ejecta from DSDP Site 612, *Meteoritics,* v. 24, pp. 209- 218.

Glass, B.P., 2000. Cenozoic microtektites and clinopyroxene-bearing spherule layers marine sediments. *In: Terrestrial and Cosmic Spherules*. (ed) D.C. Detre, Akademiai Kiado, pp. 55-71.

Glass, B.P., 2002. Upper Eocene impact ejecta/spherule layers in marine sediments. *Chemie der Erde*, v. 62, pp. 173-96.

Glass B.P., 2003. Australasian microtektites in the South China Sea: Implications regarding the location and size of the source crater (abs) *Lunar and Planetary Science* XXXIV, #1092

Glass, B.P., and Zwart, M.J., 1977. North American microtektites, radiolarian extinctions and the age of the Eocene-Oligocene boundary. In: F.M. Swain, (ed) *In:* Stratigraphic Micropaleontology of the Atlantic Basin and Borderlands. Elsevier, Amsterdam, pp. 553-568.

Glass, B.P., and Zwart, M.J., 1979. North American microtektites in Deep Sea Drilling Project cores from the Caribbean Sea and Gulf of Mexico. *Geological Society of America Bulletin,* v. 90, pp. 595-602.

Glass, B.P., and Burns, C.A., 1987. Late Eocene crystal-bearing spherules: Two layers or one? *Meteoritics*, v. 22, pp. 265-79.

Glass, B.P., and Burns, C.A., 1988. Microkrystites: A new term for impact produced glassy spherules containing primary crystallites. *Proc. 18th Lunar and Planetary Sci. Conference*, pp. 455-58.

Glass, B.P. and Wu, J., 1993. Coesite and shocked quartz discovered in the Australian and North American microtektite layers. *Geology*, v. 21, pp. 435-38.

Glass, B.P. and Koeberl, C., 1999. ODP Project Hole 689B spherules and upper Eocene microtektite and clinopyroxene-bearing spherule strewn fields. *Meteoritics and Planet. Science,* v. 34, pp. 197-208.

Glass, B.P., and Liu, S. 2001. Discovery of high-pressure ZrSiO4 polymorph in naturally occurring shock metamorphosed zircons. *Geology*, v. 29, pp. 371-73.

Glass, B.P., Baker, R.N., Storzer, D., Wagner, G.A., 1973. North American microtektites from the Caribbean Sea and their fission track age. *Earth and Planetary Science Letters*, v. 19, pp. 184-92.

Glass, B.P., Burns, C.A., Lerner, D.H., and Sanfilippo, A. 1984. North American tektites and microtektites from Barbados, West Indies. *Meteoritics,* v. 19, pp. 228.

Glass, B.P., Burns, C.A., Crosbie, J.R., DuBois, D.L., 1985. Late Eocene North American microtektites and clinopyroxene-bearing spherules. *Proc. of the 16th Lunar and Planetary Science Conf. Journal of Geophysical Research* 90:D175-D196.

Glass, B.P., Hall, C.M., York, D., 1986. $^{40}Ar/^{39}Ar$ laser probe dating of North American tektite fragments from Barbados and the age of the Eocene-Oligocene boundary. *Chemical Geology,* v. 59, pp. 181-86.

Glass, B.P., Kent, D.V., Schneider, D.A., Tauxe, L., 1991. Ivory Coast microtektite strewn field: description and relation to the Jaramillo geomagnetic event. *Earth and Planetary Science Letters*, v. 107, pp. 182-96.

Glass, B.P., Koeberl, C., Blum, J.D., McHugh, C.M.G. 1998, Upper Eocene tektite ejecta layer on the continental slope off New Jersey. *Meteoritics and Plan. Sci.,* v. 33, pp. 229-241.

Glass, B.P., Huber, H., Koeberl, C., 2004a. Geochemistry of Cenozoic microtektites and clinopyroxene-bearing spherules. *Geochimica et Cosmochimica Acta*, v. 68, no. 19, pp. 3971-4006.

Glass, B.P., Liu, S., Montanari, A., 2004b. Impact ejecta in upper Eocene deposits at Massignano, Italy. *Meteoritics and Planetary Science*, v. 39, pp. 589-97.

Greenburg, J.M., 1998. Making a comet nucleus. *Astron., Astrophys.,* v. 330, pp. 375-80.

Greenwood, D.R., and Wing, S.L., 1995. Eocene continental climates and latitudinal temperature gradients. *Geology*, v. 23, no. 11, pp. 1044-48.

Greive, R.A., Cintala, M.J., Tagle, R., 2007. Planetary Impacts. *In:* (eds) L.A. McFadden, P.R. Weissman, T.V. Johnson, Encyclopedia of the Solar System, 2nd edition. Elsevier, Amsterdam, pp. 813-28.

Guinasso, N.L., and Schink, D.R., 1975. Quantitative estimates of biological mixing rates in abyssal sediments. *Journal of Geophysical Research*, v. 18, pp. 3032-43.

Hays, J.D., Imbrie, J., Shackleton, N.J., 1976. Variations in the earth's orbit: pacemaker of the ice ages. *Science*, v. 194, pp. 1121-1132.

Hesselbo, S.P., Robinson, S.A., Surlyk, F., Piasecki, S., 2002. Terrestrial and marine extinction at the Triassic-Jurassic boundary synchronized with major carbon-cycle perturbation: A link to initiation of massive volcanism? *Geology*, v. 30, no. 3, pp. 251-54.

Hesselbo, et *al.,* 2007. Triassic-Jurassic boundary events: Problems, progress, possibilities. *Palaeogeography, Palaeoclimatology, Palaeoecology*., v. 244, pp. 1-10.

Hildebrand, A.R., Penfield, G.T., Kring, D.A., Pilkington, M., Camargo Z., A., Jacobsen, S.B., Boynton, W.V., 1991. Chicxulub crater: A possible Cretaceous/Tertiary boundary impact crater on the Yucatan peninsula, Mexico. *Geology,* v. 19, pp. 867-871.

Hodych, J.P., and Dunning, G.R., 1992. Did the Manicouagan impact trigger end-of-Triassic mass extinction? *Geology*, v. 20, pp. 51-54.

Holland, H.D., 1978. The chemistry of the atmosphere and oceans. Wiley, New York.

Holser, W.T., Schonlaub, H.P., Attrep Jr., M., Boeckelmann, K., Klein, P., Magaritz, M., et *al*., 1989. A unique geochemical record at the Permian-Triassic boundary. *Nature*, v. 337, 39-44.

Hooker, J.J., 1996. Mammalian biostratigraphy across the Paleocene-Eocene boundary in the Paris, London, and Belgian basins, *In: Correlations of the Early Paleogene in Northwest Europe,* (eds) R.O. Knox et *al*., *Geological Society of America Special Publication*, 101, pp. 205-18.

Hooker, J.J., and Dashzeveg, D., 2003. Evidence for direct mammalian faunal interchange between Europe and Asia near the Paleocene-Eocene boundary. *In: Causes and Consequences of Globally Warm Climates in the Early Paleogene, Geological Society of America Special Publication*, 369, Geological Society of America, Boulder, CO, pp. 463-78.

Horton, J.W., and Izett, G.A., 2005. Crystalline rock ejecta and shocked minerals of the CBIS, USGS-NASA Langley core, Hampton, Virginina, *In:* Horton, J.R., Powars, D.S., Gohn, G.S., (eds), Studies of the Chesapeake Bay impact structure. *USGS Professional Paper* 1688, pp. E1-30.

Houghton, R.A., 2005. The Contemporary Carbon Cycle. *In:* W. H. Schlesinger (ed), Biogeochemistry: *Treatise on Geochemistry*, v. 8, Elsevier Press, Oxford, UK, pp. 473-514.

Howard, H.H., 1968. Glass pieces that hit the Earth 33 million years ago are found in Georgia. *Macon News*, v. 85, no. 187, pp. 6.

Hsu, K.J., and Mckenzie, J.A., 1985. A "Strangelove" Ocean in the early Tertiary. *In:* In: Sundquist, E.T., and Broecker, W.S., (eds), *The Carbon Cycle and Atmospheric CO_2: Natural Variations Archean to Present, Am. Geophys. Un., Geophys. Monograph*: vol. 32*,* pp. 469-486.

Hsu, K.J., and Mckenzie, J.A., 1990. Carbon-isotope anomalies at era boundaries; Global catastrophes and their ultimate cause. *In: Global Catastrophes in Earth history; An interdisciplinary conference on impacts, volcanism, and mass mortality*. *Geological Society of America Special Publication*, 247, Geological Society of America, Boulder, CO, pp. 61-70.

Hsu, K.J., He, Q., McKenzie, J.A., et *al.*, 1982. Mass mortality and its environmental and evolutionary consequences. *Science*, v. 216, no. 4543, pp. 249-56.

Huber, M., Sloan, L.C., Shellito, C., 2003. Early Paleogene oceans and climate: A fully coupled modeling approach using the NCAR CCSM. *In: Causes and Consequences of Globally Warm Climates in the Early Paleogene, Geological Society of America Special Publication*, 369, Geological Society of America, Boulder, CO, pp. 25-47.

Hutchison, R., 2004. The chondrites: chemistry and classification. *In*: Meteorites: A Petrologic, Chemical, and Isotopic synthesis. The Press Syndicate of the Uni. of Cambridge, Cambridge, UK.

Imbrie, J., Hays, J.D., Martinson, D.G., McIntyre, A., Mix, A.C., Morley, J.J., Pisias, N.G., Prell, W.L., Shackleton, N.J., 1984. The orbital theory of Pleistocene climate: support from a revised chronology of the marine ^{18}O record. *In,* Berger, A., Imbrie, J., Hays, J., Kukla, G., Saltzman, B., (eds), Milankovich and Climate. Reidel, Norwell, MA, pp. 269-306.

Imbrie, J., Boyle, E.A., Clemens, S.C., Duffy, A., Howard, W.R., Kukla, G., Kutzbach, J., Martinson, D.G., McIntyre, A., Mix, A.C., Molfino, B., Morley, J.J., Peterson, L.C., Pisias, N.G., Prell, W.G., Raymo, M.E., Shackleton, N.J., Toggweiler, J.R., 1992. On the nature and origin of major glaciation cycles: 1. Linear responses to Milankovitch forcing. *Paleoceanography*, v. 7, pp. 701-38.

Imbrie, J., Berger, A., Boyle, E.A., Clemens, S.C., Duffy, A., Howard, W.R., Kukla, G., Kutzbach, J., Martinson, D.G., McIntyre, A., Mix, A.C., Molfino, B., Morley, J.J., Peterson, L.C., Pisias, N.G., Prell, W.G., Raymo, M.E., Shackleton, N.J., Toggweiler, J.R., 1993. On the structure and origin of major glaciation cycles: 2. The 100,000 year cycle. *Paleoceanography*, v. 8, pp. 699-735.

Isozaki, Y., 2001. An extraterrestrial impact at the Permian-Triassic Boundary? *Science*, v. 293, no. 5539, p. 2343a.

Jenkyns, H.C., 1980. Cretaceous anoxic events: from continents to oceans. *Journal of the Geological Society, London*, v. 137, pp. 171-88.

Jessberger, E.K. and Kissel, J., 1991. Chemical properties of cometary dust and a note on carbon isotopes, *In:* R.L. Newburn, M. Neugebauer, J.H. Rahe (eds), Comets in the Post-Halley Era, v. 2, Kluwer Academic, Amsterdam, pp. 1075-92.

Jin, Y.G., Wang, Y., Wang, W., Shang, Q.H., Cao, C.Q., Erwin, D.H., 2000. Pattern of marine mass extinction near the Permian-Triassic boundary in south China. *Science*, v. 289, pp. 432-36.

John, C., and Glass, B.P., 1974. Clinopyroxene-bearing glass spherules associated with North American microtektites. *Geology* v. 2, pp. 599-602.

Kaiho, K., Kajiwara, Y., Nakano, T., Miura, Y., Kawahata, H., Tazaki, K., Ueshima, M., Chen, Z., Shi, G.R., 2001. End-Permian catastrophe by a bolide impact: Evidence of a gigantic release of sulfur from the mantle. *Geology*, v. 29, no. 9, pp. 815-18.

Katz, M.E., Pak, D.K., Dickens, G.R., Miller, K.G., 1999. The source and fate of massive carbon input during the latest Paleocene thermal maximum. *Science*, v. 286, pp. 1531-33.

Katz, M.E., Cramer, B.S., Mountain, G., Katz, S., Miller, K.G., 2001. uncorking the bottle: What triggered the Paleocene/Eocene thermal maximum methane release? *Paleoceanography*, v. 16, no. 6, pp. 549-62.

Kaye, C.A., Schnetzler, C.C., Chase, J.N., 1961. Tektite from Martha's Vineyard, Mass. *Geological Society of America Bulletin*, v. 72, pp. 339-40.

Keith, M.L., and Weber, J.N., 1964. Carbon and oxygen isotopic composition of selected limestones and fossils. *Geochimica et Cosmochimica Acta*, v. 28, no. 10-11, pp. 1787- 1816.

Keller, G., 1986a. Late Eocene impact events and stepwise mass extinctions. *In:* Pomerol, C.H., and Premoli-Silva, I., (eds), Terminal Eocene Events. Elsevier, Amsterdam, pp. 403-12.

Keller, G., D'Hondt, S.L., Orth, C.J., Gilmore J.S., Oliver, P.Q., Shoemaker, E.M., and Molina, E., 1987. Late Eocene Microspherules: Stratigraphy, age, and geochemistry. *Meteoritics,* v. 22, pp. 25-60.

Kelly, D.C., Bralower, T.J., Zachos, , J.C., Premoli-Silva, I., Thomas, E., 1996. Rapid diversification of planktonic foraminifera in the tropical Pacific (ODP Site 865) during the late Paleocene thermal maximum. *Geology*, v. 24, pp. 423-26.

Kennett, J.P., and Stott, J.D. 1990. Proteus and Proto-Oceanus: ancestral Paleogene oceans as revealed from Antarctic stable isotopic results; ODP Leg 113. In Barker, P.F., Kennett, J.P., et al., *Proceedings of the Ocean Drilling Program, Scientific Results, 113:* 865-880.

Kennett, J.P., and Stott, J.D. 1991. Abrupt deep-sea warming, paleoceanographic changes and benthic extinctions at the end of the Paleocene: *Nature*, v. 353, pp. 225-229.

Kent, D.V., Cramer, B.S., Lanci, L., Wang, D., Wright, J.D., Van der Voo, R., 2003. A case for a comet impact trigger for the Paleocene/Eocene thermal maximum and carbon isotope excursion, *Earth and Planetary Science Letters*, v. 211, pp. 13-26.

Klein, C., 2002. Manual of Mineral Science 22nd ed. John Wiley & Sons: New York, pp. 425-427.

Koch, P.L., Zachos, J.C., and Gingerich, P.D., 1992. Correlation between isotope records in marine and continental carbon reservoirs near the Paleocene/Eocene boundary. *Nature*, v. 358, pp. 319-322.

Koeberl, C., 1989. New estimates of area and mass for the North American tektite strewn field. *Proc. of the 19th Lunar and Planetary Sci. Conf.*, pp. 745-51.

Koeberl, C., 2001. The sedimentary record of impact events. *In:* B. Peucker-Ehrenbrink and B. Schmitz (eds), Accretion of Extraterrestrial Material Throughout Earth's History. Kluwer Academic/Plenum Pubs., New York, NY, pp. 333-78.

Koeberl, C., Bottomley, R.J., Glass, B.P., Storzer, D., York, D., 1989. Geochemistry and age of the Ivory Coast tektites, (abs) *Meteoritics* , v. 24 pp. 287.

Koeberl, C., Sharpton, V.L., Schuraytz, B.C., Shirey, S.B., Blum, J.D., Marin, L.E., 1994. Evidence for a meteoritic component in impact melt rock from the Chicxulub structure. *Geochimica et Cosmochimica Acta*, v. 58, pp. 1679-84.

Koeberl, C., Poag, C.W., Reimold, W.U., Brandy, D., 1996. Impact origin of the Chesapeake Bay structure, source of the North American tektites. *Science*, v. 271, pp. 1263-66.

Koeberl C., Bottomley, R., Glass, B.P., Storzer, D., 1997. Geochemistry and age of Ivory Coast tektites and microtektites. *Geochim. Cosmochim. Acta.* v. 61, pp. 1745-1772.

Koeberl C., Reimold, W.U., Blum, J.D., and Chamberlain, C.P., 1998. Petrology and geochemistry of target rocks from Bosumtwi impact structure, Ghana, and comparison with Ivory Coast tektites. *Geochimica Cosmochimica Acta*. v. 62, pp. 2179-2196.

Koeberl, C., Huber, H., Sephton, M., 2001. (abs) A extraterrestrial component at the Permo-Triassic boundary? Clues from siderophile element abundances. *Geologigical Society of America Annual Meeting*, November, session no. 132.

Kroopnick, P., 1974. The dissolved O_2-CO_2-^{13}C system in the eastern equatorial Pacific. *Deep Sea Research*, v. 21, pp. 211-27.

Kroopnick, P., 1980. The distribution of ^{13}C in the Atlantic Ocean. *Earth and Planetary Science Letters,* v. 49, pp. 469-84.

Kroopnick, P., 1985. The distribution of ^{13}C of ΣCO_2 in the world oceans, *Deep Sea Research,* vol. 32, pp. 57-84.

Kroopnick, P., Weiss, R.F., Craig, H., 1972. Total CO_2, ^{13}C, and dissolved oxygen-18 at GEOSECS II in the North Atlantic. *Earth and Planetary Science Letters*, v. 16, pp. 103-10.

Ku, T.L., and Luo, S., 1992. Carbon isotopic variations on glacial-to-interglacial time scales in the ocean: modeling and implications. *Paleoceanography*, v. 7, pp. 543-62.

Kump, L.R., and Arthur, M.A., 1999. Interpreting carbon-isotope excursions: carbonates and organic matter. *Chemical Geology*, v. 161, pp. 181-98.

Kurtz, A.C., Kump, L.R., Arthur, M.A., Zachos, J.C., Paytan, A., 2003. Early Cenozoic decoupling of the global carbon and sulfur cycles. *Paleoceanography*, v. 18, PA4.

Kyte, F.T., 1998. A meteorite from the Cretaceous/Tertiary boundary. *Nature*, v. 396, pp. 237-39.

Kyte, F.T., 2001. Identification of late Eocene impact deposits at ODP Site 1090. *In* Gersonde R., Hodell, D.A., and Blum, P. (Eds.), *Proc. ODP, Sci. Results,* 177, 1-9 [CD-ROM]. Available from: Ocean Drilling Program, Texas A&M University, College Station TX 77845-9547, USA.

Kyte, F.T. and Liu, S., 2002. Iridium and spherules in late Eocene impact deposits. *Proceedings of Lunar and Planetary Science Conference.* XXXIII, (abstract) #1981.

Kyte, F.T., Shukolyukov, A., Hildebrand, A.R., Lugmair, G.W., Hanova, J., 2004. Initial Cr-isotopic and iridium measurements of concentrations from late Eocene cpx-spherule deposits. *Proceedings of Lunar and Planetary Science Conference* XXXV, (abstract) #1824.

Lanci, L., Lowrie, W., Montanari, A., 1996. Magnetostratigraphy of the Eocene/Oligocene boundary in a short drill core. *Earth and Planetary Science Letters*, v. 143, pp. 37-48.

Langenhorst, F., 1996. Characteristics of shocked quartz in late Eocene impact ejecta from Massignano (Ancona, Italy): clues to shock conditions and source crater. *Geology*, v. 24, pp. 487-90.

Lasaga, A.C., Berner, R.A., Garrels, R.M., 1985. An improved geochemical model of atmospheric CO_2: *In*: Sundquist, E.T., and Broecker, W.S., (eds), *The Carbon Cycle and Atmospheric CO_2: Natural Variations Archean to Present, Am. Geophys. Un., Geophys. Monograph*: v. 32*,* pp. 397-411.

Latimer, J.C. and Filippelli, G.M., 2002. Eocene to Miocene terrigenous inputs and export production: geochemical evidence from ODP Leg 177, Site 1090. *Palaeogeography, Palaeoclimatology, Palaeoecology*, v. 182, pp. 151-164.

Lear, C.H., Rosenthal, Y., Coxall, H.K., Wilson, P.A., 2004. Late Eocene to early Miocene ice sheet dynamics and the global carbon cycle. *Paleoceanography*, v. 19, PA4015.

Lee, M.-Y. and Wei, K.-Y. 2000. Australasian microtektites in the South China Sea and the Philippine Sea: Implications for age, size, and location of the impact crater. *Meteoritics Planet. Sci*. v. 35, pp. 1151-1155.

Lee, S.R., Horton, J.W., Walker, R.J., 2006. Confirmation of a meteoritic component in impact-melt rocks of the Chesapeake Bay impact structure, Virginia, USA-Evidence from osmium isotopic and PGE systematics. *Meteoritics and Planetary Science*, v. 41, no. 6, pp. 819-33.

Liu, S., and Glass, B.P., 2001. Upper Eocene impact ejecta/spherule layers in marine sediments: New sites. *Proceedings of Lunar and Planetary Science* XXXII, (abstract) #2027.

Liu, S., Kyte, F.T., Glass, B.P., Gersonde, R., 2000. Upper Eocene spherules at ODP Site 1090B. *Meteoritics Planetary Sci.,* (abs) v. 35, pp. A98–A99.

Liu, S. et *al*. 2001. Sr and Nd data for Upper Eocene spherule layers. *Proceedings of Lunar and Planetary Science Conference* XXXII, (abstract) #1819.

Liu, S., Papanastassiou, D.A., Ngo, H.H., Glass, B.P., 2006. Sr and Nd analyses of upper Eocene spherules and their implications for target rocks. *Meteoritics and Planetary Science*, v. 41, no. 5, pp. 705-14.

Lowrie, W., and Lanci, L., 1994. Magnetostratigraphy of Eocene-Oligocene boundary sections in Umbria, Italy: no evidence for short subchrons within chron 13r. *Earth and Planetary Science Letters*, v. 126, pp. 247-58.

Lyle, M., Wilson, P.A., Janecek, T.R., et *al*., 2002. *Proc. ODP, Init. Repts.,* 199: College Station, TX (Ocean Drilling Program). doi:10.2973/odp.proc.ir.199.2002.

Maas, M.C., Anthony, M.R., Gingerich, P.D., Gunnell, G.F., Krause, D.W., 1995. Mammalian generic diversity and turnover in the late Paleocene and Early Eocene of the Bighorn and Crazy Mountain Basins, Wyoming and Montana (USA). *Palaeogeo., Palaeoclim., Palaeoecology*, v. 115, pp. 181-207.

Mackensen, A., and Ehrmann, W.U., 1992. Middle Eocene through early Oligocene climate history and paleoceanography in the Southern Ocean: stable oxygen and carbon isotopes from ODP Sites on Maud Rise and Kerguelen Plateau, *Marine Geology*, v. 108, pp. 1-27.

MacLeod, N., Keller, G., Kitchell, J.A., 1990. Progenesis in Late Eocene populations of *Subbotina linaperta* (Foraminifera) from the western Atlantic. *Marine Micropaleontology*, v. 16, pp. 219-40.

Magaritz, A., Bart, R., Baud, A., Holser, W.T., 1988. The carbon-isotope shift at the Permian/Triassic boundary in the souther Alps is gradual. *Nature*, v. 331, pp. 337-39.

Makjanic, J., Vis, R.D., Hovenier, J.W., Heymann, D., 1993. Carbon in the matrices of ordinary chondrites. *Meteoritics*, v. 28, pp. 63-70.

Mankinen, E., Donelly-Nolan, J.M., Gromme, C.S., Hearn, B.C., 1980. Paleomagnetism of the Clear Lake volcanics and new limits on the age of the Jaramillo normal-polarity event. *USGS Prof. Pap.* 1141, pp. 67-82.

Marino, M., and Flores, J.A., 2002. Middle Eocene to early Oligocene calcareous nannofossil stratigraphy at Leg 177 Site 1090: *Marine Micropaleonontology,* v. 45**,** pp. 383-398.

Martinson, D., Pisias, N., Hays, J., Imbrie, J., Moore Jr. T., Shackleton, N., 1987. Age dating and the orbital theory of the ice ages: Development of a high-resolution 0 to 300,000-year chronostratigraphy. *Quaternary Research*, v. 27, pp. 1-29.

Masaitis, V.L., 1992. Impactites from Popigai crater (abs). *International Conference on Large Meteorite Impacts and Planetary Evolution*, LPI Contribution no. 790, p. 51.

Masaitis, V.L., Naumov, M.V., Mashchak, M.S., 2005. Original diameter and depth of erosion of the Popigai impact crater, Russia. *In:* T. Kenkmann, F. Horz, A. Deutsch, (eds), *Large Meteorite Impacts III*, *Geological Society of America Special Publication*, 384, pp. 131-40.

Mason, B., 1963. *Space Science Reviews,* v. 1, pp. 621.

Maurrasse, F., and Glass, B.P., 1976. Radiolarian stratigraphy and North American microtektites in Caribbean core RC9-58: Implications concerning the age of the Eocene-Oligocene boundary. *Trans. Caribbean Geological Conference 7th*, pp. 205-12.

Mead, G.A., Hodell, D.A., Ciesielski, P.F., 1992. Late Eocene to Oligocene Vertical Oxygen Isotopic Gradients in the South Atlantic: Implications for Warm Saline Deep Water. *In: The Antarctic Paleoenvironment: A Perspective on Global Change, Antarctic Research Series*, vol. 60, (eds) J.P. Kennett and D.A. Warnke, pp. 27-48, AGU, Washington, D.C.

Messenger, S., 2000. Identification of molecular-cloud material in interplanetary dust particles. *Nature*, v. 404, 968-71.

Milankovitch, M.M., 1941. Canon of insolation and the ice-age problem: Koniglich Serbische Akademie, Beograd. (English translation by the Israel program for scientific translation, published for the U.S. Dept. of Commerce and the National Science Foundation, Washington, D.C.).

Milkov, A., 2004. Global estimates of hydrate-bound gas in marine sediments: How much is really out there? *Earth Science Reviews*, v. 66, no. 3-4, pp. 183-97.

Miller, K.G. and Fairbanks, R.G., 1983. Evidence for Oligocene-Middle Miocene abyssal circulation changes in the western North Atlantic. *Nature*, v. 306, pp. 250-53.

Miller, K.G. and Fairbanks, R.G., 1985. Oligocene to Miocene global carbon isotope cycles and abyssal circulation changes, *In*: Sundquist, E.T., and Broecker, W.S., eds., *The Carbon Cycle and Atmospheric CO2: Natural Variations Archean to Present, American Geophysical Union, Geophysical Monograph*: vol. 32*,* pp. 469-486.

Miller, K.G., and Katz, M.E., 1987. Eocene benthic foraminiferal biofacies of the New Jersey Transect, *In:* Poag, C.W., Watts, A., et *al., Init, Rep. Deep Sea Drilling Project*, 95, 253-65.

Miller, K.G., and Kent, D.V., 1987. Testing Cenozoic eustatic changes: The critical role of stratigraphic resolution. *Cushman Foundation Foraminiferal Res. Special Pub.* V. 24, pp. 51-56.

Miller, K.G., Fairbanks, R.G., and Mountain, G.S., 1987. Tertiary oxygen isotope synthesis, sea-level history, and continental margin erosion, *Paleoceanography*, v. 2, pp. 1-19.

Miller, K.G., Berggren, W.A., Zhang, J., and Palmer-Julson, A., 1991. Biostratigraphy and Isotope stratigraphy of upper Eocene microtektites at Site 612: How Many Impacts? *Palaios*, v. 6, pp. 17-38.

Miller, K.G., Katz, M.E., Berggren, W.A., 1992. Cenozoic deep-sea benthic foraminifera: A tale of three turnovers. *In:* Takayanagi, Y., and Saito, T., (eds), Studies of Benthic Foraminifera: *Proc. of the 4th International Symposium on Benthic Foraminifera (Benthos '90)*, Sendai, Japan, Tokai Uni. Press, pp. 67-75.

Miller, K.G., Thompson, P.R., and Kent, D.V., 1993. Integrated stratigraphy of the Alabama coastal plain: Relationship of upper Eocene to Oligocene unconformities to glacioeustatic change. *Paleoceanography*, v. 8, pp. 313-331.

Miller, K.G., Browning, J.V., Aubry, M.P., Wade, B.S., Katz, M.E., Kulpecz, A.A., Wright, J.D., *in press*. Eocene-Oligocene Global Climate and Sea-level Changes: St. Stephens Quarry, Alabama. *Geological Society of America Bulletin*.

Montanari, A., and Koeberl, C., 2000. Impact Stratigraphy: The Italian Record: Lecture Notes in Earth Sciences, v. 93, Springer Verlag, Heidelberg, 364 p.

Montanari, A., Drake, R., Bice, M.D., Alvarez, W., Curtis, G.H., Turrin, B.D., DePaolo, D.J., 1985. Radiometric time scale for the upper Eocene and Oligocene based on K/Ar and Rb/Sr dating of volcanic biotites from the pelagic sequence of Gubbio, Italy. *Geology*, 13:596-99.

Montanari, A., Deino, A., Drake, R., Turrin, B.D., DePaolo, D.J., Odin, G.S., Curtis, G.H., Alvarez, W., Bice, D.M., 1988. Radioisotopic dating of the Eocene-Oligocene boundary in the pelagic sequence of the Northern Apennines: *In:* Premoli Silva, I., Coccioni, R., Montanari, A., (eds) The Eocene-Oligocene Boundary in the Marche-Umbria Basin (Italy): I.U.G.S. Memoir, F.lli Aniballi Pubs, Anacona, pp. 195-208.

Montanari, A., Asaro, F., Michel H.V., Kennett, J.P., 1993. Iridium anomalies of Late Eocene age at Massignano (Italy) and ODP Site 689B, Maud Rise, Antarctica. *Palaios*, v. 8, pp. 420-37.

Morrison, D., Chapman, C.R., Slovic, P., 1994. The impact hazard. In: Gehrels T (ed) Hazards due to comets and asteroids. University of Arizona Press, Tucson, pp. 59-91.

Moore, C.L., and Lewis, C.F., 1967. Total carbon content of ordinary chondrites. *Journal of Geophysical Research*, v. 72, pp. 6289-92.

Norris, R.D., and Rohl, U., 1999. Carbon cycling and chronology of climate warming during the Paleocene/Eocene transition. *Nature*, v. 401, pp. 775-78.

Oberli, F., and Meier, M., 1991. Age of Eocene-Oligocene boundary in the Marche-Umbria basin, Italy, by high resolution U-Th-Pb dating. *Terra*, v. 3, no. 1, pp. 286.

Obradovich, J.D., Snee, L.W., and Izett, G.A., 1989. Is there more than one glassy impact layer in the Late Eocene?, *Geological Society of America,* Abstracts with Programs, A134.

Odin, G.S., Montanari, A., Deino, A., Drake, R., Guise, P.G., Kreuzer, H., Rex, D.C., 1991. Reliability of volcano-sedimentary biotite ages across the Eocene-Oligocene boundary (Apennines, Italy). *Chemical Geology*, v. 86, pp. 203-24.

Officer, C.B., and Drake, C.L., 1985. Terminal Cretaceous environmental events. *Science*, v. 227, pp. 1161-67.

Okada, H., Bukry, D., 1980. Supplementary modification and introduction of code number to the low latitude coccolith biostratigraphic zonation (Bukry, 1973, 1975). *Marine Micropaleontology,* v. 5, pp. 321-25.

O'Keefe, J.A., 1976. Tektites and Their Origin. Elsevier Scientific Publishing Co., Amsterdam, Germany, p. 254.

Olsen, P.E., Shubin, N.H., Ander, M., 1987. New Early Jurassic tetrapod assemblages constrain Triassic-Jurassic tetrapod extinction event. *Science*, v. 237, pp. 1025-29.

Olsen, P.E., Koeberl, C., Huber, H., Montanari, A., Fowell, S.J., Et-Touhami, M., Kent, D.V., 2002. Continental Triassic-Jurassic boundary in central Pangea: Recent progress and discussion of an Ir anomaly. *In: Catastrophic Events and Mass Extinctions: Impacts and Beyond,* (eds) C. Koeberl, and K.G. MacLeod, *Geological Society of America Special Publication*, 356, pp. 505-522.

Olsson, R.K., Miller, K.G., Browning, J.V., Wright, J.D., Cramer, B.S., 2002. Sequence stratigraphy and sea-level change across the Cretaceous-Tertiary boundary on the New Jersey passive margin. *In: Catastrophic Events and Mass Extinctions: Impacts and Beyond,* (eds) C. Koeberl, and K.G. MacLeod, *Geological Society of America Special Publication*, 356, pp. 97-108.

Oppo, D.W., and Fairbanks, R.G., 1987. Variability in the deep and intermediate water circulation of the Atlantic Ocean during the past 25,000 years: Northern Hemisphere modulation of the Southern Ocean. *Earth and Planetary Science Letters*, v. 86, pp. 1-15.

Otting, W., and Zahringer, J., 1967. Total carbon content and primordial rare gases in chondrites. *Geochimica et Cosmochimica Acta*, v. 31, pp. 1949-60.

Pak, D.K., and Miller, K.G., 1992. Paleocene to Eocene benthic foraminiferal isotopes and assemblages: Implications for deepwater circulation: *Paleoceanography*, v. 7, pp. 405-22.

Palfy, J., Mortensen, J.K., Carter, E.S., Smith, P.L., Friedman, R.M., Tipper, H.W., 2000. Timing of the end-Triassic mass extinction: first on land, then in the sea? *Geology*, v. 28, pp. 39-42.

Perch-Nielsen, K., McKenzie, J., He, Q., 1982. Biostratigraphy and isotope stratigraphy and the "catastrophic" extinction of calcareous nannoplankton at the Cretaceous Tertiary boundary. *Geological Society of America Special Paper* 190, pp. 353-71.

Pierrard, O., Robin, E., Rocchia, R., Montanari, A., 1998. Extraterrestrial Ni-rich spinel in upper Eocene sediments from Massignano, Italy. *Geology*, v. 26, no. 4, pp. 307-10.

Poag, W.C., and Low, D., 1987. Unconformable sequence boundaries at Deep Sea Drilling Project Site 612, New Jersey Transect: Their characteristics and stratigraphic significance. In *Initial Reports of the Deep Sea Drilling Project,* C.W. Poag, A.B. Watts *et al.* (eds), 95, pp. 453-98.

Poag, W.C., and Aubry, M.P., 1995, Upper Eocene impactites of the U.S. East Coast: Depositional origins, biostratigraphic framework, and correlation. *Palaios*, v. 10, pp. 16-43.

Poag, W.C., and Poppe, L.J., 1998. The Toms Canyon structure, New Jersey outer continental shelf; a possible late Eocene impact crater. *Marine Geology*, v. 145, no. 1-2, pp. 23-60.

Poag, W.C., Powars, D.S., Poppe, L.J., Mixon, R.B., Edwards, L.E., Folger, D.W., Bruce, S., 1992. Deep Sea Drilling Project Site 612 bolide event – New evidence of a late Eocene impact-wave deposit and a possible impact site, U.S. East Coast. *Geology*, v. 20, no. 9, pp. 771-74.

Poag, W.C., Powars, D.S., Poppe, L.J., Mixon, R.B., 1994. Meteoroid mayhem in Ole Virginny: Source of the North American tektite strewn field. *Geology,* v. 22, pp. 691-94.

Poag, W.C., Mankinen, E., Norris, R.D., 2003. Late Eocene Impacts: Geologic record, correlation, and paleoenvironmental consequences. In: Prothero, D.R., Yvany, L.C., Nesbitt, E., (eds) From Greenhouse to Icehouse: The Marine Eocene-Oligocene Transition. Columbia University Press, New York, pp 495-510.

Poag, W.C., Koeberl, C., and Reimold, W.U., 2004, The Chesapeake Bay Crater: Springer, New York, 522 p.

Pope, K.O., Ocampo, A.C., and Duller, C.E., 1993. Surficial geology of the Chicxulub impact crater, Yucatan, Mexico. *Earth Moon and Planets* v. 63, pp. 93-104.

Prell, W.L., Imbrie, J., Martinson, D.G., Morley, J.J., Pisias, N.G., Shackleton, N.J., Streeter, H.F., 1986. Geographic correlation of oxygen isotope stratigraphy application to the late Quaternary. *Paleoceanography*, v. 1, no. 2, pp. 137-62.

Premoli Silva, I., and Jenkins, D.J., 1993. Decision on the Eocene-Oligocene boundary stratotype. *Episodes*, v. 16, pp. 379-81.

Prothero, D. R., 2004, Did impacts, volcanic eruptions, or climate change affect mammalian evolution? *Palaeogeography, Palaeoclimatology, Palaeoecology,* v. 214, pp. 283-294.

Raup, D., 1979. Size of the Permo-Thriasic bottleneck and its evolutionary implications. *Science*, v. 206, pp. 217-18.

Raup, D., and Sepkoski, J.J., 1982. Mass extinctions in the fossil record. *Science*, v. 215, pp. 217-18.

Raup, D.M., and Sepkoski, J.J., 1986. Periodic extinction of families and genera. *Science*, v. 231, no. 4740, pp. 833-36.

Raymo, M.E., 1991. Geochemical evidence supporting TC Chamberlin's theory of glaciation. *Geology*, v. 19, pp. 344-47.

Retallack, G.J., Seyedolali, A., Krull, E.S., Holser, W.T., Ambers, C.P., Kyte, F.T., 1998. Search for evidence of impact at the Permian-Triassic boundary in Antarctica and Australia. *Geology*, v. 26, no. 11, pp. 979-82.

Ryder, G., Fastovsky, D., Gartner, S., (eds), 1996. The Cretaceous-Tertiary Event and other Catastrophes in Earth history. *Geological Society of America Special Publication,* 307, Geological Society of America, Boulder, CO, 556 p.

Sanfilippo, A., Riedel, W.R., Glass, B.P., Kyte, F.T., 1985. Late Eocene microtektites and radiolarian extinctions on Barbados, *Nature*, v. 314, pp. 613-15.

Sanford, W.E., Gohn, G.S., Powars, D.S., Horton, Jr., J.W., Edwards, L.E., and Self-Trail, J.M., 2004. Drilling the Central Crater of the Chesapeake Bay Impact Structures: A first Look, *EOS,* v. 85, pp. 369-377.

Sarmiento, J.L., 1993. Ocean carbon cycle. *Chemical and Engineering News*, May 31, pp. 30-43.

Sarnthein, M., Winn, K., Duplessy, J.C., Fontugne, M.R., 1988. Global variations of surface ocean productivity in low and mid latitudes: influence on CO_2 reservoirs of the deep ocean and atmosphere during the last 21,000 years. *Paleoceanography*, v. 3, pp. 361-99.

Saunders, J.B., Bernoulli, D., Muller-Merz, E., Oberhansli, H., Perch-Nielsen, K., Riedel, W.R., Sanfilippo, A., Torrini, R. Jr., 1984. Stratigraphy of the late Middle Eocene to Early Oligocene In the Bath Cliff section, Barbados, West Indies. *Micropaleontology*, v. 30, pp. 390-425.

Savin, S.M., Douglas, R.G., and Stehli, F.G., 1975. Tertiary marine paleotemperatures. *Geological Society of America Bulletin*, v. 86, pp. 1499-1510.

Schidlowski, M., 2001. Carbon isotopes as biogeochemical recorders of life over 3.8 Ga of Earth history: evolution of a concept. *Precambrian Research*, v. 106, pp. 117-34.

Schlanger, S.O., and Jenkyns, H.C., 1976. Cretaceous anoxic events: causes and consequences. *Geol. Mijnbouw.* v. 55, pp. 179-84.

Schmitz, B., Speijer, R.P., and Aubry, M.-P., 1996. Latest Paleocene benthic extinction event on the southern Tethyan shelf (Egypt): Foraminiferal stable isotopic ($\delta^{13}C$, $\delta^{18}O$) records. *Geology,* v. 24, pp. 347-350.

Schmitz, B., Asaro, F., Molina, E., Monechi, S., von Salis, K., Speijer, R.P., 1997. High-resolution iridium, $\delta^{13}C$, $\delta^{18}O$, foraminifera and nannofossil profiles across the latest Paleocene benthic extinction event at Zumaya, Spain. *Palaeogeography, Palaeoclimatology, Palaeoecology*, v. 133, pp. 49-68.

Schmitz, B., Pujalte, V., Nunez-Betelu, K., 2001. Climate and sea-level perturbations during the Initial Eocene Thermal Maximum: evidence from siliclastic units in the Basque Basin (Ermua, Zumaia, and Trabakua Pass), northern Spain. *Palaeogeography, Palaeoclimatology, Palaeoecology*, v. 165, pp. 299-320.

Schneider, D.A., Kent, D.V., Mello, G.A., 1992. A detailed chronology of the Australasian impact event: Brunhes/Matuyama geomagnetic polarity reversal, and climate change. *Earth and Planetary Sci. Lett.,* v. 111, pp. 395-405.

Schneider, D.A., and Kent, D.V., 1990. Ivory Coast microtektites and geomagnetic reversals. *Geophysical Research Letters*, v. 17, no. 2, pp. 163-66.

Schuraytz, B.C., Lindstrom, D.J., Marin, L.E., Martinez, R.R., Mittlefehldt, D.W., Sharpton, V.L., Wentworth, S.J., 1996. Iridium metal in Chicxulub impact melt: forensic chemistry on the K-T smoking gun. *Science*, v. 271, no. 5255, pp. 1573-76.

Scott, E.R.D., and Krot, A.N., 2005. Chondritic meteorites and high-temperature nebular origins of their components. *Chondrites and the Protoplanetary Disk*, v. 341, pp. 15.

Sephton, M.A., Verchovsky, A.B., Bland, P.A., Gilmour, I., Grady, M.M., Wright, I.P., 2003. Investigating the variations in carbon and nitrogen isotopes in carbonaceous chondrites. *Geochimica et Cosmochimica Acta*, v. 67, no. 11, pp. 2093-2108.

Sexton, P.F., Wilson, P.A., Norris, R.D., 2006. Testing the Cenozoic multisite composite $\delta^{18}O$ and $\delta^{13}C$ curves: New monospecific Eocene records from a single locality, Demerara Rise (Ocean Drilling Program Leg 207), *Paleoceanography*, v. 21, no. 2, PA2019.

Shackleton, N.J., 1967. Oxygen isotope analyses and Pleistocene temperatures reassessed. *Nature*, v. 215, pp. 15-17.

Shackleton, N.J., 1977. Carbon-13 in Uvigerina: Tropical rainforest history and the equatorial Pacific carbonate dissolution cycles. In: *The Fate of Fossil Fuel CO_2 in the Oceans* (eds) Anderson, N.R., and Malahoff, A., 401-27.

Shackleton, N. J., 1986. Paleogene stable isotope events. *Palaeogeography, Palaeoclimatology, Palaeoecology*, v. 57, pp. 91-102.

Shackleton, N.J., and Opdyke, N.D., 1973. Oxygen Isotope and Paleomagnetic Stratigraphy of Equatorial Pacific Core V28-238: Oxygen Isotope Temperatures and Ice Volumes on a 10^5 Year and 10^6 Year Scale. *Quaternary Research*, v. 3, pp. 39-55.

Shackleton, N.J., and Kennett, J.P., 1975. Paleotemperature history of the Cenozoic and the initiation of Antarctic glaciation: oxygen, and carbon isotope analyses in DSDP Sites 277, 279, and 281. *In:* Kennett, J.P., Homtz, R.E. et *al.*, (eds), *Initial Reports Deep Sea Drilling Project*, 29, pp. 599-612.

Shackleton, N.J., and Opdyke, N.D., 1976. Oxygen Isotope and Paleomagnetic Stratigraphy of Equatorial Pacific Core V28-239 late Pliocene to latest Pleistocene. *In: Investigation of late Quaternary Paleoceanography and Paleoclimatology: Geological Society of America Memoir*, 145 (eds) R.M. Cline and J.D. Hays. Geological Society of America. Boulder CO, pp. 449-64.

Shackleton, N.J., Hall, M.A., Boersma, A., 1984. Oxygen and carbon isotope data from Leg 74 foraminifers. *In: Initial Deep Sea Drilling Project*, 74, pp. 599-612.

Sharpton, V.L., Burke, K., Camargo-Zanoguera, A., Hall, S.A., Lee, D.S., Marin, L.E., Suarez-Reynoso, G., Quezada-Muneton, J.M., Spudis, P.D., Urrutia-Fucugauchi, J., 1993. Chicxulub multiring impact basin: Size and other characteristics derived from gravity analysis. *Science,* v. 261, pp. 1564-1567.

Shaw, H.F., and Wasserburg, G.J., 1982. Age and provenance of the target materials for tektites and possible impactites as inferred from Sm-Nd and Rb-Sr systematics. *Earth and Planetary Science*, v. 60, pp. 155-77.

Shukolyukov, A., and Lugmair, G.W., 1998. Isotopic evidence for the Cretaceous-Tertiary impactor and its type. *Science*, v. 282, pp. 927-29.

Siegenthaler, U., and Sarmiento, J., 1995. Atmospheric carbon dioxide and the ocean. *Nature*, v. 365, pp. 119-25.

Speiss, V., 1990. Cenozoic magnetostratigraphy of Leg 113 drill sites, Maud Rise, Weddell Sea, Antarctica, *in* Barker, P.F., Kennett, J.P., et al., *Proc. of the Ocean Drilling Prog., Sci. Res*., 113: College Station, Texas, Ocean Drilling Program, pp. 261-318.

Spezzaferri, S., Basso, D., Coccioni, R., 2002. Late Eocene planktonic foraminiferal response to an extraterrestrial impact at Massignano GSSP (Northeastern Apennines, Italy), *Journal of Foraminiferal Research*, v. 32, pp. 188-99.

Staudacher, Th., Jessberger, E.K., Dominik, B., Kirsten, T., Schaeffer, O.A., 1982. $^{40}Ar/^{39}Ar$ ages of rocks and glasses from the Nordlinger Ries crater and the temperature history of impact breccias. *Journal of Geophysical Research*, v. 51, pp. 1-11.

Stahl, W., 1979, Carbon isotopes in petroleum geochemistry. *In:* Jager, E., Hunziker, J.C., (eds), Lectures in Isotope Geology. Springer, Berlin, pp. 274-82.

Stecher, O., Ngo, H.H., Papanastassiou, D.A., Wasserburg, G.J., 1989. Nd and Sr isotopic evidence for the origin of tektite material from DSDP Site 612 off the New Jersey Coast. *Meteoritics*, v. 24, pp. 89-98.

Stott, L.D., and Kennett, J.P., 1990. The paleoceanographic and paleoclimatic signature of the Cretaceous/Tertiary boundary in the Antarctic: Stable isotopic results from ODP Leg 113, *In: Proc. Ocean Drill. Program Sci. Results,* v. 113, pp. 829-48.

Stott, L.D., Kennett, J.P., Shackleton, N.J., Corfield, R.M., 1990. The evolution of Antarctic surface waters during the Paleogene: Inferences from stable isotopic composition of planktonic foraminifers, ODP Leg 113. *In: Proc. Ocean Drill. Program Sci. Results,* v. 113, pp. 849-63.

Stott, L.D., Sinha, A., Thiry, M., Aubry, M.-P., and Berggren, W.A., 1996. Global $\delta^{13}C$ changes across the Paleocene-Eocene boundary; Criteria for terrestrial-marine correlations: in Knox, R.W. O'B., Corfield, R.M., and Dunay, R.E., (eds), *Correlation of the early Paleogene in Northwest Europe*, Geological Society Special Publications 101, London (geological Society of London): pp. 381-99.

Sundquist, E.T., 1985. Geological perspectives on carbon dioxide and the carbon cycle. *In:* E.T. Sundquist and W.S. Broecker, (eds) *The Carbon Cycle and Atmospheric CO_2 variations Archean to the Present*, *Geophysical Research Monograph*, v. 32, pp. 5-60. American Geophysical Union, Washington, DC.

Sundquist, E.T., and Visser, K., 2005. The Geologic History of the Carbon Cycle. *In:* W. H. Schlesinger (ed), Biogeochemistry: *Treatise on Geochemistry*, v. 8, Elsevier Press, Oxford, UK, pp. 425-72.

Svensen, H., Planke, S., Malthe-Serenssen, A., Jamtveit, B., Myklebust, R., Eldem, T.R., Rey, S.S., 2004. Release of methane from a volcanic basin as a mechanism for initial Eocene global warming. *Nature*, v. 429, pp. 542-45.

Swisher, C.C., Grajales-Nishimura, J.M., Montanari, A., Margolis, S.V., Claeys, P., Alvarez, W., Renne, P., Cedillo-Pardo, E., Maurrasse, J.M, Curtis, G.H., Smit, J., McWilliams, M.O., 1992. Coeval $^{40}Ar/^{39}Ar$ ages of 65.0 million years ago from Chicxulub crater melt rock and Cretaceous-Tertiary boundary tektites. *Science,* v. 257, pp. 954-958.

Tagle, R. and Claeys, P., 2004. Comet or asteroid shower in the late Eocene? *Science*, v. 305, p. 492.

Tagle, R. and Claeys, P., 2005. An ordinary chondrite impactor for the Popigai crater, Siberia. *Geochimica et Cosmochimica Acta*, v. 69, no. 11, pp. 2877-89.

Thein, J., 1987. A tektite layer in upper Eocene sediments of the New Jersey continental slope (Site 612, Leg 95). In *Initial Reports of the Deep Sea Drilling Project* (eds. C.W. Poag, A.B. Watts *et al.*), pp. 565-79. vol. 95, U.S. Government Printing Office, Washington D.C., USA.

Thomas, E., 1990. Late Cretaceous-early Eocene mass extinctions in the deep sea. *In,* Sharpton, V.L., and Ward, P.D., (eds) Global catastrophes in earth history: An interdisciplinary conference on impacts, volcanism, and mass mortality. *Geological Society of America Special Publication,* v. 101, pp. 401-41.

Tingle, T.N., 1998. Accretion and differentiation of carbon in the early Earth. *Chemical Geology*, v. 147, pp. 3-10.

Tjalsma, L.A., and Lohmann, G.P., 1983. Paleocene-Eocene bathyal and abyssal benthic foraminifera from the Atlantic Ocean. *Micropaleontology Spec. Pub.* v. 4, 1-90.

Toon, O.B., Zahnle, K., Turco, R.P., Covey, C., 1994. Environmental perturbations caused by asteroid impacts. *In:* Gehrels, T., (ed), Hazards due to comets and asteroids. University of Arizona Press, Tucson, pp. 791-826.

Urey, H.C., 1947. The thermodynamic properties of isotopic substances. *Journal of the Chemical Society*, London, April, pp. 562-81.

Vincent, E., Killingley, J.S., Berger, W.H., 1984. Miocene oxygen and carbon isotope stratigraphy of the tropical Indian Ocean. *In:* (ed) J.P. Kennett, Miocene Paleoceanography and Biogeography, *Geological Society of America*.

Vincent, E., and Berger, W.H., 1985. Carbon dioxide and polar cooling in the Miocene; the Monterey Hypothesis. *In:* E.T. Sundquist and W.S. Broecker, (eds) *The Carbon Cycle and Atmospheric CO_2 variations Archean to the Present*, *Geophysical Research Monograph*, v. 32, pp. 455-68. American Geophysical Union, Washington, DC.

Vinot-Bertouille, A.C., and Duplessy, J.C., 1973. Individual isotopic fractionation of carbon and oxygen in benthic foraminifera. *Earth and Planetary Science Letters*, v. 18, no. 2, pp. 247-52.

Vonhof, H.B., and Smit, J., 1999. Late Eocene microkrystites and microtektites at Maud Rise (Ocean Drilling Project Hole 689B: Southern Ocean) suggest a global extension of the approximately 35.5 Ma Pacific impact ejecta strewn field. *Meteoritics and Planetary Science*, v. 34, pp. 747-755.

Vonhof, H.B., Smit, J., Brinkhuis, H., Montanari, A., Nederbragt, A.J., 2000. Global cooling accelerated by early late Eocene impacts? *Geology*, v. 28, no. 8, pp. 687-90.

Walkden, G., Parker, J., Kelley, S., 2002. A Late Triassic impact ejecta layer in southwestern Britian. *Science*, v. 298, pp. 2185-88.

Wade, B.S., and Palike, H., 2004. Oligocene climate dynamics. *Paleoceanography*, v. 19, PA4019, doi:10.1029/2004PA001042.

Ward, P.D., Haggart, J.W., Carter, E.S., Wilbur, D., Tipper, H.W., Evans, T., 2001. Sudden productivity collapse associated with the Triassic-Jurassic boundary mass extinction. *Science*, v. 292, pp. 1148-51.

Whitehead, J., Papanastassiou, D.A., Spray, J.G., Grieve, R.A.F., Wasserburg, G.J. 2000. Late Eocene impact ejecta: geochemical and isotopic connections with the Popigai impact structure. *Earth and Planetary Sci. Lett.,* v. 181, pp. 473-87.

Wolfe, J.A., 1980. Tertiary climates and floristic relationships at high latitudes in the Northern Hemisphere. *Palaeogeography*, *Palaeoclimatology, Palaeoecology*, v. 30, pp. 313-23.

Wood, J.A., 2005. The chondrite types and their origins. *In:* (eds) Krot, A.N., Scott, E.R.D., Reipurth, B., Chondrites and the Protoplanetary Disk. *Astronomical Society Pacific Conference Series*, v. 341, pp. 953-71.

Worthington, L.V., 1976. On the North Atlantic Circulation. John Hopkins University Press, Woods Hole, MA, pp.110.

Wright, J.D., and Miller, K.G., 1992. Southern Ocean influences on late Eocene to Miocene deep-water circulation, in *The Antarctic Paleoenvironment: A Perspective on Global Change, Antarctic Research Series*, vol. 60, (eds) J.P. Kennett and D.A. Warnke, pp. 1-25, AGU, Washington, D.C.

Wyckoff, S., Kleine, M., Peterson, B., Wehinger, P., Ziurys, L., 2000. Carbon isotope abundances in comets. *The Astrophysical Journal*, v. 535, pp. 991-999.

Zachos, J.A., and Arthur, M.A., 1986. Paleoceanography of the Cretaceous/Tertiary boundary event: Inferences from stable isotope data. *Paleoceanography*, v. 1, no. 1, pp. 5-26.

Zachos, J.A., Stott, L.D., Lohmann, K.C., 1994. Evolution of early Cenozoic marine temperatures. *Paleoceanography*, v. 9, pp. 353-87.

Zachos, J.A., Pagani, M., Sloan, L., Thomas, E., Billups, K., 2001**.** Trends, rhythms, and aberrations in global climate 65 Ma to present. *Science,* v. 292, pp. 686-693.

Zahringer, J., 1963. K-Ar measurements of tektites. *In:* Radioactive Dating, International Atomic Energy Agency, pp. 289-305.

Equations for Tables 1, and 5 – 8

from Kent et *al*. (2003):

$$C_a = C_i \left[\frac{(\Delta\delta^{13}C)}{(\delta^{13}C_a - \delta^{13}C_i - \Delta\delta^{13}C)} \right]$$

$\Delta\delta^{13}C$ = -0.45‰ = change in the $\delta^{13}C$ value of the oceanic deep-water reservoir
$\delta^{13}C_i$ = 0.5‰ = mean isotopic composition of deep-water at Site 1090
$\delta^{13}C_a$ = mean isotopic composition of reservoir adding C to the deep-water reservoir
C_i = 37,000 Gt = initial mass of C in the deep-water reservoir
C_a = mass of C added to the deep-water reservoir needed to decrease the $\delta^{13}C$ value

---

[a] Siegenthaler and Sarmiento (1993)
[b] Falkowski (2005)
[c] Houghton et *al*. (2001)
[d] Milkov (2004)
[e] Cramer and Kent (2005)
[f] Broecker and Peng (1982)
[g] Deines (1992)
[h] Keith and Weber (1964)
[i] Kump and Arthur (1999)
[j] Faure (1986)
[k] Schidlowski (2001)
[l] Dickens et *al*. (1995, 1997)
[m] Farmer and Baxter (1974)
[n] Wyckoff et *al*. (2000)
[o] Arpigny et *al*. (2003)
[p] Messenger (2000)
[q] Sundquist and Visser (2005)
[r] Francey et *al*. (1999)
[st] Alexander et *al* (1990, 1998)
[u] Jessberger and Kissel (1991)
[v] Sephton et al., (2003)
[w] Greenberg (1998)
[x] Makjanic et *al* (1993)
[y] Tingle (1998)
[z] Mason (1963)

0.45‰ $\delta^{13}C$ decrease in deep-water (37,000 Gt exchangeable reservoir)

requires ~370 Gt of cometary carbon ($\delta^{13}C$ composition = -45‰)

Assuming comets are ~25 wt.% carbon[u] with a bulk-density[w] of 1500 kg/m^3

volume of a sphere = (4/3)πr^3

Equals **12 km** diameter comet

requires ~920 Gt of L-type chondritic carbon ($\delta^{13}C$ composition = -18‰)

Assuming ordinary chondrites are ~0.15 wt.% carbon[xy] with a bulk-density[z] of 2500 kg/m^3

A **225 km** diameter L-type chondrite would only inject ~7 Gt of carbon

Table 1
Size in gigatons (Gt) and the isotopic ratio of the exchangeable carbon reservoirs

Carbon reservoir	Pre-Industrial[a] (Gt)	Recent (1980-present) (Gt)	$\delta^{13}C$ (PDB)	Perturbation required to change deep-water $\delta^{13}C$ ratio by - 0.45 ‰
ATMOSPHERE	600	720[b] - 750[a]	-6 to -7[fr] (-6.5)	**2,540**
OCEANS		38,400[b]		
total inorganic		37,400[b]	0[f]	
surface layer (inorganic)	1,000	670[b] - 1,020[a]	2 - 4[f] (3)	**-5,640**
deep layer (inorganic)	**38,000**	**36,730[b] - 38,100[a]**	**1 - 2[f] (0.5)**	
dissolved organic	700	600[b] - 700[a]	-17[f]	**975**
LITHOSPHERE		115 million[q]		
volcanism (mantle)		35 million[q]	-5[g]	**3,290**
sedimentary carbonates (inorganic)		>60 million[b]	0.56[h] to 1[i] (1)	**-17,530**
kerogens (organic)		15 million[b]	-15 to -40[j] (-30)	**550**
TERRESTRIAL BIOSPHERE		2,000[b]		
living biomass	610	550[a] - 1,000[b]	-5 to -35[jk] (-25)	**665**
dead biomass (soil and detritus)	1,560	1,200[b] - 1,500[a]	-10 to -30[jq] (-29)	**570**
AQUATIC BIOSPHERE	3	1[b] - 3[a]	-6 to -23[j] (-23)	**720**
FOSSIL FUELS		4,000[a] - 4,130[b]		
coal		3,150[b] - 3,700[c]	-25[j]	**665**
oil		230[b] - 700[c]	-18 to -34[j] (-28)	**590**
gas		140[b] - 500[c]	-40 to -70[j] (-60)	**275**
peat		250[b] - 500[d]	-25[f]	**665**
methane hydrates		500 to 2,500[d]	-40 to -70[im] (-60[l])	**275**
comet		up to 2,000[e]	-110[oo]	**150**
interplanetary dust particles		up to 2,000[e]	-45[p]	**370**
ordinary chondrite		< 500[e]	-15 to -20[st] (-18)	**920**
carbonaceous chondrite		up to 6,000[e]	-10 to -20[tv] (-15)	**1,100**

Table 2.
Counts (in #s) of benthic foraminifera species from the genus *Cibicidoides*. Full names of species listed at the end of table.

Core /Section	Depth (cm)	*C. dic*	*C. prae*	*C. eoc*	*C. grim*	*C. brad*	Other
31X-CC	18 - 19.5			2			
31X-7	30 – 31.5			2	1		
31X-6	144 – 145.5			4			
31X-6	104.5 – 106		2	1			
31X-6	65 – 66.5			1			
31X-6	25 – 26.5	1	2	6			
31X-5	134 – 135.5		2	2			
31X-5	88 – 89.5	1	2		3		
31X-5	48.5 - 50		1				
31X-5	12 – 13.5			4		1	1 *C. rob*
31X-4	122 – 123.5		1	2			
31X-4	82.5 - 84			6	3		
31X-4	42 – 43.5						
31X-3	144 – 145.5			1	1		
31X-3	123 – 124.5	1			1	1	
31X-3	105 – 106.5		1		1	1	
31X-3	83 – 84.5		2	3	1		
31X-3	63 – 64.5		2	5	1		
31X-3	45 – 46.5		4	3		3	1 *C. ha*
31X-3	25 – 26.5				1	3	1 *C. rob*
31X-3	6 – 7.5					4	
31X-2	135 – 136.5			7	1	2	
31X-2	113.5 – 115		4	2		3	
31X-2	95.5 – 97			4	1	2	
31X-2	75.5 – 77		3	2		2	
31X-2	57 – 58.5		1	2		3	
31X-2	37 – 38.5		4	1		5	
31X-2	18 – 19.5		4	4			
31X-1	145.5 – 147		2	4	1	3	
31X-1	125 – 126.5	1	5			1	
31X-1	105 – 106.5		1	2		2	
31X-1	85 – 86.5		1			5	
31X-1	65 – 66.5						
31X-1	45.5 – 47					1	
31X-1	25.5 – 27		4	1		1	
31X-1	6.5 – 8		1	4			
30X-7	44 – 45.5		1	13		5	2 *C. hav*
30X-7	25.5 – 27			7		4	
30X-7	5.5 – 7	2		9		1	1 *C. lau*
30X-6	133 – 134.5						
30X-6	107.5 – 109		1	1		4	
30X-6	87 – 88.5	1	1	12		7	
30X-6	67 – 68.5	1	1	1		5	
30X-6	48.5 – 50	6	2	2		2	
30X-6	33 – 34.5			3		1	
30X-6	12 – 13.5	1		4		1	
30X-5	138 – 139.5		1	5	1	7	

Table 2.

Core/Section	Depth (cm)	*C. dic*	*C. prae*	*C. eoc*	*C. grim*	*C. brad*	Other
30X-5	118.5 – 120						
30X-5	**105 – 106 ~ ~ ~ ~ ~ ~ IR ANOMALY (954 ppt) ~ ~ ~ ~ ~ ~ ~ ~ ~ ~ ~ IR ANOMALY~**						
30X-5	**114 – 115 ~ ~ ~ ~ ~ EJECTA LAYERS ~ ~ ~ ~ ~ ~ ~ ~ ~ ~ EJECTA LAYERS ~ ~ ~**						
30X-5	94 – 95.5		1	1	1	3	
30X-5	75.5 – 77	1	1	3		2	
30X-5	58.5 – 60	1		2	2	1	
30X-5	36 – 37.5	1				1	
30X-5	18.5 – 20	1				3	
30X-4	143.5 – 145					4	
30X-4	123 – 124.5					3	
30X-4	104 –105.5					7	
30X-4	86 – 87.5					1	
30X-4	66 – 67.5					3	
30X-4	46 – 47.5					2	
30X-4	26 – 27.5					7	
30X-4	6 – 7.5					7	
30X-3	137 – 138.5					4	1 *C. hav*
30X-3	116 – 117.5					9	
30X-3	96 – 97.5					4	1 *C. rob*
30X-3	76 – 77.5					7	1 *C. hav*
30X-3	58.5 – 60					5	
30X-3	36.5 – 38					3	
30X-3	18 – 19.5					1	
30X-2	148.5 – 150					4	1 *C. rob*
30X-2	130 – 131.5					2	
30X-2	111 – 112.5					3	
30X-2	91 – 92.5					2	
30X-2	71.5 – 73	1		1		1	
30X-2	51 – 52.5					2	
30X-2	32 – 33.5					4	
30X-2	11 – 12.5			1		1	
30X-1	142 – 143.5	1				4	
30X-1	121.5 – 123					2	
30X-1	101 – 102.5						
30X-1	76 – 77.5					3	1 *C. rob*
30X-1	58.5 – 60					5	
30X-1	36 – 37.5					2	
30X-1	18 – 19.5						
29X-CC	14 – 15.5						
29X-7	36 – 37.5					4	
29X-7	18.5 – 20					3	1 *C. rob*
29X-6	144 – 145.5						
29X-6	124 – 125.5						
29X-6	104.5 – 106					2	
29X-6	84 – 85.5					3	
29X-6	64 – 65.5		1			3	
29X-6	44 – 45.5						
29X-6	24 – 25.5						
29X-6	4.5 – 6					1	
29X-5	126 – 127.5					1	
29X-5	86 – 87.5	5					
29X-5	43.5 – 45					5	
29X-5	5 – 6.5	5					

Table 2.

Core/Section	Depth (cm)	*C. dic*	*C. prae*	*C. eoc*	*C. grim*	*C. brad*	Other
29X-4	107 – 108.5					6	
29X-4	65 – 66.5	1				4	
29X-4	25.5 – 27						1 *C. rob*
29X-3	136 – 137.5					5	
29X-3	84 – 85.5	1				5	
29X-3	42.5 – 44					1	
29X-3	6 – 7.5						
29X-2	115 – 116.5			1		5	
29X-2	75.5 – 77					6	
29X-2	35.5 – 37					3	
29X-1	145 – 146.5					3	
29X-1	105.5 – 107			1		5	
29X-1	65 – 66.5					4	
29X-1	25 – 26.5			3		5	
28X-7	22 – 23.5					4	
28X-6	135 – 136.5			1		3	
28X-6	94 – 95.5					3	
28X-6	54 – 55.5						
28X-6	14 –15.5					5	
28X-5	124 –125.5			3		4	
28X-5	84 – 85.5					5	1 *C. lau*
28X-5	43 – 44.5	1				4	
28X-5	5 – 6.5						
28X-4	113 – 114.5					2	
28X-4	73 – 74.5					7	
28X-4	36 – 37.5					5	
28X-3	148 – 149.5			4	1	4	
28X-3	105 – 106.5					3	
28X-3	65 – 66.5					3	
28X-3	25 – 26.5			2		8	1 *C. lau*
28X-2	138 – 139.5			1		4	
28X-2	95 – 96.5	1		2		2	
28X-2	55 – 56.5			2		3	
28X-2	15 – 16.5			3		6	1 *C. mic*
28X-1	135.5 – 137			1		1	
28X-1	96 – 97.5				1	2	
28X-1	54.5 – 56		1	3	2	2	
28X-1	16 – 17.5					1	
27X-6	72.5 – 74		1	7		4	1 *C. lau*
27X-6	34 – 35.5		2	5	1	1	
27X-5	148 – 149.5	1	4	3		1	
27X-5	113 – 114.5			3		2	
27X-5	72 – 73.5			1		4	
27X-5	33.5 – 35	3		2		2	
27X-4	134 – 135.5			2		1	
27X-4	94 – 95.5	2		3	1		
27X-4	58 – 59.5			2		2	
27X-4	18 – 19.5			4	1	2	
27X-3	122 –123.5			2		2	
27X-3	83 – 84.5	2		3		1	
27X-3	44 –45.5			3		1	
27X-3	6 – 7.5		2		3	1	
27X-2	113.5 – 115	1		1		4	

Table 2.

Core/Section	Depth (cm)	*C. dic*	*C. prae*	*C. eoc*	*C. grim*	*C. brad*	Other
27X-2	72 – 73.5			4		2	
27X-2	33.5 – 35			2		4	
27X-1	137 – 138.5			7		1	
27X-1	93 – 94.5			3			
27X-1	63 – 64.5			3			
27X-1	18 – 19.5						
26X-7	12 – 13.5						
26X-6	143 – 144.5						
26X-6	103 – 104.5						
26X-6	63 – 64.5						
26X-6	24 – 25.5						
26X-5	138.5 – 140						
26X-5	92 – 93.5						
26X-5	48 – 49.5	1		1		1	
26X-5	12 – 13.5	2		8			

Main *Cibicidoides*:

C. dic
C. prae
C. eoc
C. grim
C. brad

***Cibicidoides*:**

C. dickersoni
C. praemundulus
C. eoceanus
C. grimsdalei
C. bradyi

Other

C. rob
C. hav
C. lau
C. mic

C. robertsonianus
C. havanensis
C. laurisae
C. micrus

Table 3

Sample	Site/Hole	Core	Sec.	Depth	*Cibicidoides*	Age Ma	mbsf	$\delta^{13}C$	$\delta^{18}O$
#				(cm)	*spp.*				
1	1090B	26X	5	12	D/E	33.7910	239.320	0.77	1.24
2	1090B	26X	6	48	D/E/B	33.8005	239.680	0.64	1.01
3	1090B	27X	1	63	E	33.9023	243.530	0.18	0.85
4	1090B	27X	1	93	E	33.9102	243.830	0.36	0.79
5	1090B	27X	1	137	E/B	33.9218	244.270	0.56	0.91
6	1090B	27X	2	33.5	E/B	33.9341	244.735	0.45	0.90
7	1090B	27X	2	72	E/B	33.9443	245.120	0.49	0.96
8	1090B	27X	2	113.5	D/E/B	33.9553	245.535	0.30	0.53
9	1090B	27X	3	6	P/B/G	33.9665	245.960	0.29	0.71
10	1090B	27X	3	44	E/B	33.9766	246.340	0.16	0.46
11	1090B	27X	3	83	D/E	33.9869	246.730	0.86	0.92
12	1090B	27X	3	122	E/B	33.9972	247.120	0.58	0.58
13	1090B	27X	4	18	E/B	34.0093	247.580	0.75	0.90
14	1090B	27X	4	94	D/E	34.0294	248.340	0.48	0.67
15	1090B	27X	4	134	E/B	34.0400	248.740	0.78	0.88
16	1090B	27X	5	33.5	D/E	34.0531	249.235	0.56	0.83
17	1090B	27X	5	72	E/B	34.0632	249.620	0.10	1.01
18	1090B	27X	5	113	E	34.0741	250.030	0.58	0.79
19	1090B	27X	5	148	P/D/E	34.0833	250.380	0.34	0.70
20	1090B	27X	6	34	P/E/B	34.0928	250.740	0.80	1.06
21	1090B	27X	6	72.5	P/E/B	34.1030	251.125	0.23	0.85
22	1090B	28X	1	54.5	P/E/B	34.1564	253.145	0.60	0.82
23	1090B	28X	1	96	G/B	34.1674	253.560	0.70	1.06
24	1090B	28X	2	15	E/M/B	34.1856	254.250	0.07	0.86
25	1090B	28X	2	55	E/B	34.1962	254.650	0.34	0.83
26	1090B	28X	2	95	D/E/B	34.2067	255.050	0.29	0.62
27	1090B	28X	2	138	E/B	34.2181	255.480	0.42	0.69
28	1090B	28X	3	25	E/ B	34.2279	255.850	0.42	1.09
29	1090B	28X	3	148	E	34.2604	257.080	0.43	0.65
30	1090B	28X	4	73	B	34.2802	257.830	0.02	1.19
31	1090B	28X	5	43	D/B	34.3119	259.030	0.26	1.03
32	1090B	28X	5	84	L/B	34.3227	259.440	0.00	1.06
33	1090B	28X	5	124	E/B	34.3333	259.840	0.45	0.74
34	1090B	28X	6	135	E/B	34.3759	261.450	0.32	0.96
35	1090B	29X	1	25.5	B	34.4049	262.550	0.42	1.04
36	1090B	29X	1	65	B	34.4155	262.950	0.31	1.14
37	1090B	29X	1	105.5	E/B	34.4262	263.355	0.84	0.82
38	1090B	29X	2	75.5	B	34.4579	264.555	0.15	0.94
				P	*praemundulus*				
				D	*dickersoni*				
				E	*eoceanus*				
				B	*bradyi*				
				G	*grimsdalei*				
				H	*havanensis*				
				R	*robertsonianus*				
				M	*micrus*				
				L	*laurisae*				
#	1090B	30X	#	#	Duplicates	#	#	(avg.)	(avg.)

Table 3

Sample #	Site/Hole	Core	Sec.	Depth (cm)	*Cibicidoides spp.*	Age Ma	mbsf	$\delta^{13}C$	$\delta^{18}O$
39	1090B	29X	3	84	D/B	34.4998	266.140	0.48	0.91
40	1090B	29X	3	136	B	34.5136	266.660	0.34	1.03
41	1090B	29X	4	65	D/B	34.5344	267.450	0.60	1.03
42	1090B	29X	4	107	B	34.5455	267.870	0.44	0.90
43	1090B	29X	5	5	D	34.5582	268.350	0.61	0.59
44	1090B	29X	5	43.5	B	34.5684	268.735	0.42	0.76
45	1090B	29X	5	86	D	34.5796	269.160	0.65	0.75
		29X	6	24	MICROTEKTITE	34.6029	270.040		
46	1090B	29X	6	64	P/B	34.6134	270.440	0.15	0.69
47	1090B	*29X*	7	18.5	B/R	34.6711	272.180	0.08	0.73
48	1090B	30X	1	58.5	B	34.7096	272.585	0.26	0.70
49	1090B	30X	1	76	B/R	34.7262	272.760	0.08	0.80
50	1090B	30X	1	142	D/B	34.7889	273.420	0.06	0.51
51	1090B	30X	2	148.5	B/H	34.9375	274.985	0.09	0.73
52	1090B	30X	3	58.5	B	35.0559	275.585	0.27	0.90
53	1090B	30X	3	76	B	35.0912	275.760	0.25	0.85
54	1090B	30X	3	96	B/R	35.1315	275.960	0.35	0.99
55	1090B	30X	3	116	B	35.1719	276.160	0.42	0.97
56	1090B	30X	3	137.5	B/H	35.2142	276.370	0.45	0.82
57	1090B	30X	4	6	B	35.2525	276.560	0.21	0.43
58	1090B	30X	4	26	B	35.2928	276.760	0.03	0.75
59	1090B	30X	4	66	B	35.3491	277.160	0.21	0.74
60	1090B	30X	4	104	B	35.3646	277.540	0.27	0.59
		30X	4	123	MICROTEKTITE	35.3723	277.730		
61	1090B	30X	5	58.5	D/E/G/B	35.4071	278.585	0.83	0.47
62	1090B	30X	5	75.5	P/D/E/B MICRTEK	35.4140	278.755	0.72	0.31
63	1090B	30X	5	94	P/E/G/B MICRTEK	35.4215	278.940	0.43	0.34
*******	**1090B**	**30X**	**5**	**105**	**IR (295 ppt)**	**35.4260**	**279.050**	********	*******
*******	**1090B**	**30X**	**5**	**114**	**EJECTA LAYERS**	**35.4300**	**279.150**	********	*******
64	1090B	30X	5	138	P/E/G	35.4394	279.380	0.96	0.98
65	1090B	30X	6	12	D/E/B	35.4491	279.620	0.74	0.40
66	1090B	30X	6	33	E/B	35.4577	279.830	0.91	0.54
67	1090B	30X	6	48.5	P/E/B	35.4640	279.985	1.00	0.73
68	1090B	30X	6	67	P/D/E/B	35.4715	280.170	0.70	0.61
69	1090B	30X	6	87	E	35.4796	280.370	0.87	0.70
70	1090B	30X	6	107.5	P/E/B	35.4880	280.575	0.90	0.67
71	1090B	30X	7	5.5	D/E	35.5075	281.055	1.09	0.78
72	1090B	30X	7	25.5	E	35.5156	281.255	0.95	0.65
73	1090B	30X	7	44	E	35.5232	281.440	1.01	0.70
74	1090B	31X	1	6.5	P/E	35.5422	281.765	0.97	0.56
75	1090B	31X	1	25.5	P/E/B	35.5543	281.955	0.84	0.69
76	1090B	31X	1	85	P/B	35.5922	282.550	0.68	1.07
77	1090B	31X	1	105	P/E/B	35.6049	282.750	0.97	0.70
78	1090B	31X	1	125	P/D	35.6176	282.950	1.03	0.63
79	1090B	31X	1	145.5	P/B	35.6306	283.155	0.85	0.43

Table 3

Sample #	Site/Hole	Core	Sec.	Depth (cm)	*Cibicidoides spp.*	Age Ma	mbsf	$\delta^{13}C$	$\delta^{18}O$
80	1090B	31X	2	18	P/E	35.6450	283.380	0.97	0.57
81	1090B	31X	2	37	P/E	35.6570	283.570	0.95	0.59
82	1090B	31X	2	57	P/E/B	35.6698	283.770	0.92	0.69
83	1090B	31X	2	75.5	P/E/B	35.6815	283.955	0.83	0.62
84	1090B	31X	2	95.5	E/G/B	35.6912	284.155	0.79	0.58
85	1090B	31X	2	113.5	P/E/B	35.6989	284.335	0.84	0.67
86	1090B	31X	2	135	E/G/B	35.7080	284.550	0.99	0.50
87	1090B	31X	3	6	B	35.7170	284.760	0.41	1.09
88	1090B	31X	3	25	G/B/R	35.7251	284.950	0.46	0.95
89	1090B	31X	3	45	P/B	35.7337	285.150	1.00	0.61
90	1090B	31X	3	63	E/P/G	35.7413	285.330	0.95	0.55
91	1090B	31X	3	83	P/E/G	35.7499	285.530	0.91	0.46
92	1090B	31X	3	105	P/G/B	35.7593	285.750	0.90	0.60
93	1090B	31X	3	123	D/G/B	35.7669	285.930	0.84	0.58
94	1090B	31X	3	144	E/G	35.7759	286.140	1.02	0.64
95	1090B	31X	4	82.5	E/G	35.8137	287.025	0.86	0.73
96	1090B	31X	4	122	P/E	35.8305	287.420	0.97	0.79
97	1090B	31X	5	12	E	35.8476	287.820	0.86	0.61
98	1090B	31X	5	48.5	P	35.8632	288.185	0.97	0.82
99	1090B	31X	5	88	P/D/G	35.8800	288.580	0.82	0.73
100	1090B	31X	5	134	E	35.8997	289.040	0.58	0.39
101	1090B	31X	6	25	P/D/E	35.9168	289.440	0.73	0.79
102	1090B	31X	6	104.5	P/E	35.9511	290.245	0.88	0.59
103	1090B	31X	6	144	E	35.9680	290.640	0.88	0.84
104	1090B	31X	7	30	E/G	35.9833	291.000	0.50	0.56
105	1090B	31X	CC	18	E	36.0008	291.410	0.81	1.12

Table 4

Site/Hole/ Core/Section		Depth (cm)	Age (Ma)	Depth (mbsf)	$\delta^{13}C$ Bulk-$CaCO_3$	$\delta^{18}O$ Bulk-$CaCO_3$
1090-B-30X-5		5	35.3853	278.05	2.12	0.07
1090-B-30X-5		10	35.3873	278.10	2.12	-0.16
1090-B-30X-5		15	35.3894	278.15	2.14	-0.26
1090-B-30X-5		20	35.3914	278.20	2.17	-0.13
1090-B-30X-5		25	35.3934	278.25	2.14	-0.26
1090-B-30X-5		30	35.3955	278.30	2.35	0.21
1090-B-30X-5		35	35.3975	278.35	2.19	0.16
1090-B-30X-5		40	35.3995	278.40	2.32	0.32
1090-B-30X-5		45	35.4016	278.45	2.26	0.34
1090-B-30X-5		50	35.4036	278.50	2.30	0.32
1090-B-30X-5		55	35.4056	278.55	2.18	0.31
1090-B-30X-5		60	35.4077	278.60	2.18	0.33
1090-B-30X-5		65	35.4097	278.65	2.15	0.29
1090-B-30X-5		70	35.4117	278.70	2.04	0.11
1090-B-30X-5		75	35.4138	278.75	2.10	0.22
1090-B-30X-5		80	35.4158	278.80	2.07	0.05
1090-B-30X-5		85	35.4178	278.85	2.02	0.01
1090-B-30X-5		90	35.4199	278.90	2.16	0.39
1090-B-30X-5		95	35.4219	278.95	2.17	0.35
1090-B-30X-5		100	35.4239	279.00	2.04	0.04
1090-B-30X-5	**Ir (295 ppt)**	**105**	**35.4260**	**279.05**	**2.06**	**0.15**
1090-B-30X-5		110	35.4280	279.10	2.06	0.00
1090-B-30X-5	**Ejecta Layers**	**115**	**35.4300**	**279.15**	**1.60**	**-0.55**
1090-B-30X-5		120	35.4321	279.20	1.85	-0.25
1090-B-30X-5		125	35.4341	279.25	2.20	0.11
1090-B-30X-5		130	35.4361	279.30	2.11	0.36
1090-B-30X-5		135	35.4382	279.35	2.21	0.10
1090-B-30X-5		140	35.4402	279.40	2.11	0.13
1090-B-30X-5		144	35.4418	279.44	2.23	0.15
1090-B-30X-5		145	35.4422	279.45	2.08	0.17
1090-B-30X-5		149	35.4439	279.49	2.17	0.41

Table 5.
Diameter (km) of a **comet**(s) required to change the deep ocean reservoir in gigatons (Gt) of carbon

Comet diameter NEO (near Earth object) (km)	Crater diameter (km)	Gt of C (w/ ρ=1.5)	Gt of C x 2 (w/ ρ=1.5)
1	12	0.2	0.4
2	30	2	4
3	**60 (Chesapeake Bay)**	**5**	**10**
4	**85**	**13**	**26**
5	100	25	50
6		45	90
7	125	70	140
8		100	200
9		150	300
10		200	400
11		260	520
12		370	740
13		430	860
14	200	540	1,080

Table 6.
Diameter (km) of an **ordinary chondrite**(s) (**OC**) required to change the deep ocean reservoir in gigatons (Gt) of carbon

OC diameter (km)	Crater diameter (km)	Gt of C (w/ ρ=2.5)	Gt of C x 2 NEO (w/ ρ=2.5)
1	12	0.002	0.004
2	30	0.017	0.034
3	60	0.06	0.12
4	85	0.13	0.26
5 (Popigai)	**100**	**0.26**	**0.52**
6		0.45	0.9
7	125	0.72	1.4
8		1.1	2.2
9		1.5	3
10		2.1	4.2
11		2.8	5.6
12		3.6	7.2
13		4.6	9.2
14	200	5.75	11.5
15	225	7.1	14.2
16	250	8.6	17.2

Table 7
Size in gigatons (Gt) and the isotopic ratio of the exchangeable carbon reservoirs required to produce a **K-T magnitude** change

Carbon reservoir	Recent (1980-present) (Gt)	$\delta^{13}C$ (PDB)	Perturbation required to change deep-water $\delta^{13}C$ ratio by **-1.5 ‰** (Gt)	Required to change the deep-water $\delta^{13}C$ by **-2 ‰** (Gt)
ATMOSPHERE	720[b] - 750[a]	-6 to -7[fr] (-6.5)	**10,090**	**14,800**
OCEANS	38,400[h]			
total inorganic	37,400[h]	0[f]		
surface layer (inorganic)	670[b] - 1,020[a]	2 - 4[f] (3)	**-13,875**	**-16,445**
deep layer (inorganic)	**36,730[b] - 38,100[a]**	**1 - 2[f] (0.5)**		
dissolved organic	600[b] - 700[a]	-17[f]	**3,470**	**4,775**
LITHOSPHERE	115 million[q]			
volcanism (mantle)	35 million[q]	-5[g]	**13,875**	**21,140**
sedimentary carbonates (inorganic)	>60 million[b]	0.56[h] to 1[i] (1)	**-27,750**	**-29,600**
kerogens (organic)	15 million[b]	-15 to -40[j] (-30)	**1,915**	**2,600**
TERRESTRIAL BIOSPHERE	2,000[b]			
living biomass	550[a] - 1,000[b]	-5 to -35[ik] (-25)	**2,310**	**3,150**
dead biomass (soil and detritus)	1,200[b] - 1,500[a]	-10 to -30[iq] (-29)	**1,980**	**2,691**
AQUATIC BIOSPHERE	1[b] - 3[a]	-6 to -23[j] (-23)	**2,525**	**3,440**
FOSSIL FUELS	4,000[a] - 4,130[b]			
coal	3,150[b] - 3,700[c]	-25[j]	**2,310**	**3,150**
oil	230[b] - 700[c]	-18 to -34[j] (-28)	**2,055**	**2,790**
gas	140[b] - 500[c]	-40 to -70[j] (-60)	**940**	**1,265**
peat	250[b] - 500[d]	-25[f]	**2,310**	**3,150**
methane hydrates	500 to 2,500[d]	-40 to -70[jm] (-60[l])	**940**	**1,265**
comet	up to 2,000[e]	-110[no]	**510**	**680**
interplanetary dust particles	up to 2,000[e]	-45[p]	**1,260**	**1,700**
ordinary chondrite	< 500[e]	-15 to -20[rt] (-18)	**3,265**	**4,485**
carbonaceous chondrite	up to 6,000[e]	-10 to -20[tv] (-15)	**3,965**	**5,480**

Table 8.
Diameter (km) of a **carbonaceous chondrite**(s) (**CC**) required to change the deep ocean reservoir in gigatons (Gt) of carbon

CC diameter Earth object) (km)	Crater diameter (km)	Gt of C (w/ ρ=2.5)	Gt of C x 2 NEO (near (w/ ρ=2.5)
1	12	0.08	0.16
2	30	0.63	1.26
3	60	2.1	4.2
4	85	5	10
5	100	10	20
6		17	34
7	125	27	54
8		40	80
9		58	116
10	**(K-T impactor)**	**80**	**160**
11		105	210
12		136	272
13		173	346
14	200	215	430
15	225	265	530
16	250	322	644

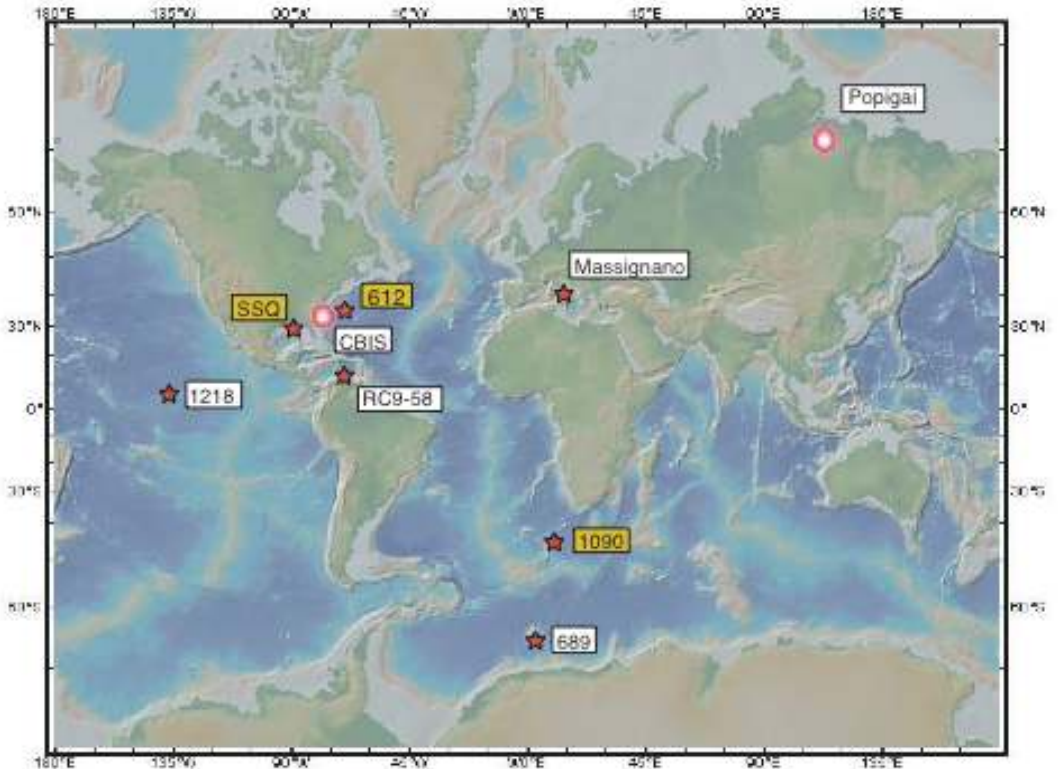

Figure 1.

Global map showing the location of the Chesapeake Bay Impact Structure (CBIS) and Popigai crater. Map displays marine sections from Deep Sea Drilling Project (DSDP) Site 612 (data from this thesis), Ocean Drilling Program (ODP) Sites 689, 1090 (data from this thesis), and 1218, Caribbean core RC9-58 and marine sections on land St. Stephens Quarry (SSQ) (data from this thesis) and Massignano. Yellow boxes indicate new data from this thesis.

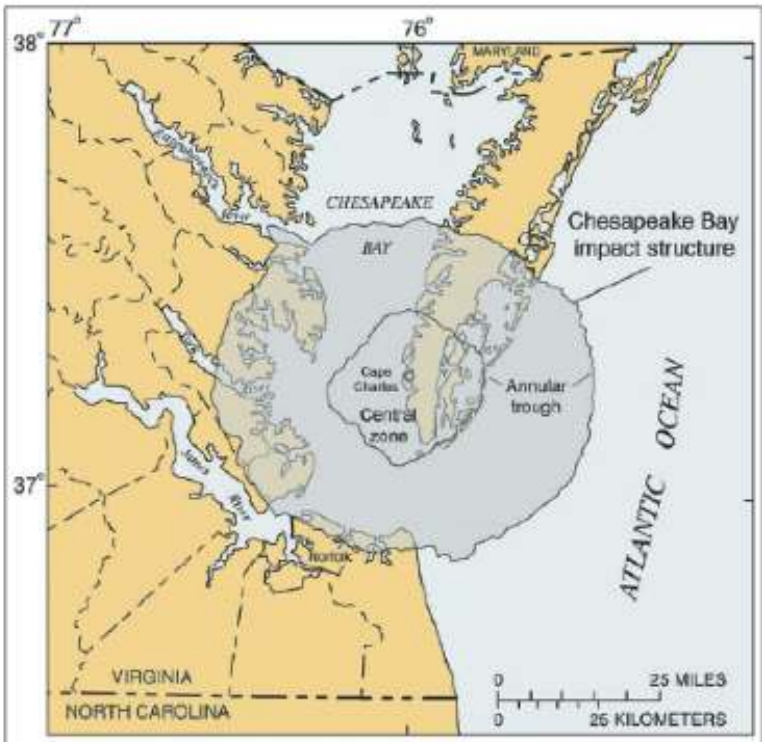

Figure 2.

Regional map of the Chesapeake Bay area, showing the location of the Chesapeake Bay Impact Structure (CBIS) (modified from Gohn et *al*., 2006).

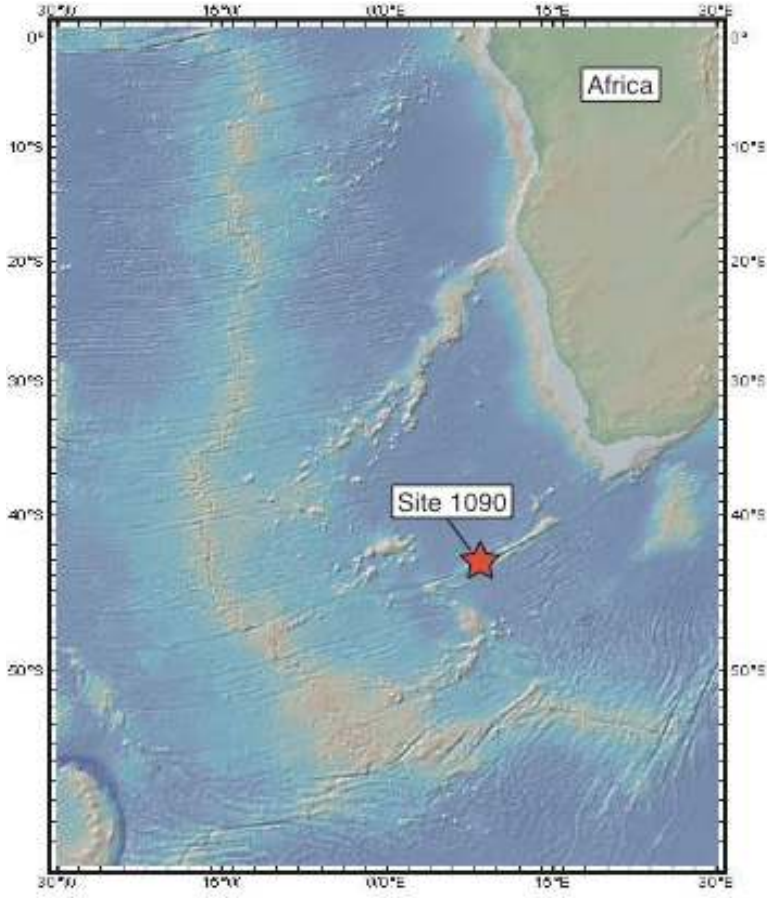

Figure 3.

Location of Ocean Drilling Program Site 1090 in the south Atlantic. Present day water depth is 3,702 mbsf and paleo-water depth was 3,200 mbsf at 34 Ma.

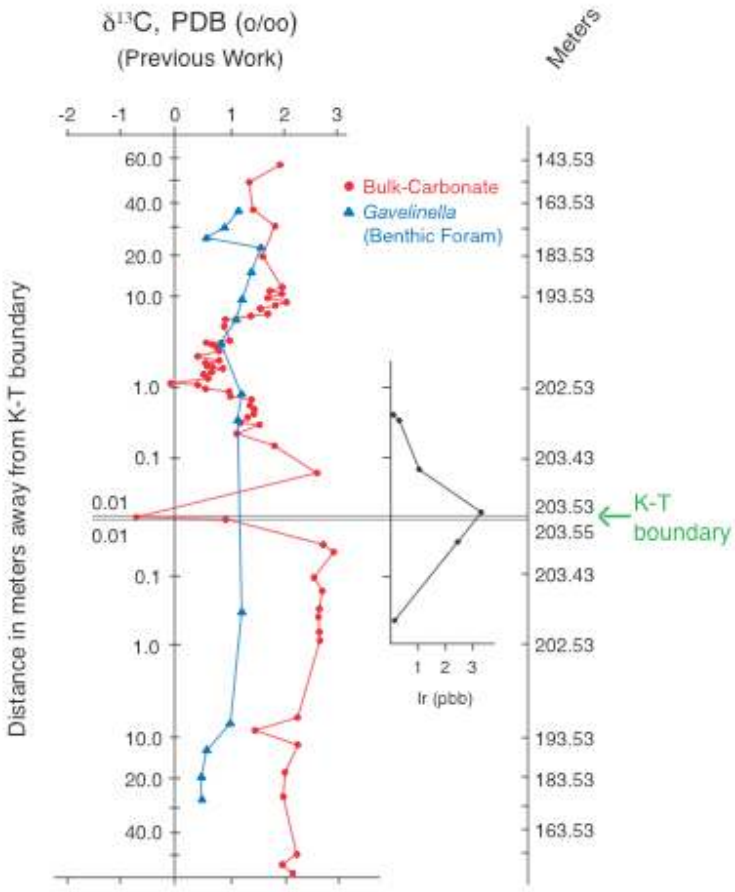

Figure 4a.

South Atlantic DSDP Site 524 carbon isotopes of bulk-carbonate (red circles) and benthic foraminifera (blue triangles) plotted with Ir data across the Cretaceous-Tertiary (K-T) boundary (modified from Hsu et *al*, 1982).

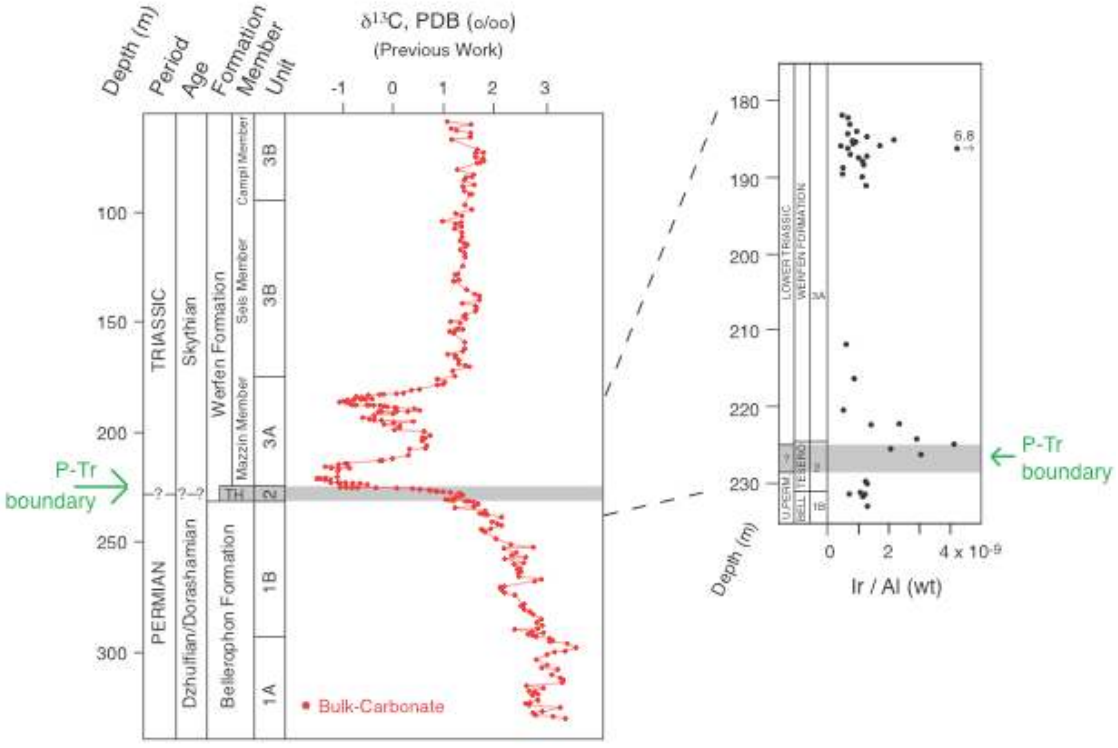

Figure 4b.

Bulk-$CaCO_3$ carbon isotopes and Ir data across the Permian-Triassic (P-Tr) boundary in northern Italy (modified from Holser et *al*, 1989).

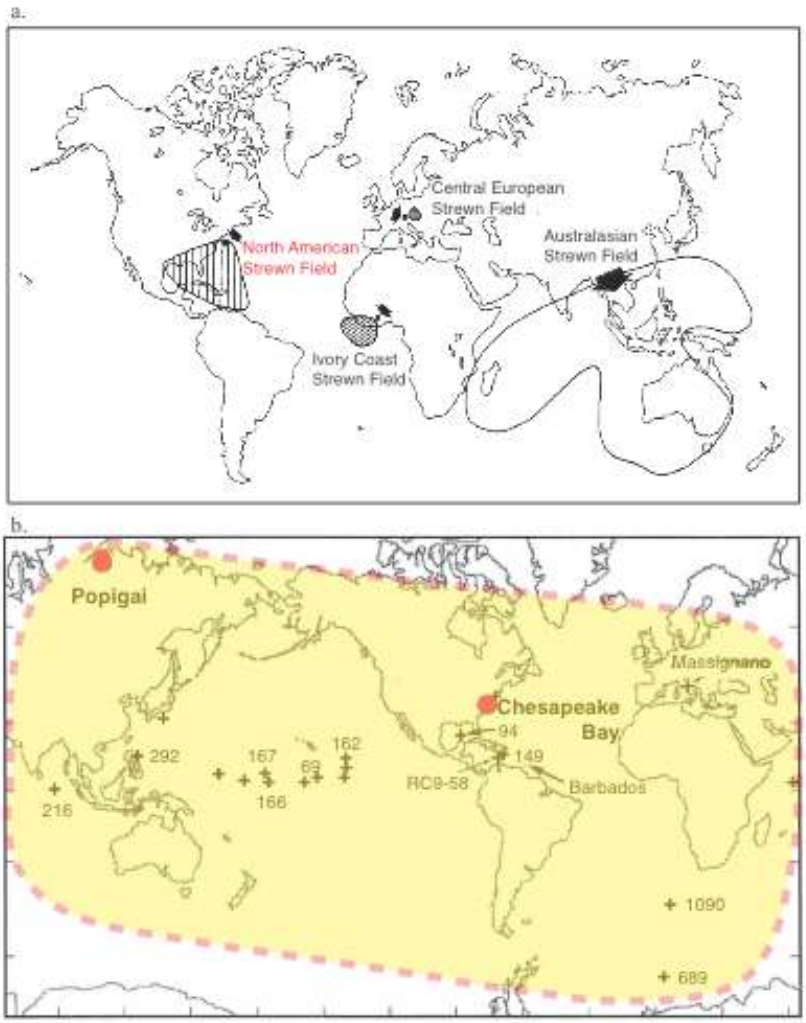

Figure 5a.

Four Cenozoic Strewn Fields, including the North American, Central European, Ivory Coast, and Australasian (modified from Koeberl, 1994).

Figure 5b.

Geographic distribution of sites with identified late Eocene cpx-spherules whose source crater is Popigai (modified from Glass, 2004).

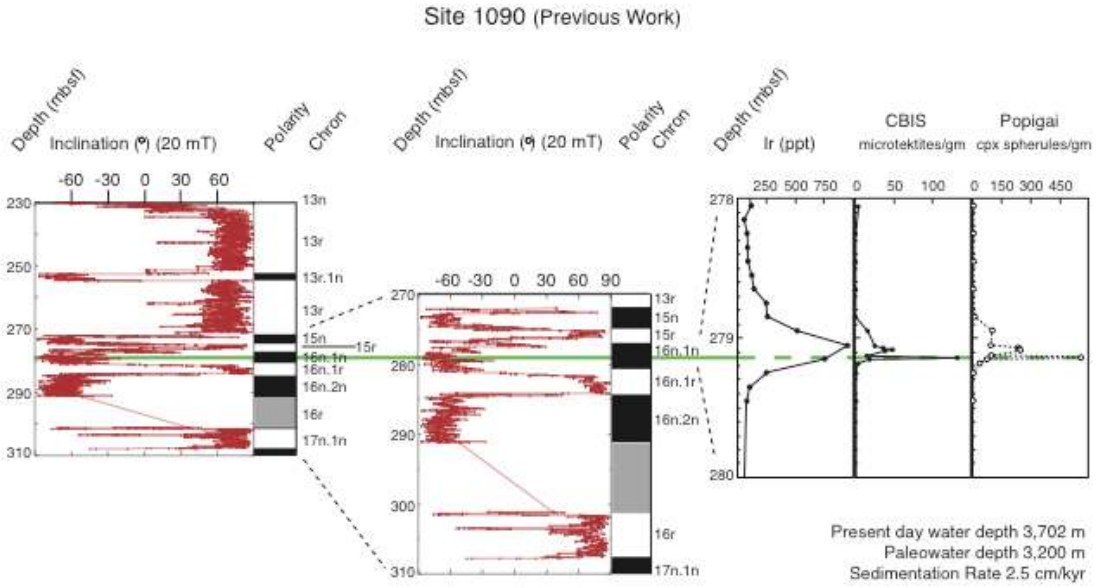

Figure 6.

Shipboard measurements of inclination of the remanent magnetization after alternating-field demagnetization (Gersonde et *al.*, 1999) and magnetic polarity chronology according to the GPTS (1995) (Channell et *al.*, 2003), providing a first-order correlation of the late Eocene ejecta layers (Kyte and Liu, 2002) to Chron C16n.1n

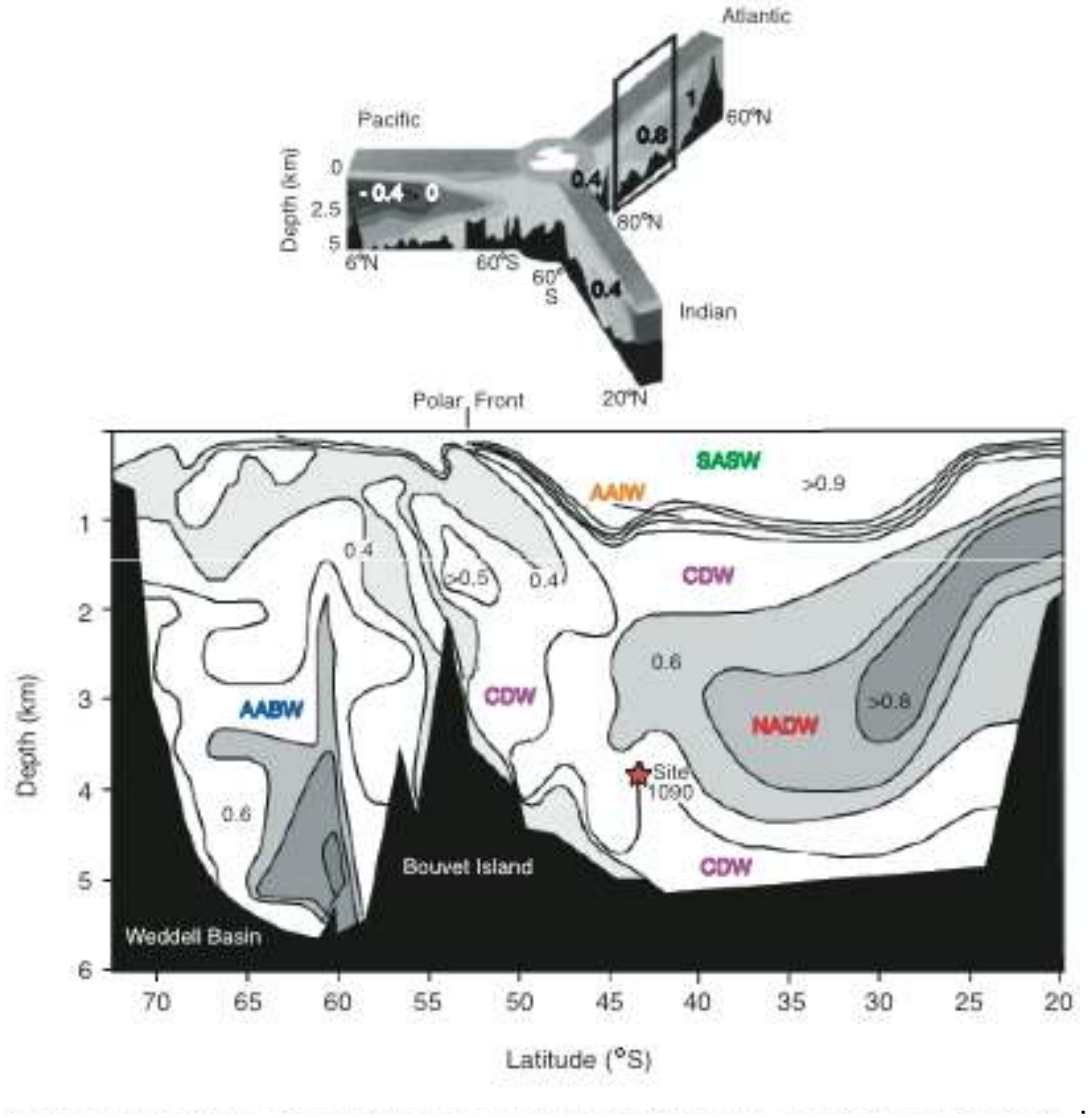

Figure 7.

Top illustration depicts the vertical and latitudinal distribution of $\delta^{13}C$ of dissolved inorganic carbon (DIC) in today's oceans using GEOSECS data (Kroopnick, 1985), after Wright and Miller (1992) (modified from Hodell et *al*., 2002). Bottom figure illustrates the position of ODP Site 1090 in the South Atlantic relative to North Atlantic Deep Water (NADW) and Circumpolar Deep Water (CDW) and their corresponding $\delta^{13}C$ values (modified from Hodell et *al*., 2002). AABW, Antarctic Bottom Water; AAIW, Antarctic Intermediate Water; SASW, Subantarctic Surface Water.

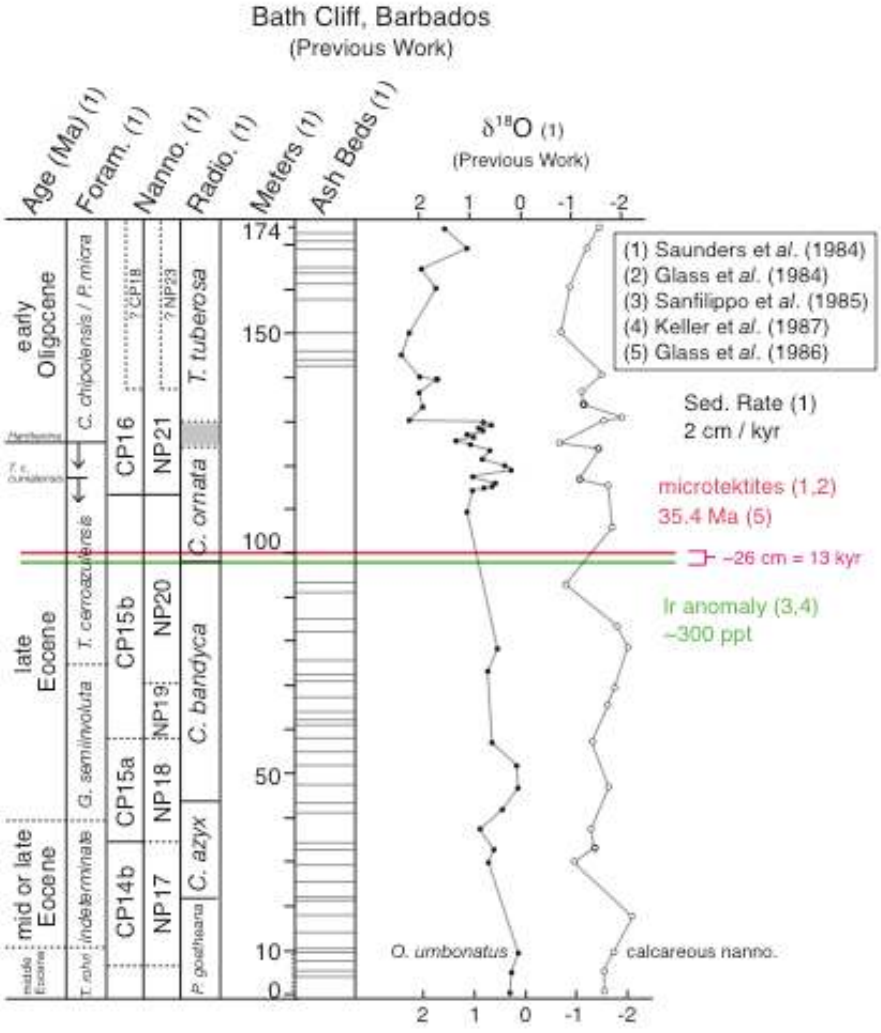

Figure 8.

Biostratigraphy, tephrastratigraphy, and oxygen isotope stratigraphy of the Bath Cliff Section, Barbados (modified from Saunders et *al*., 1984). Red line represents microtektite horizon and green line shows the location of the iridium anomaly (~300 ppt). Closed circles represent benthic foraminifera oxygen isotope values and open circles represent calcareous nannoplankton.

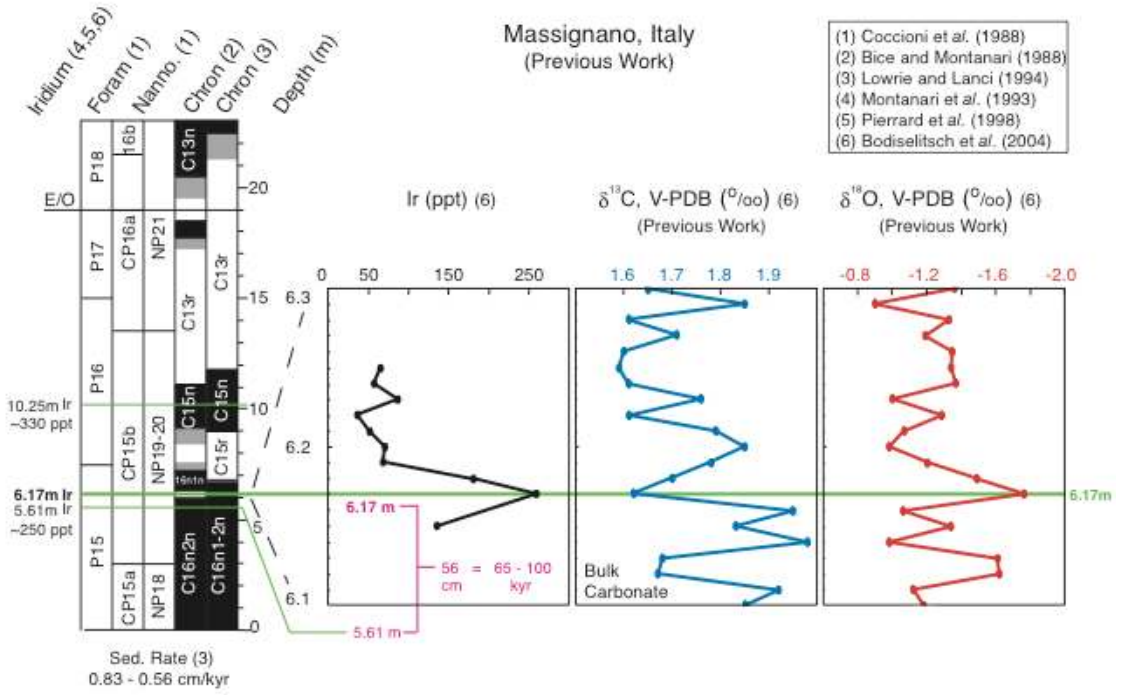

Figure 9a.

Biostratigraphy, magnetostratigraphy, and Ir anomalies of the GSSP of the E/O boundary at Massignano. Left graph displays (~250 ppt) Ir anomaly at 6.17 m, right and center graphs show high resolution carbon (blue) and oxygen (red) bulk-carbonate isotopes (Bodiselitsch et *al*., 2004).

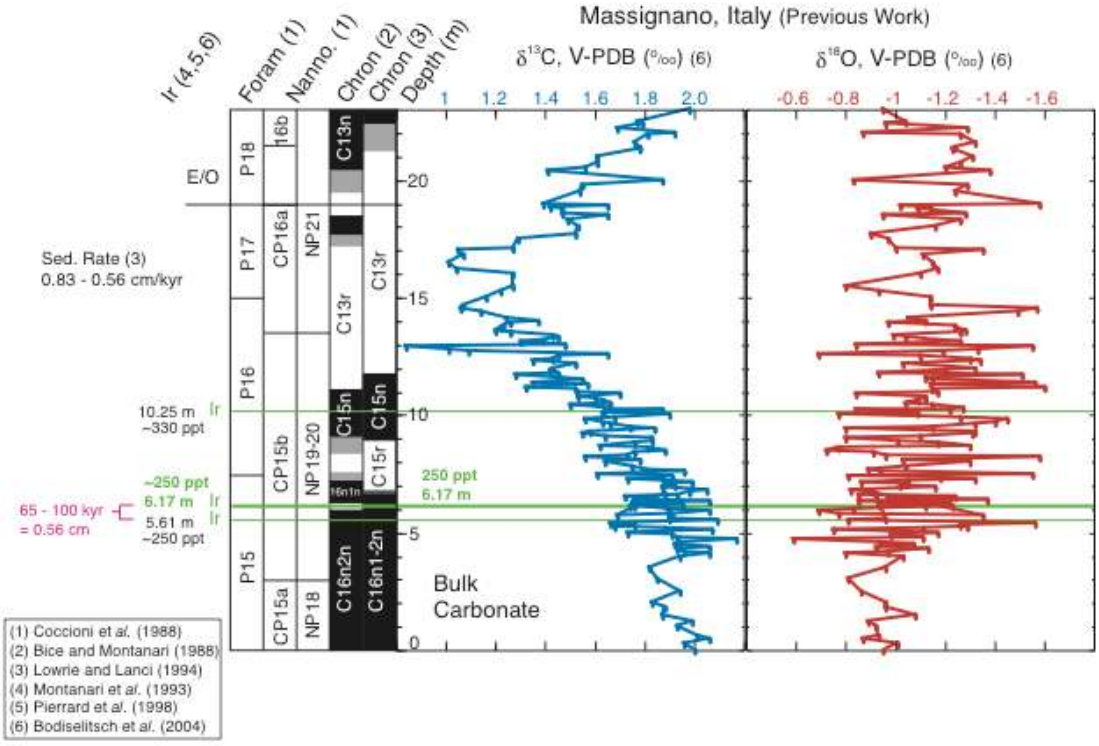

Figure 9b.

Biostratigraphy, magnetostratigraphy, and Ir anomalies (green lines) of the GSSP of the Eocene/Oligocene boundary at Massignano. Graphs show carbon (blue) and oxygen (red) bulk-carbonate isotopes for the entire section (Bodiselitsch et *al.*, 2004).

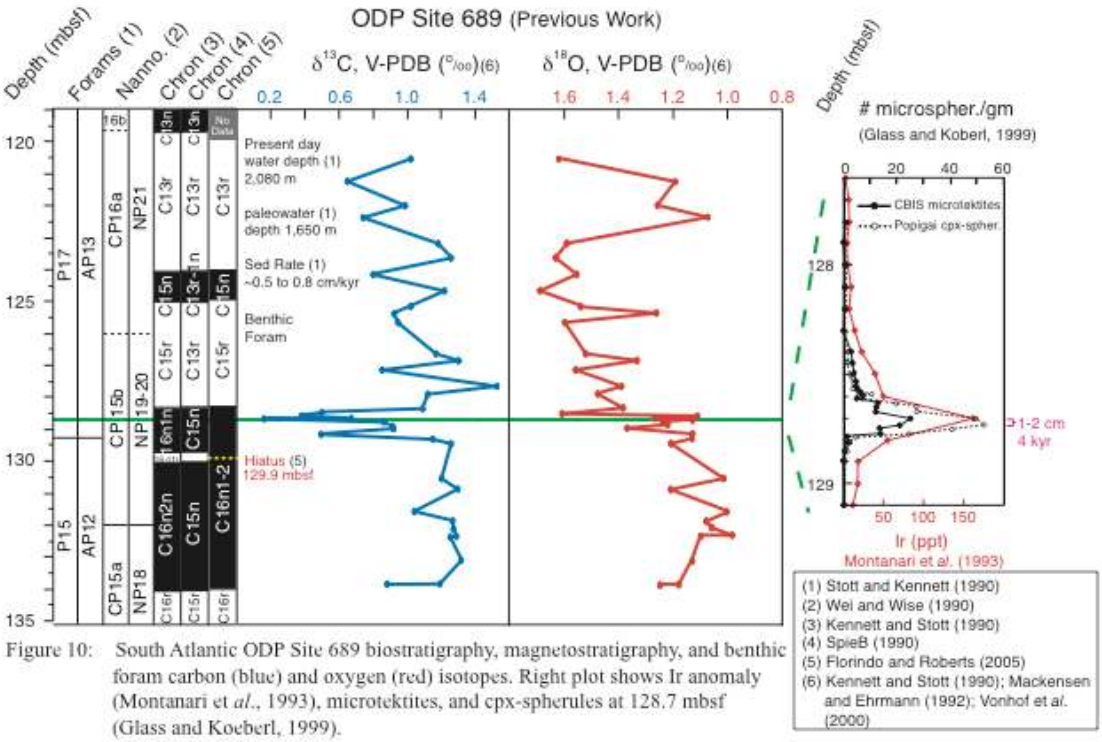

Figure 10: South Atlantic ODP Site 689 biostratigraphy, magnetostratigraphy, and benthic foram carbon (blue) and oxygen (red) isotopes. Right plot shows Ir anomaly (Montanari et *al*., 1993), microtektites, and cpx-spherules at 128.7 mbsf (Glass and Koeberl, 1999).

Figure 10.

South Atlantic ODP Site 689 biostratigraphy, magnetostratigraphy, and benthic foram carbon (blue) and oxygen (red) isotopes. Right plot shows Ir anomaly (Montanari et *al*., 1993), microtektites, and cpx-spherules at 128.7 mbsf (Glass and Koeberl, 1999).

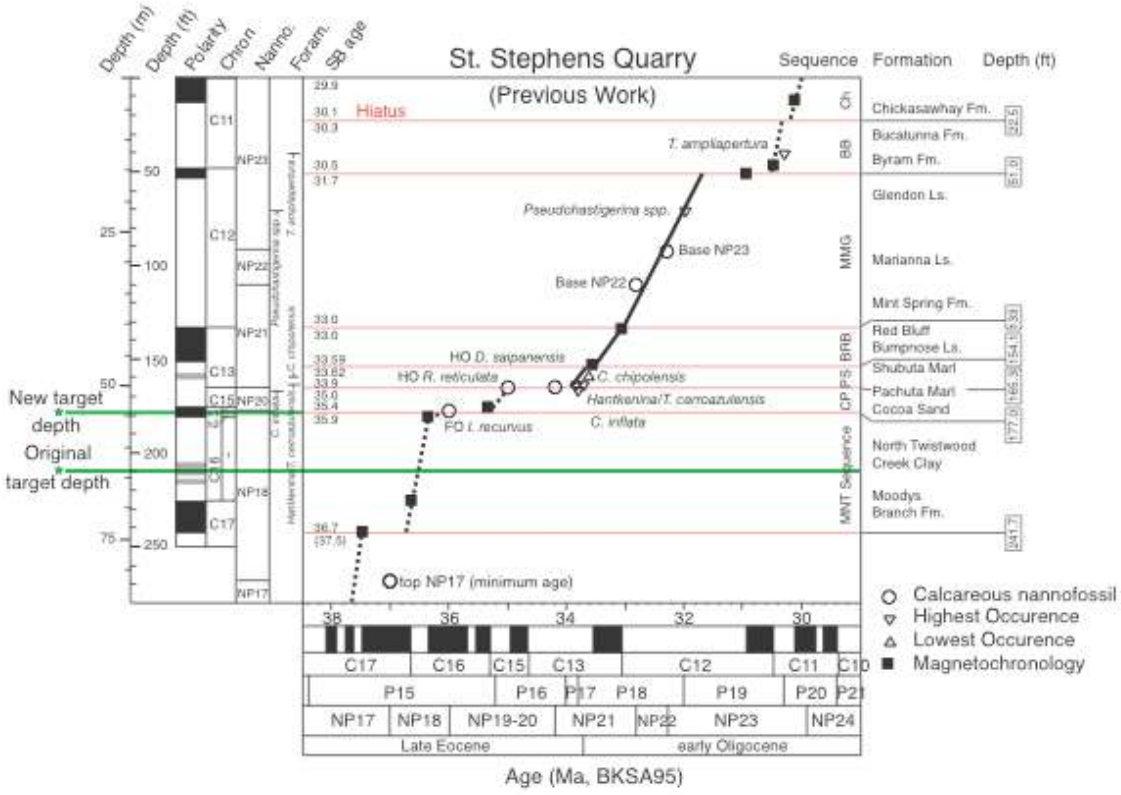

Figure 11.

St. Stephens Quarry, Alabama age-depth plot of biostratigraphy, magnetostratigraphy, and sequence stratigraphy (modified from Miller et *al.*, *in press*). Green lines show original (210 ft) (64 m) and modified (180 ft) (54.9m) target depths in magnetochron C16n.1n.

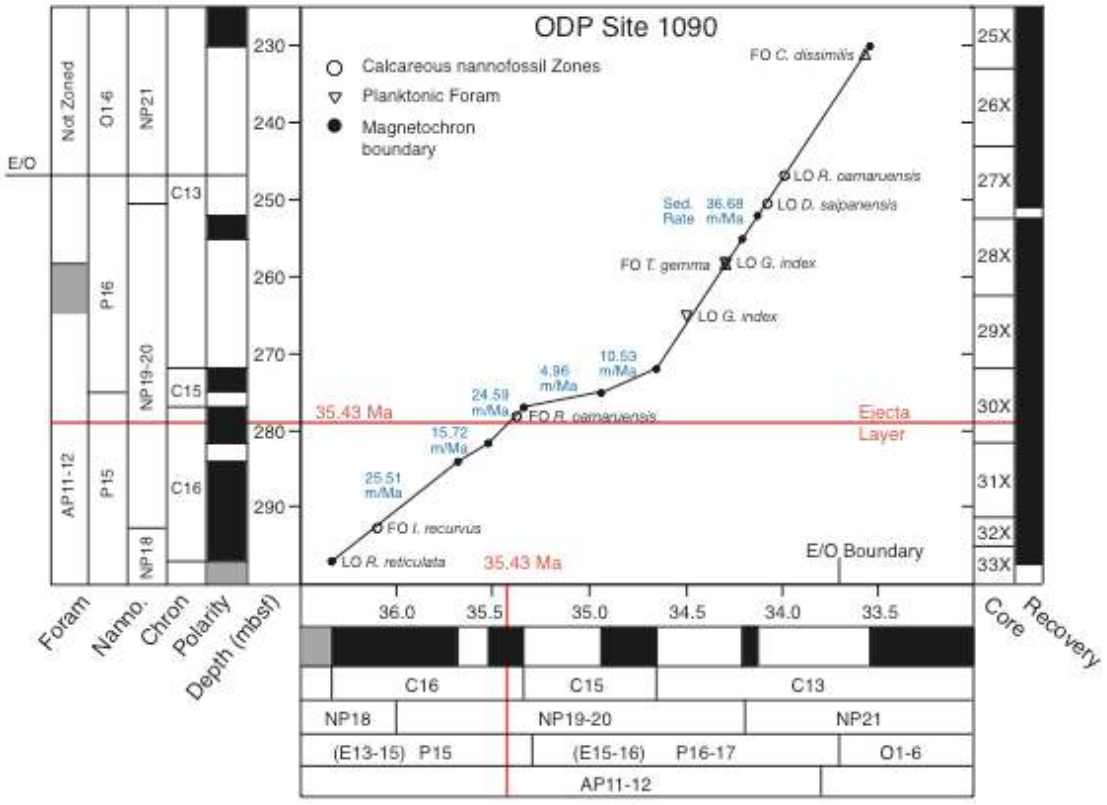

Figure 12.

South Atlantic Site 1090 age-depth plot. Red line shows ejecta layer (Kyte and Liu, 2002), nannofossil datum from Marino and Flores (2002), foram datum from Galeotti et *al*. (2002), and magnetochron data from Channell et *al*. (2003).

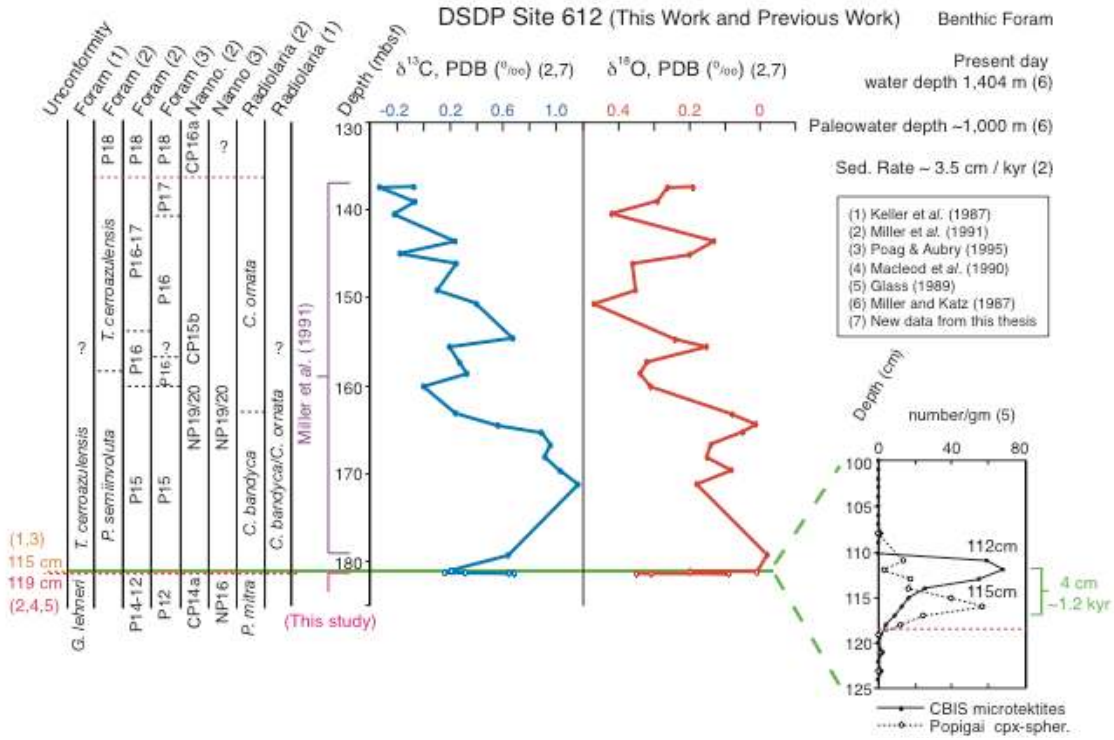

Figure 13.

DSDP Site 612 biostratigraphy and benthic foram carbon (blue) and oxygen (red) stable isotope data (open circles are new data from this thesis and closed circles are data from Miller et *al*., 1991). Dotted red line shows unconformity.

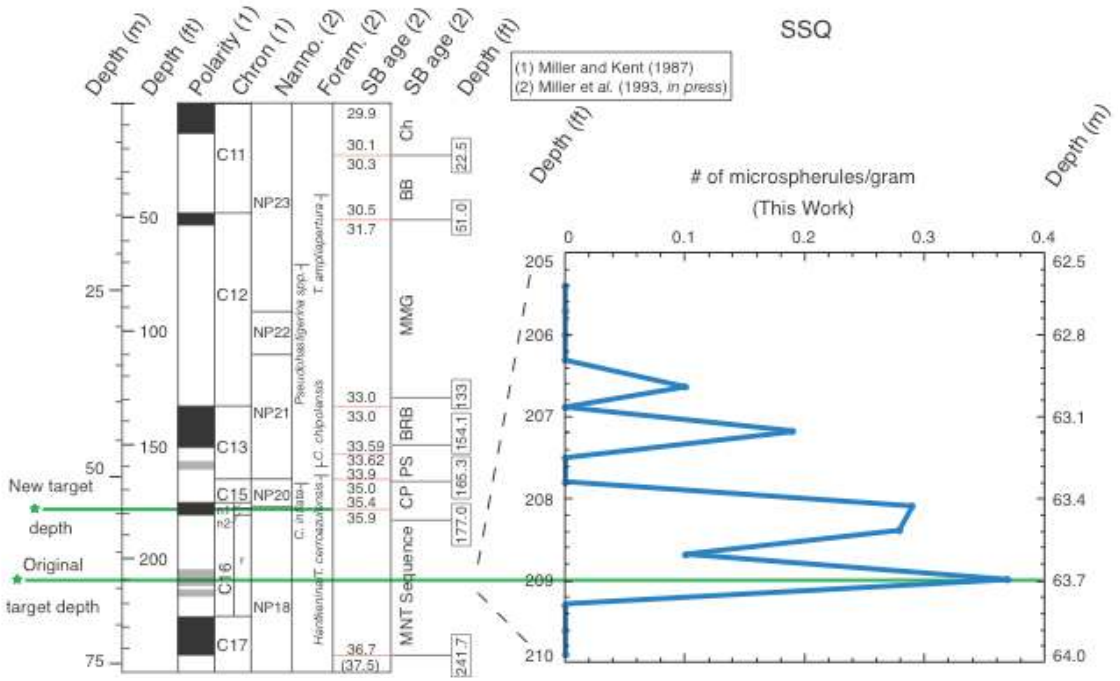

Figure 14.

Stratigraphic distribution of microspherules from SSQ. Green lines represent calculated target depths in magnetochron C16n.1n. Red lines represent hiatus.

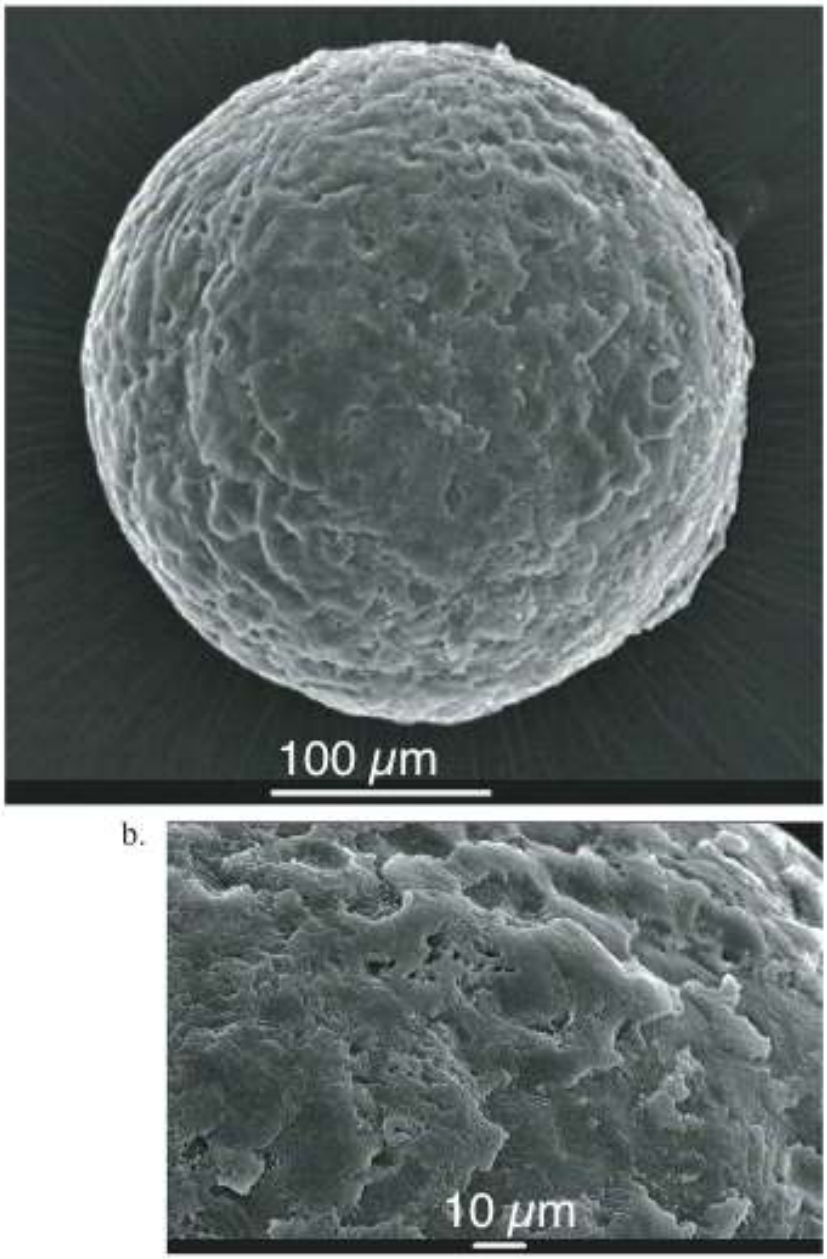

Figure 15a.

Scanning electron microscope image (SEM) magnified 272x of a 250 μm SSQ microspherule found at 204.7 ft (62 m) taken by Bridget Wade at Rutgers University.

Figure 15b.

Scanning electron microscope image (SEM) magnified 1,100x showing surface of a 250 μm SSQ microspherule found at 204.7 ft (62 m) taken by B. Wade.

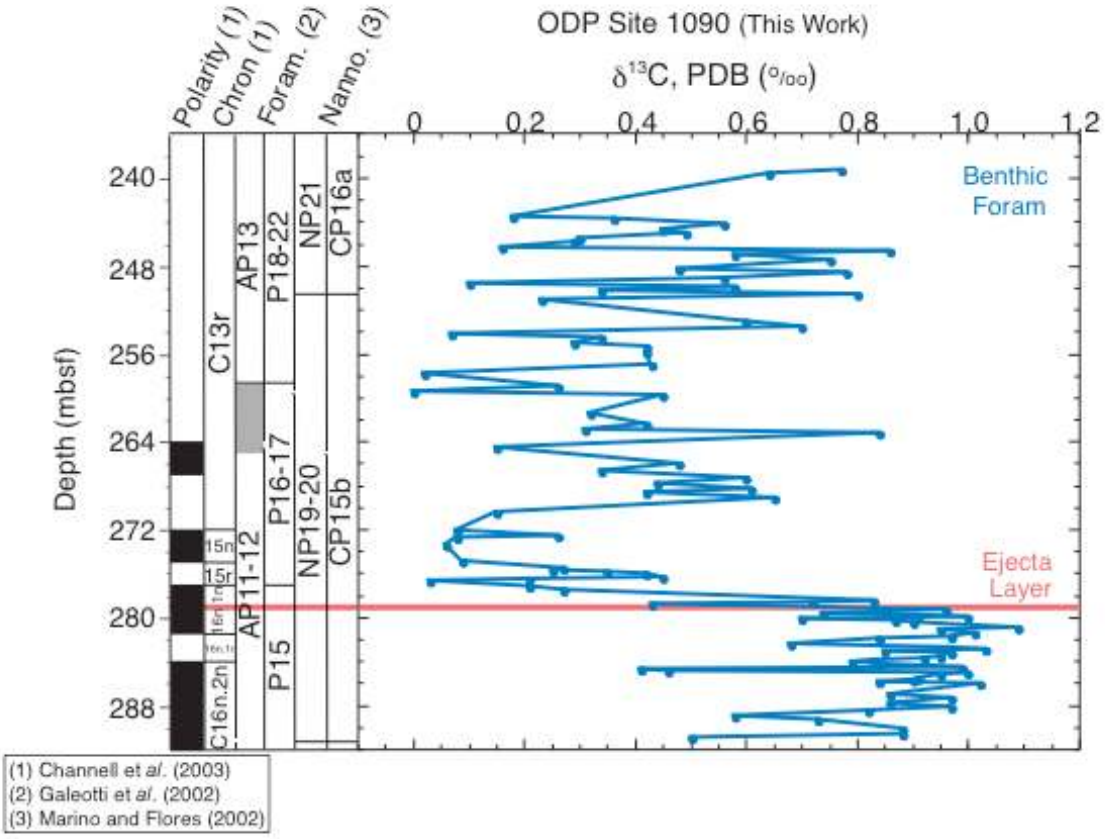

Figure 16a.

South Atlantic ODP Site 1090 benthic carbon isotopes versus depth (mbsf). Red line represents ejecta later (279 mbsf) (Kyte and Liu, 2002).

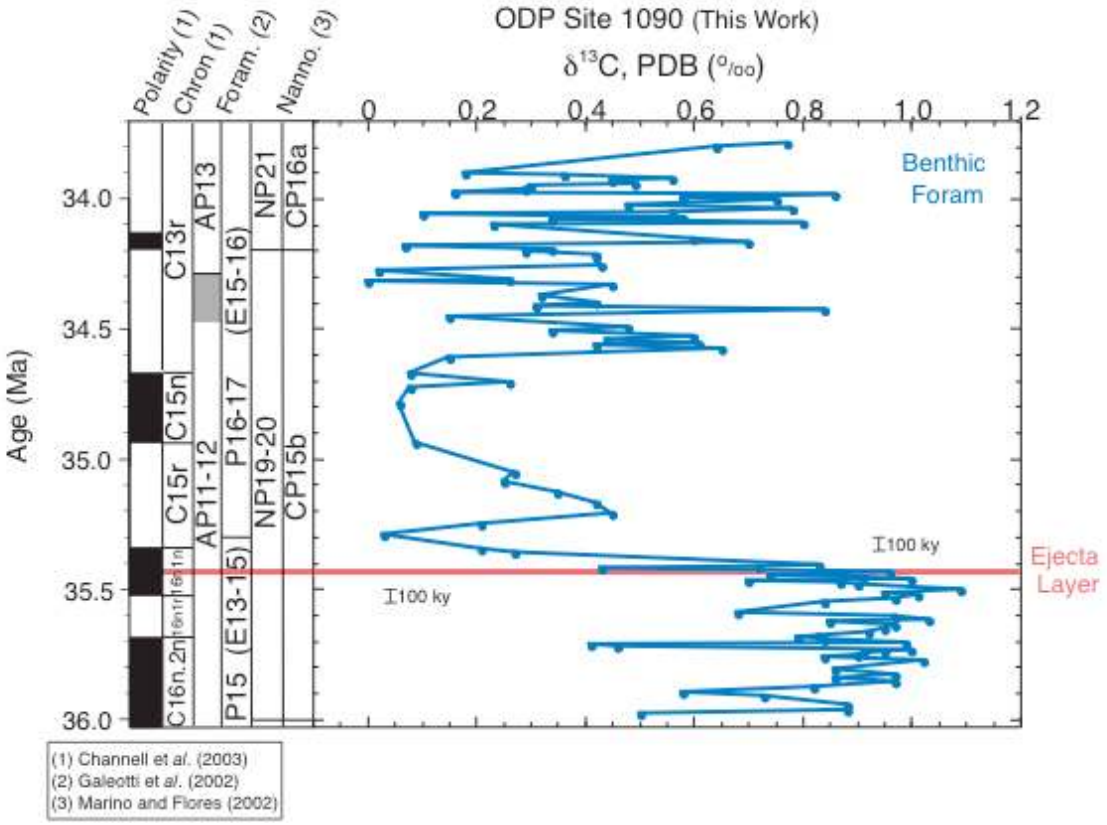

Figure 16b.

South Atlantic ODP Site 1090 benthic carbon isotopes versus age (Ma). Red line shows ejecta later (279 mbsf) (Kyte and Liu, 2002).

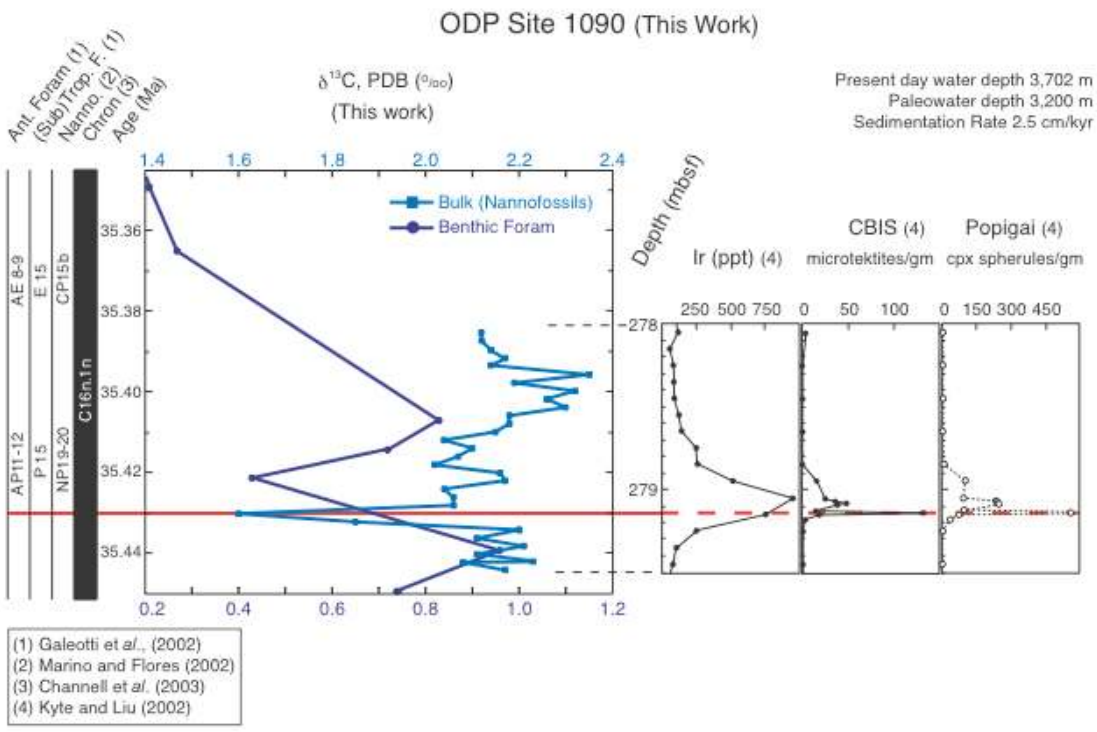

Figure 17.

ODP Site 1090 bulk-carbonate (light blue) and benthic foram (navy blue) carbon isotopes across ejecta layer (279.01 mbsf, magnetochronologic age is 35.43 Ma).

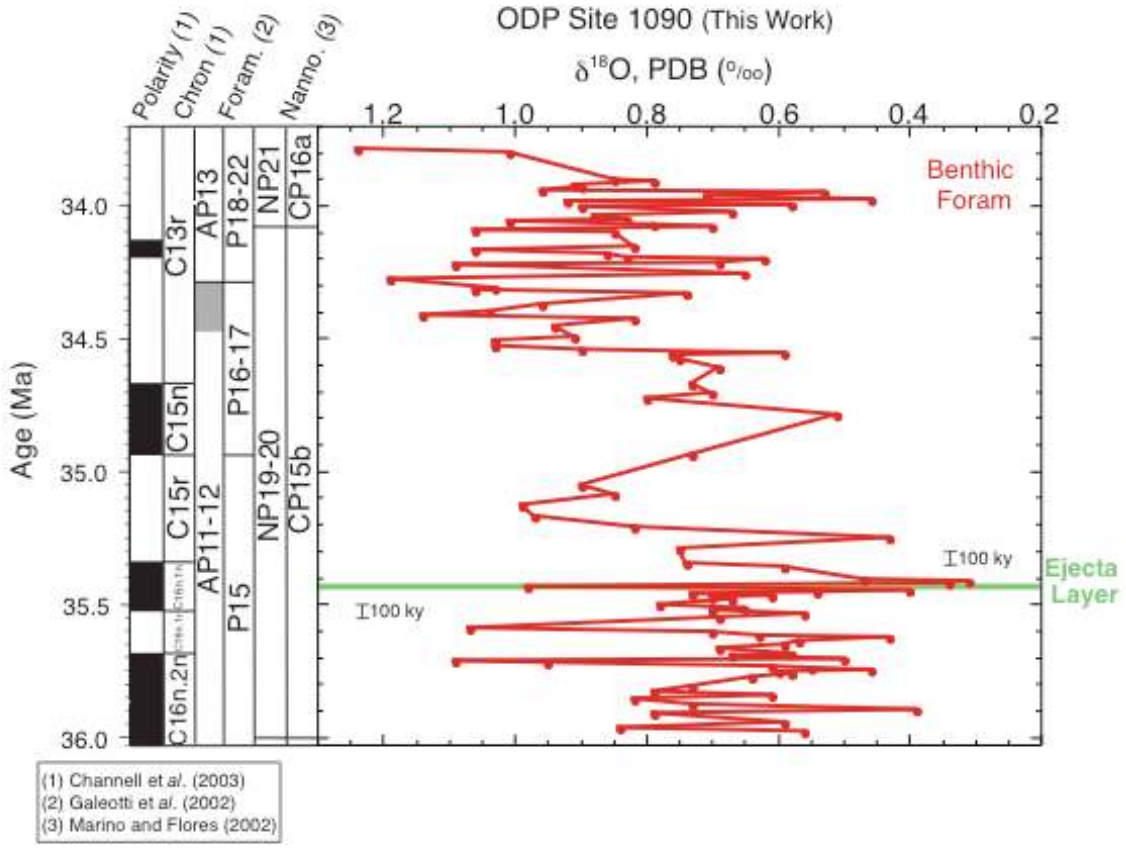

Figure 18.

South Atlantic ODP Site 1090 benthic foraminifera oxygen isotope data versus age (Ma). Green line represents impact ejecta later (Kyte and Liu, 2002) with an interpolated magnetochronologic age of 35.43 Ma.

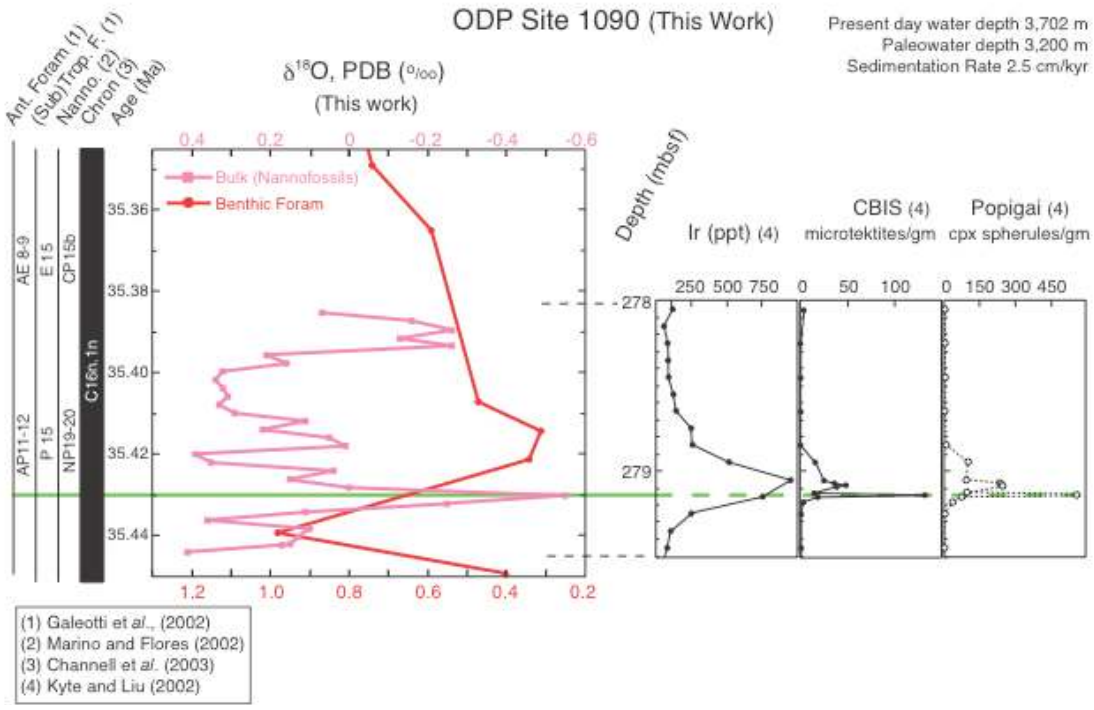

Figure 19.

ODP Site 1090 bulk-carbonate (pink) and benthic foram (red) oxygen isotopes across ejecta layer (279.01 mbsf, magnetochronolgic age is 35.43 Ma).

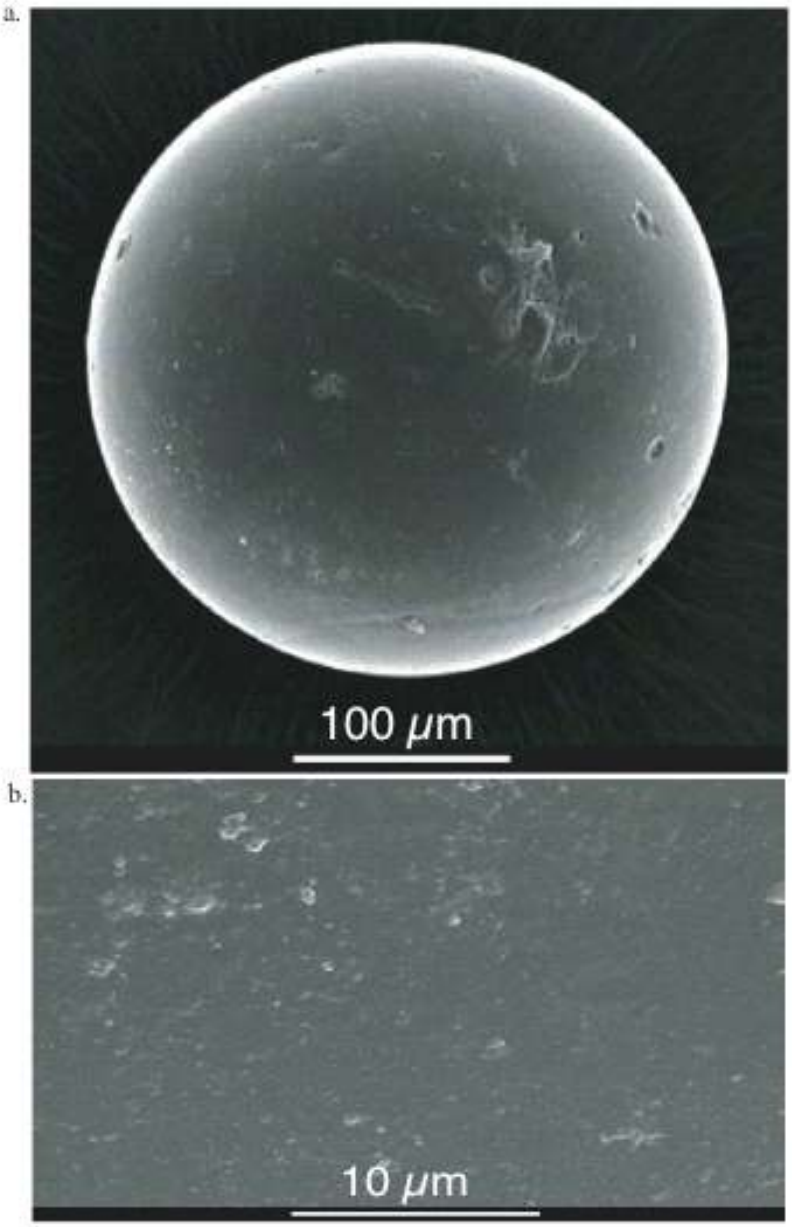

Figure 20a.

Scanning electron microscope image (SEM) magnified 306x of a 250 μm Site 1090 microtektite found in core 30X-5W; 94-95.5 cm taken by B. Wade at Rutgers University.

Figure 20b.

Scanning electron microscope image (SEM) magnified 4,460x showing surface of a 250 μm Site 1090 microtektite found in core 30X-5W; 94-95.5 cm taken by B. Wade.

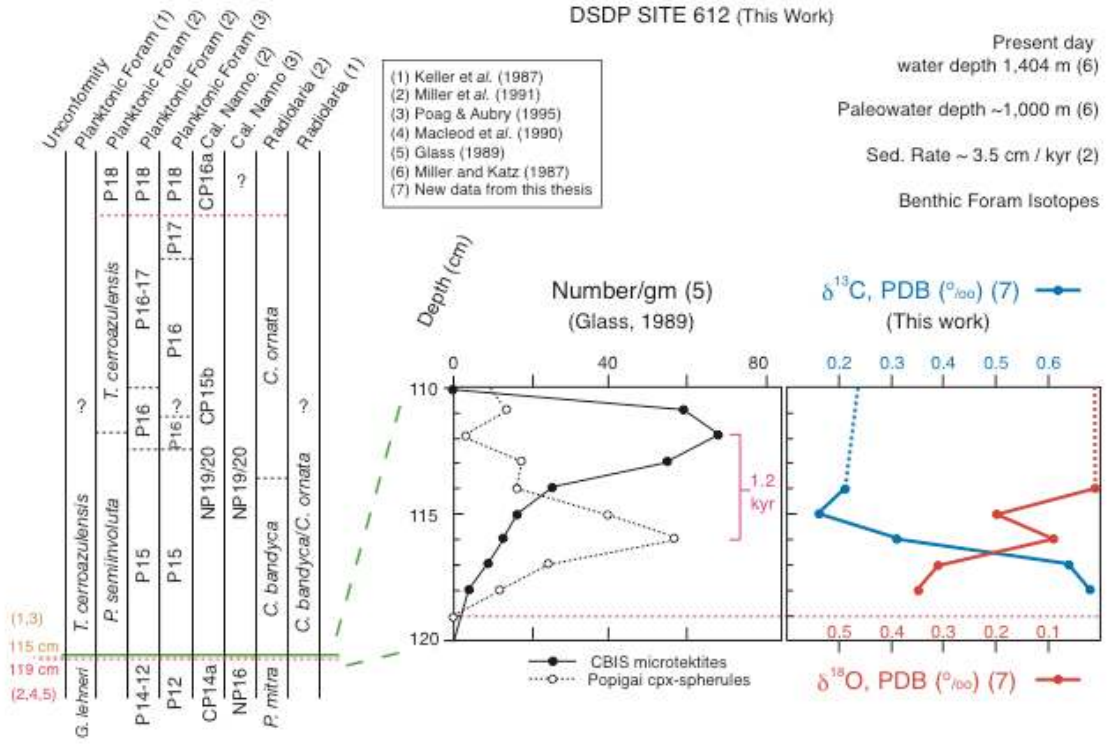

Figure 21.

Site 612 high-resolution benthic carbon and oxygen isotopes across the cpx-microspherule layer.

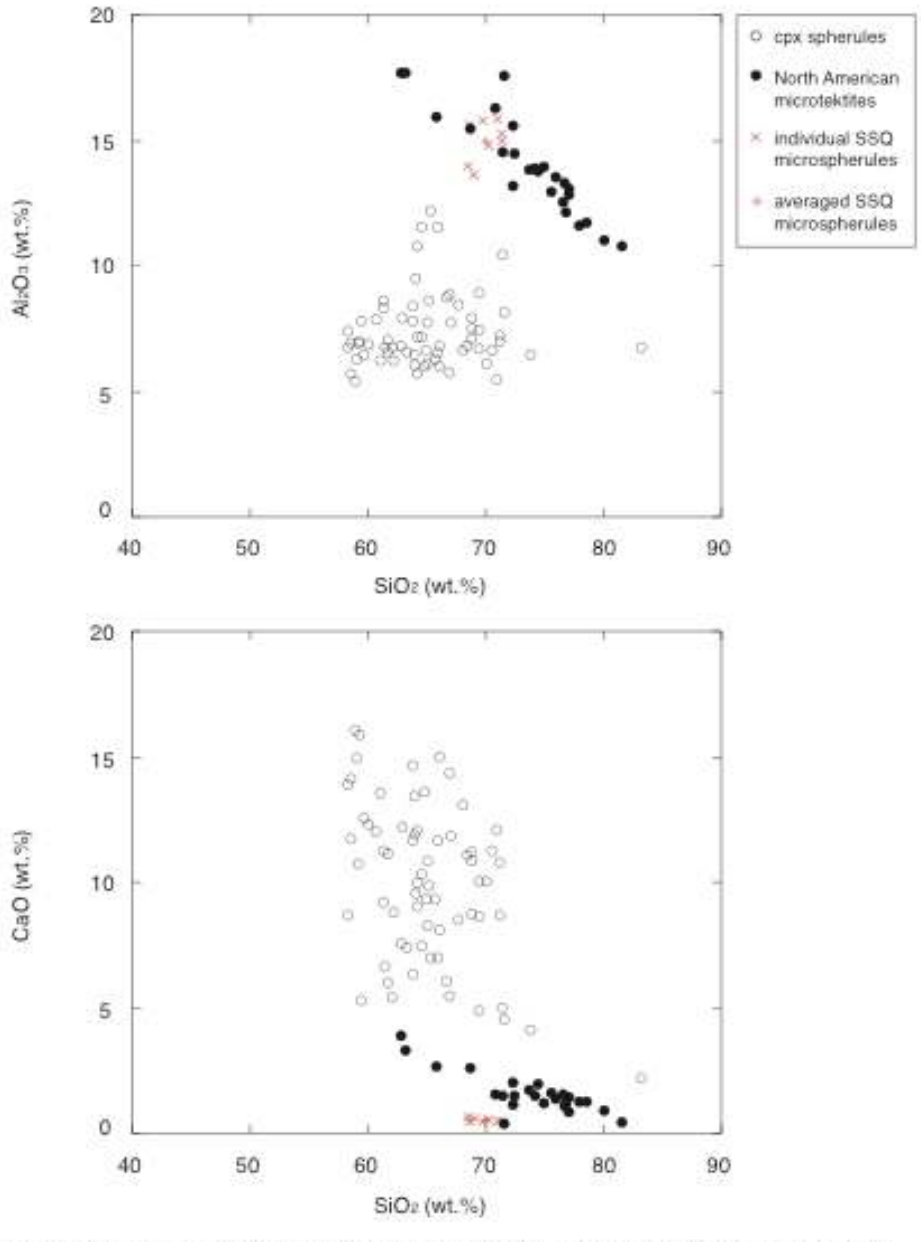

Figure 22a.

Plots display Al_2O_3 (top) and CaO (bottom) vs. SiO_2 weight percent (wt.%) concentrations of cpx-spherules (Glass et *al*., 2004a), North American microtektites (Glass et *al*., 2004a), and SSQ microspherules.

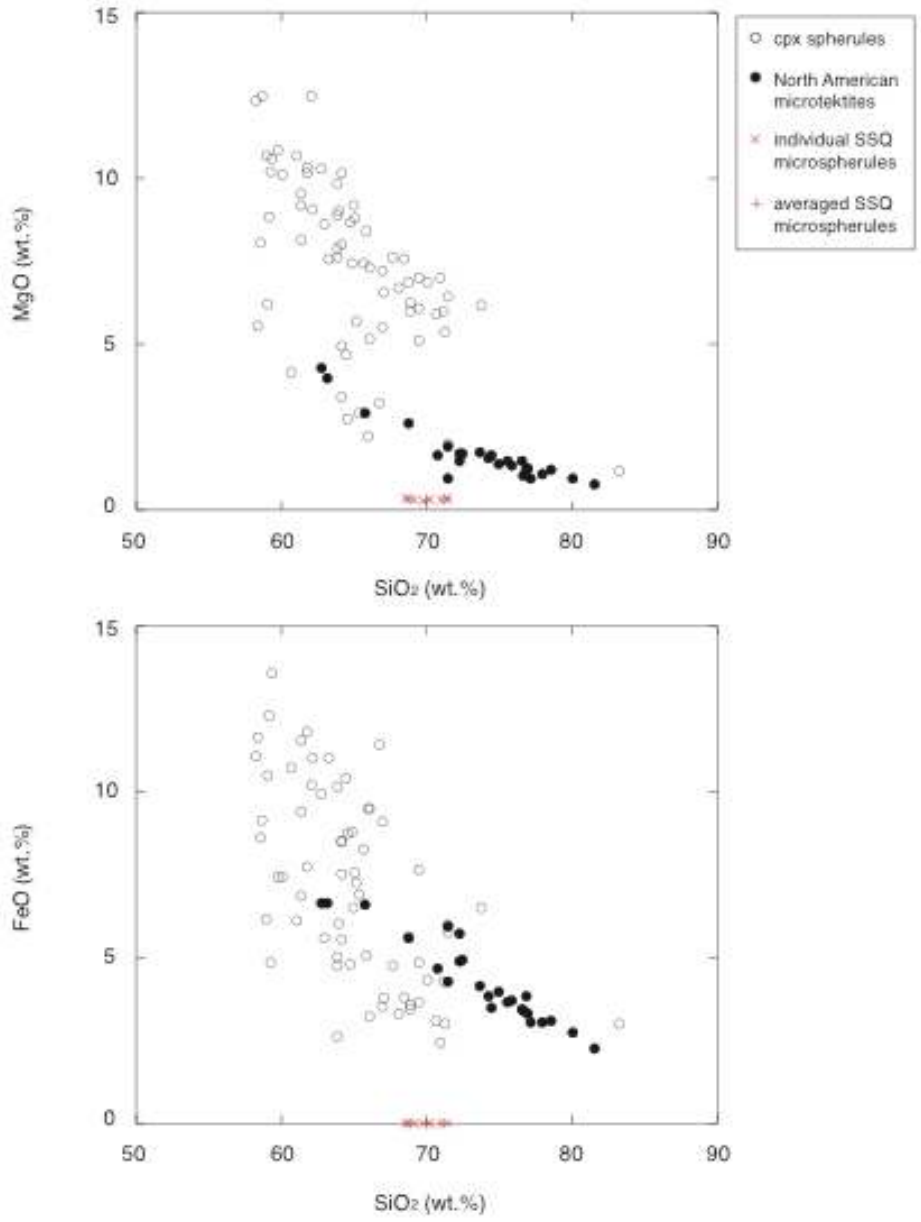

Figure 22b.

Plots display MgO (top) and FeO (bottom) vs. SiO_2 weight percent (wt.%) concentrations of cpx-spherules (Glass et *al.*, 2004a), North American microtektites (Glass et *al.*, 2004a), and SSQ microspherules.

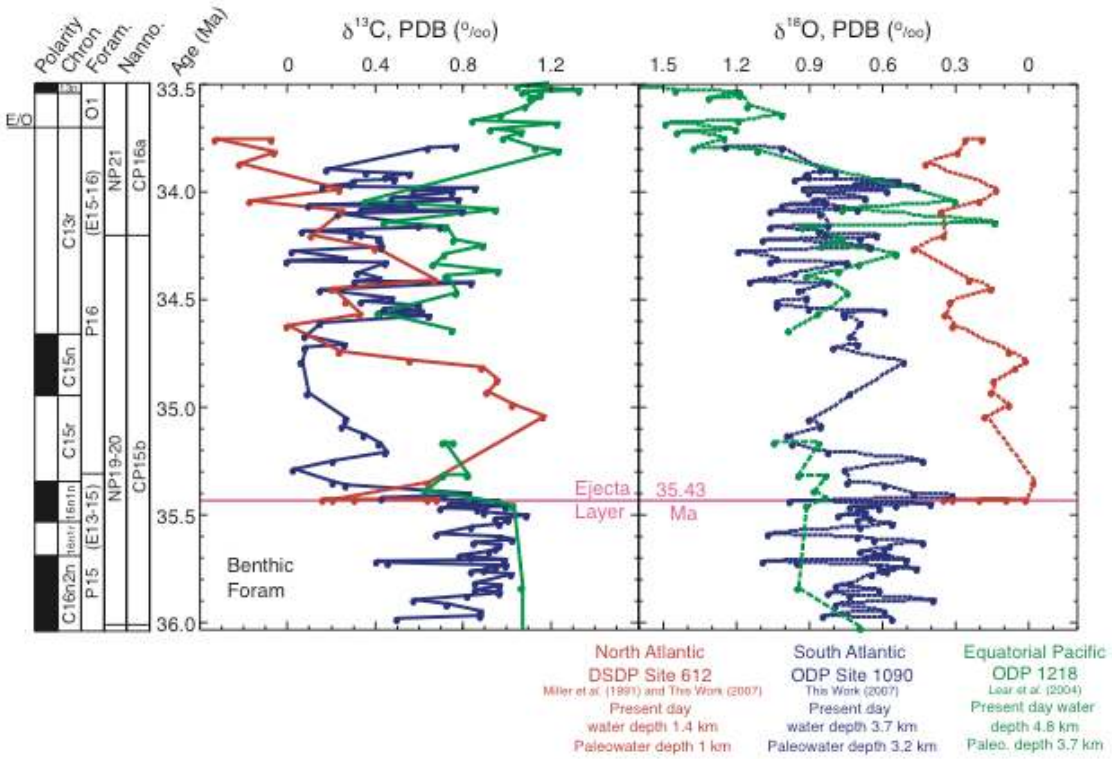

Figure 23.

North Atlantic DSDP Site 612, South Atlantic ODP Site 1090, and equatorial Pacific ODP Site 1218 benthic carbon and oxygen isotopes across ejecta layers identified at Sites 612 and 1090 by Glass (1989) and Kyte and Liu (2002), respectively.

Appendix A

SSQ BEI 1/1, 1/2

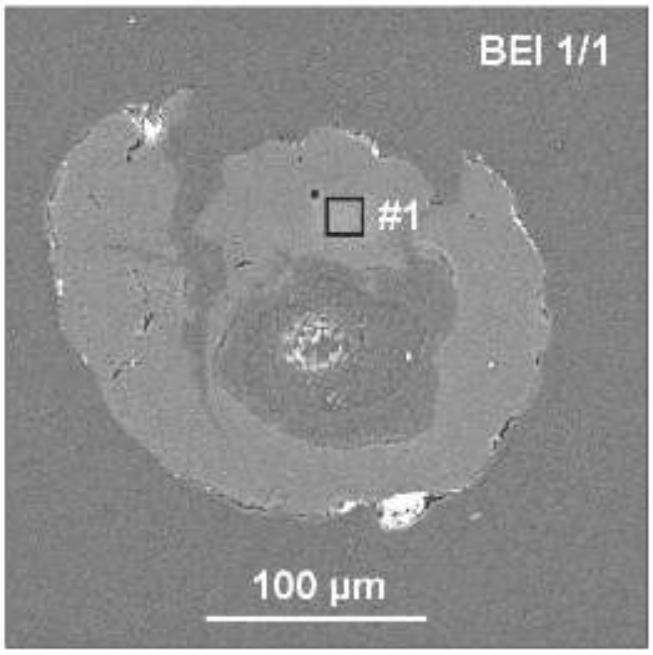

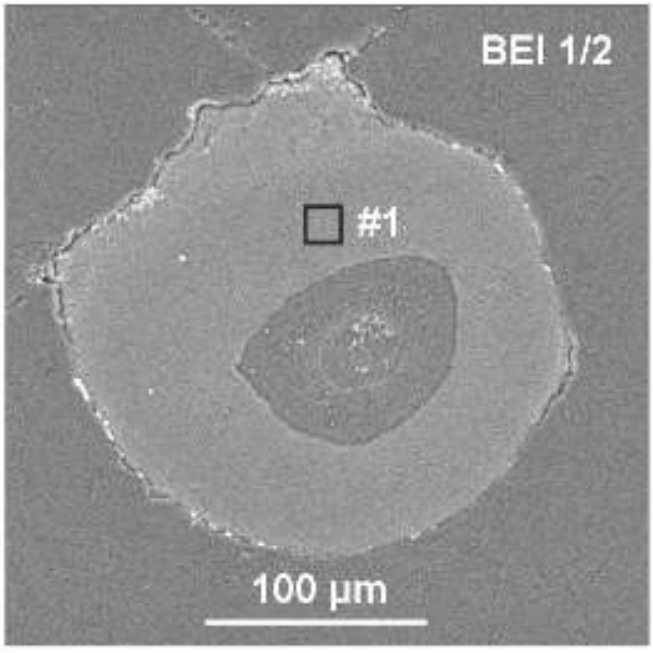

Appendix A

SSQ BEI 3/1, 3/2

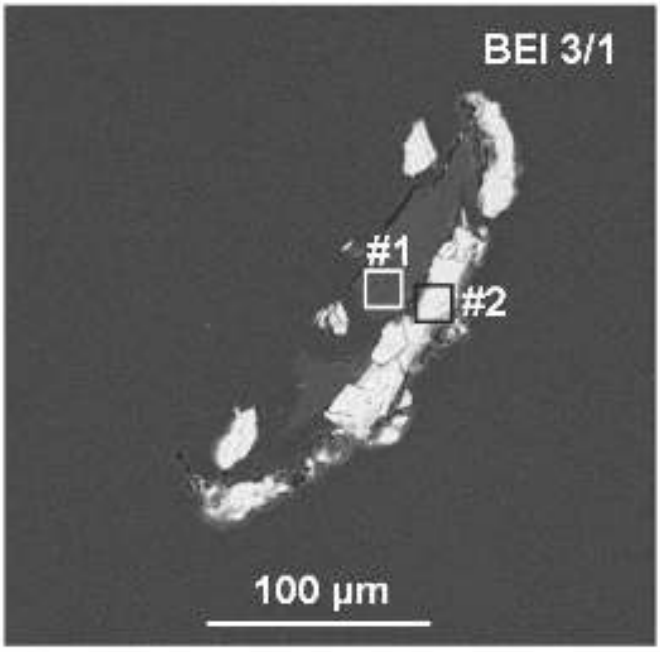

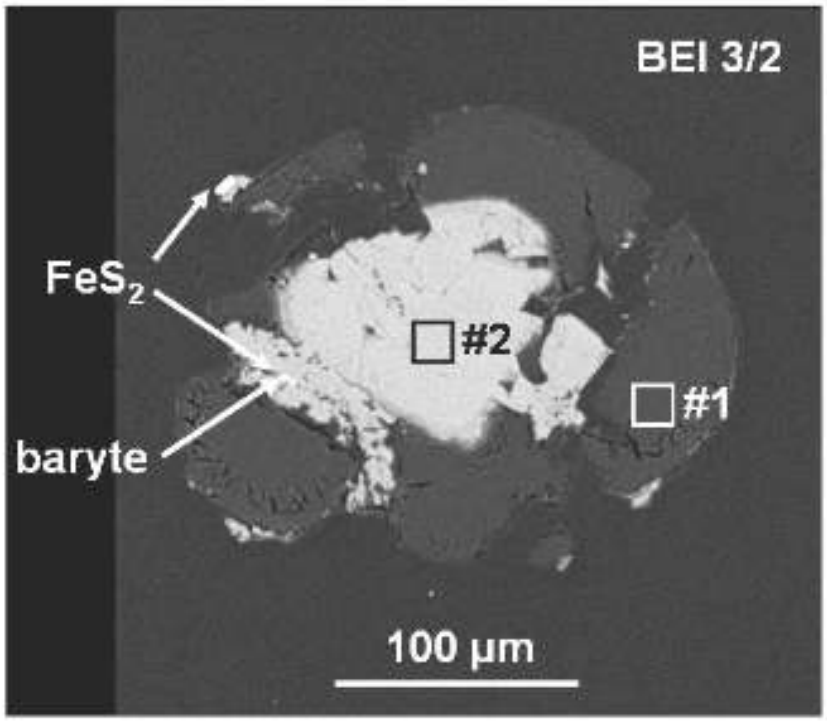

Appendix A

SSQ BEI 4/1, 4/2

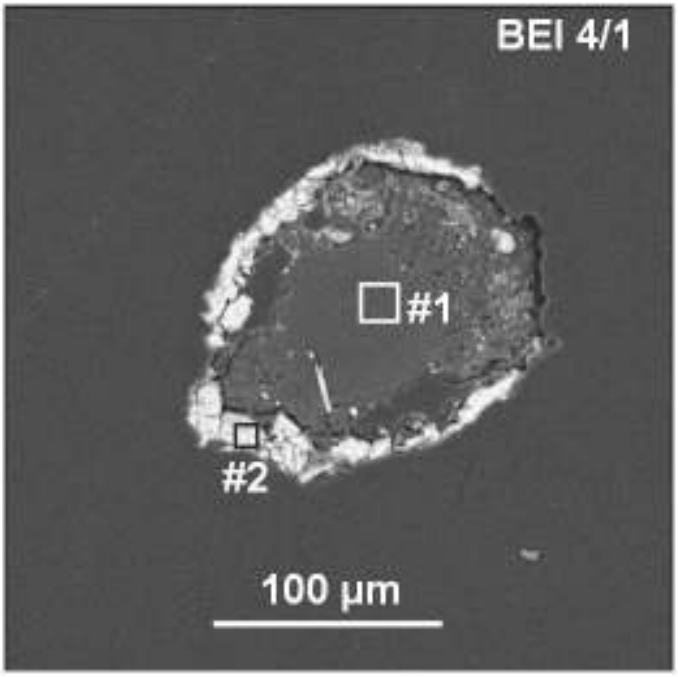

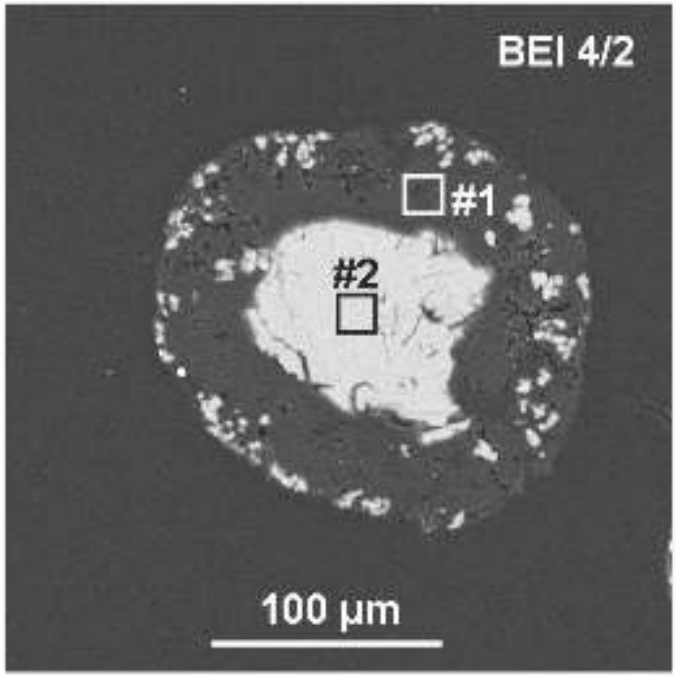

Appendix A

SSQ BEI 4/3, 4/4

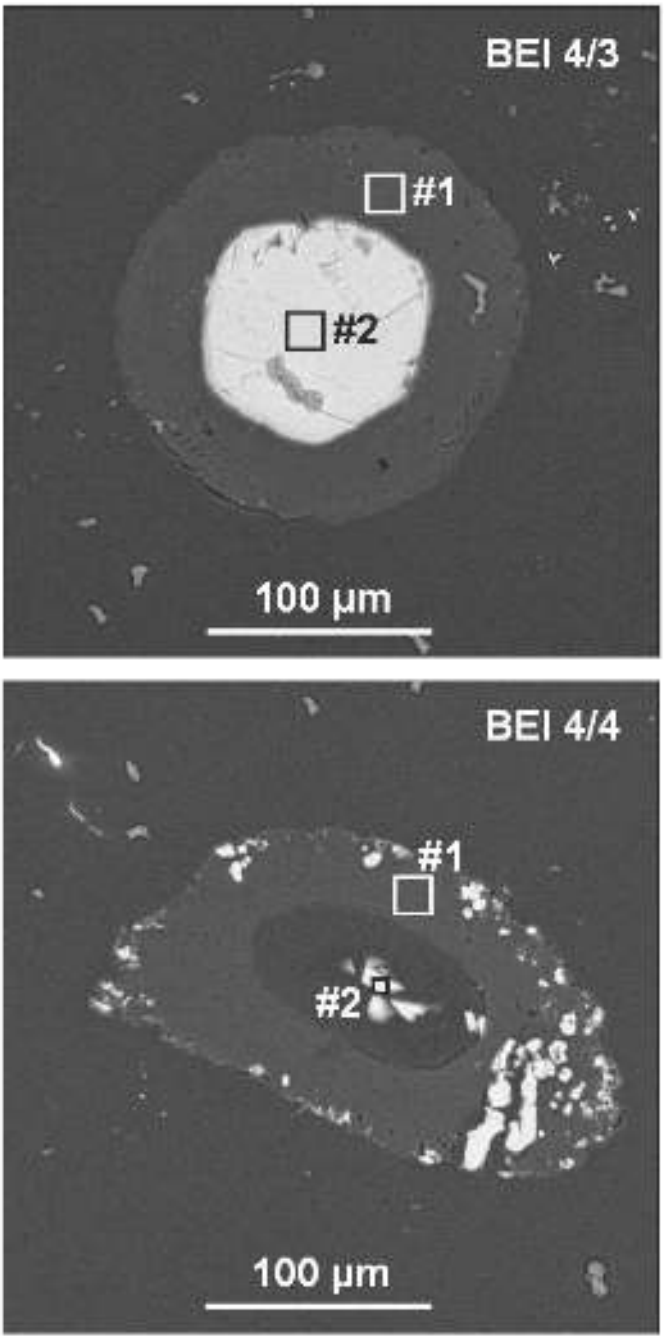

Appendix A

SSQ BEI 5/1, 6/1

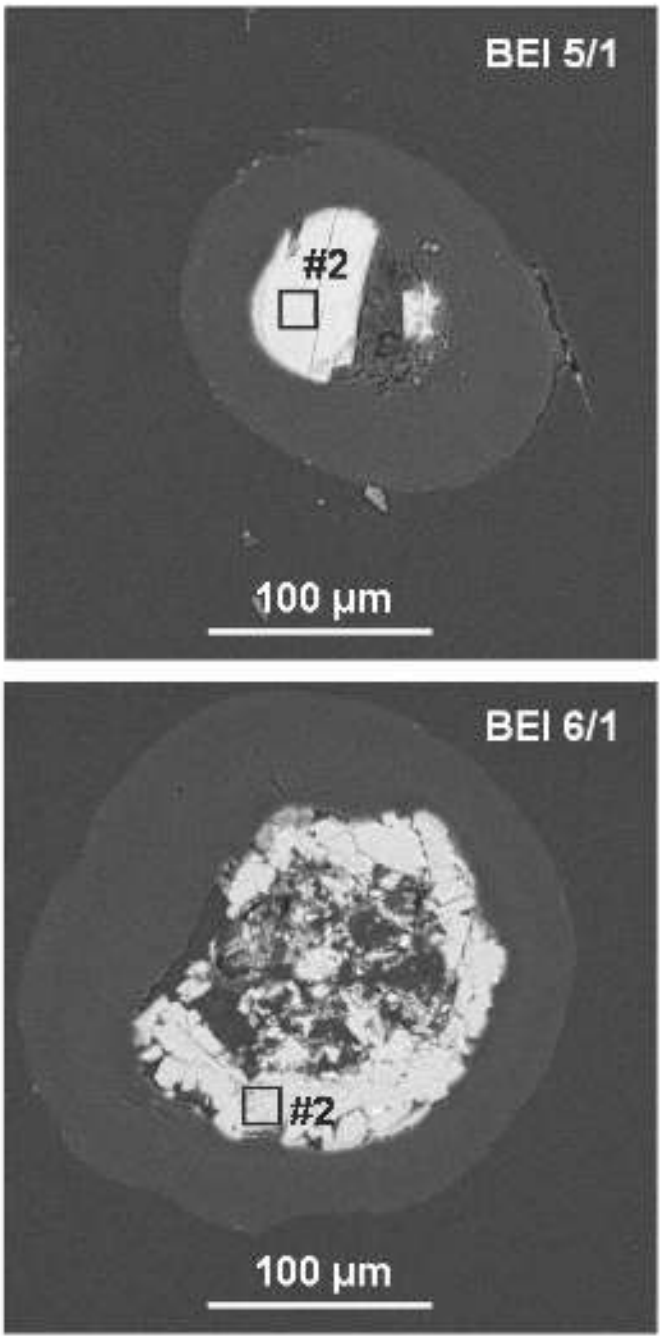

Appendix A

SSQ BEI 6/2, 7/1

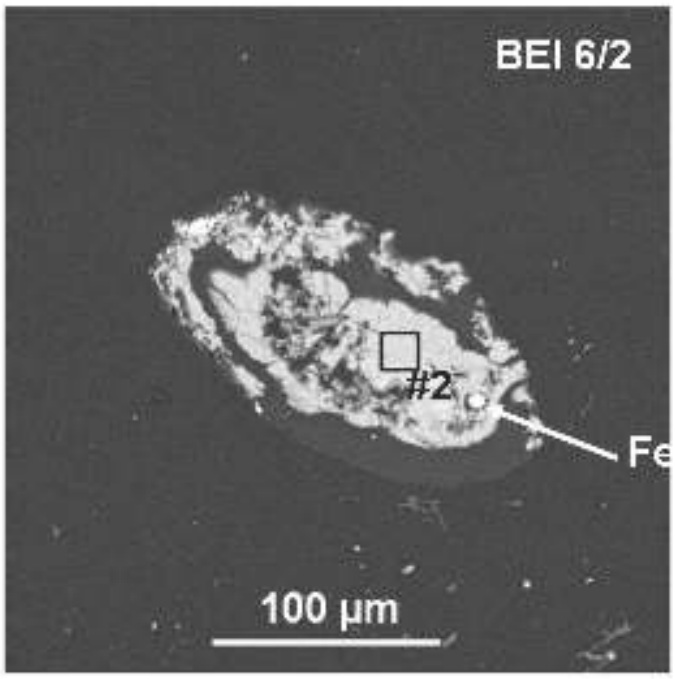

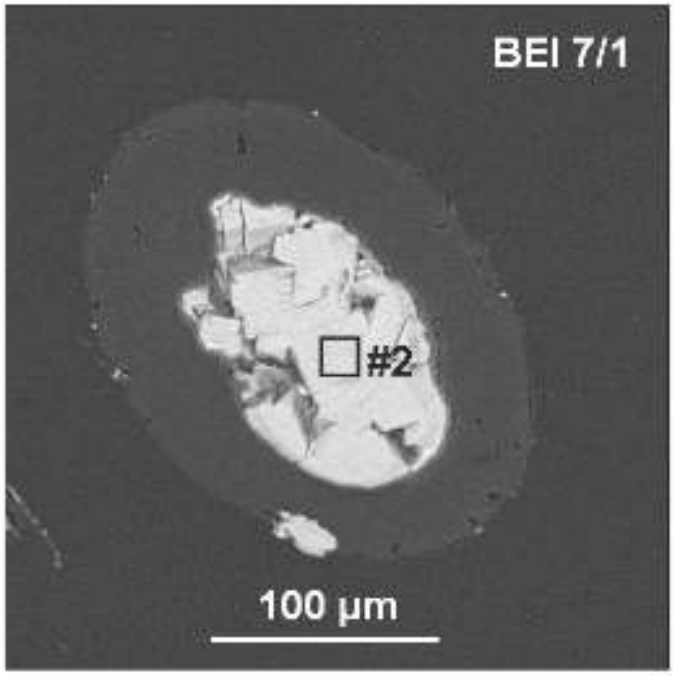

Appendix A

SSQ BEI 7/2, 7/3